Spatial Modelling of Heavy-Tailed Mineral Grades Using a Spatial Point Process

by

Cole Robert Mooney

A thesis submitted in partial fulfillment of the requirements for the degree of

Master of Science

in

Mining Engineering

Department of Civil and Environmental Engineering
University of Alberta

Abstract

Evaluating the resource contained in a precious metals deposit is a challenging task because they are often characterized by heavily-skewed grade distributions and outlier values. Traditional geostatistical modelling methods are difficult to apply in the presence of outlier values because they can lead to overestimation and bias. The economic viability of these deposits often depend on the upper few percent of samples. These outlier samples are important and should be retained; however, their influence should be reduced to prevent potential overestimation and bias.

This thesis examines the implications of modelling heavy-tailed, precious metals deposits. The limitations of traditional geostatistical modelling techniques are discussed in the context of heavy-tailed deposits and the use of a spatial point process to model grade is presented. An overview of the geologic processes that create gold deposits is presented in order to understand the nature of gold mineralization as well as provide justification for the proposed modelling technique.

A spatial point process is used to model the tail of the distribution as discrete events. A particle size distribution is given to the simulated points to calculate grade. Following that, a discrete fracture network is adapted to model mineralized quartz veins in the deposit. High-grade gold is spatially restricted to the simulated vein structures. The automatic processing of drill core photos generates the necessary input distributions for a fracture network. Finally, a thorough case study demonstrates the application of grade modelling with a spatial point process and discrete fracture network. The results are compared to traditional geostatistical techniques and limitations are discussed.

The proposed methodology presents a geologically realistic method of sim-

ulation which reduces the effect of outlier values by spatially limiting their influence. Capping or other subjective ad-hoc manipulation of assay data is not required. Final models of grade have the correct mean, variance and spatial continuity.

Acknowledgements

First, I would like to thank Jeff Boisvert. You have been a great mentor and role model in the world of geostatistics. Without your guidance, this would not have been possible. I would like to thank Clayton Deutsch for your lectures in geostatistics over the past year and a half. I would like to thank Eric Daniels for being a great friend and a source of sanity throughout graduate school.

I would like to thank Dr. Warwick Board and the rest of the team at Pretivm Resources for the financial support and giving me an opportunity to pursue graduate studies here.

I would like to thank my father. You inspired me to pursue a career in mining and your support and guidance along the way has helped make all of this possible.

Finally, I would like to thank my fiancee, Tamara, for your love, understanding and support during my time here at the CCG. We've been through a lot in the past year and a half and you've always been there for me, encouraging me along the way.

Table of Contents

List of Figures

List of Tables

List of Symbols

Symbol	Definition	First Use
X	random variable	2
F	distribution function	2
$\mathbf{h}$	distance vector	10
$\gamma(\mathbf{h})$	the variogram	10
$\mathbf{u}$	a vector of locations	10
$z(\mathbf{u})$	known data at a location	10
$\mathbb{R}^d$	real number domain	27
E	a set within $\mathbb{R}^d$	27
ε	collection of sets in E	27
A	a domain	27
μ	population mean	27
λ	intensity measure	27
k	number of occurances	28
$\lambda(\mathbf{u})$	intensity at location $\mathbf{u}$	33
L	length of veins	43
k	vein scaling constant	43

List of Abbreviations

Abbrv.	Definition	First Use
SK	simple kriging	12
OK	ordinary kriging	12
IK	indicator kriging	12
CDF	cumulative frequency distribution	14
ppb	parts per billion	20
VMS	volcanogenic massive sulphide	21
SPP	spatial point process	27
SMU	selective mining unit	27
PSD	particle size distribution	29
SGS	sequential Gaussian simulation	30
DFN	discrete fracture network	37
MCS	Monte Carlo simulation	44
RGB	red-green-blue color space	53
Lab	lightness-scaled color space	53
HSV	hue-saturation-value color space	53
CIE	International Commission on Illumination	58

DGM	discrete Gaussian model	72
SIS	sequential indicator simulation	94
TPG	truncated pluri-Gaussian	94

Chapter 1

Introduction

An important step in the development of a mine is the assessment of the value of the ore body. Exploration samples are collected early on in the project and used to create an estimate of the mineral resource which is the amount and concentration of the mineral of interest, and a geological model that describes the extents of the ore body. Mining and economic considerations are applied to the mineral resource estimate to create a mineral reserve which is the amount of calculated mineral which can be economically extracted (Rossi and Deutsch, 2014). Many geostatistical techniques have been developed over the years to provide accurate and unbiased measures of the mineral of interest. All of these techniques rely on a careful constructed sampling program to ensure reliable data collection. An accurate interpretation of the deposit geology is needed to construct statistically stationary mineralized domains. There are entire works concerning sampling protocol and geologic modelling both of which are outside the scope of this thesis. The interested reader is referred to Francois-Bongarcon and Gy (2001).

1.1 Background

Metal deposits, particularly precious metal deposits such as gold deposits, often display highly skewed grade distributions with assay values spanning four or five orders of magnitude. A small number of samples in the tail of the distribution have a disproportionately large effect on the total contained metal of a deposit when assessed by typical estimation techniques; failure to properly

deal with outlier values can lead to overestimation of the recoverable resource (Rossi and Deutsch, 2014). These heavy-tailed distributions have a number of well-documented problems, such as obtaining a representative distribution, accurately accounting for change of support and smearing of grade (Dominy et al., 2000; Maleki, Madani and Emery, 2014).

1.1.1 Heavy-Tailed Distributions

The definition of a heavy-tailed distribution varies among disciplines. In probability theory, a heavy-tailed distribution is one in which the tail is not exponentially bounded; they have heavier tails than the exponential distribution (Asmussen, 2003) (Figure 1.1). Other definitions in use include any distribution which does not have finite variance or, in some cases, any distribution which has tails heavier than a Normal distribution. In general terms, the tail can be considered heavy if the distribution of a random variable X with a distribution function F satisifies the following (Asmussen, 2003):

$$\lim_{x\to\infty} \mathrm{e}^{\lambda} \Pr[X > x] = \infty, \forall \lambda > 0 \tag{1.1}$$

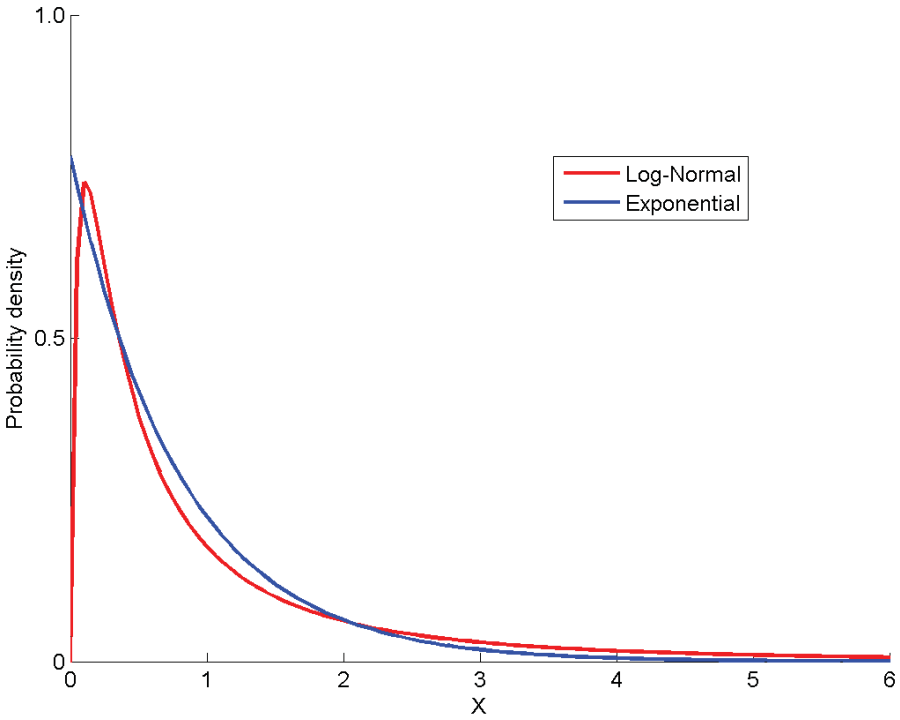

Figure 1.1: The log-normal distribution is classified as heavy-tailed when compared to the exponential distribution.

The definition of a heavy-tailed distribution means that there is a larger probability of getting very large values. These large values, often termed outlier values, can be real in the case of deposits characterized by heavy-tailed distributions. The implications of this can be seen when calculating summary statistics; a small number of samples will have a very strong affect on the mean, variance and measures of spatial continuity (Rossi and Deutsch, 2014).

Mandelbrot (1997) defines seven states of randomness; ranging from proper mild randomness (normal distribution) to extreme randomness where all moments are infinite and a single observation can impact the total in a very disproportionate way. In the context of heavy-tailed, precious metal deposits, the state of randomness falls somewhere to the right of center because they are often characterized by distributions which have heavier tails than a log-normal distribution. This implies that precious metals deposits characterized by heavy tails have an inherent randomness which cannot be ignored.

For this work, the exact definition of a heavy-tailed deposit is not overly important. The important points are i) to recognize that there is an increased level of inherent randomness in the statistical population, ii) accept the existance of high outlier values as real, and iii) understand that these samples have a strong effect on the overall distribution.

1.1.2 Outlier Values

Observations which stand out from the general population have been recognized for over one-hundred years in the statistical literature. These observations, often termed outlier values, must be examined and understood in the context of the problem at hand before proceeding. There is no strict mathematical definition of what constitutes an outlier value. Grubbs (1969) simply defines an outlier as: "an observation point that is distant from the rest". He then subdivides outliers into two types: i) a value which is an extreme manifestation of the random variability inherent in the data, and ii) a value which is the result of gross deviation from the prescribed experimental procedure or an error in calculating or recording the numberical value. In the case of the former, the value should be retained and processed in the same manner as other observations. In the case of the latter, the value should be discarded. In a mining context, outlier assay values must be carefully observed to ensure that they are in fact a result of the underlying heavy-tailed distribution and not an error from the assay lab.

Deciding whether or not an observation is an outlier value is a highly subjective exercise; however, there are many methods of detection. One common method is to examine the values on a lognormal cumulative frequency plot and look for breaks or changes in slope. Figure 1.2 illustrates an example of using a probability plot to detect outliers. A clear inflection point in the grade frequency distribution indicates the presence of a small outlier population.

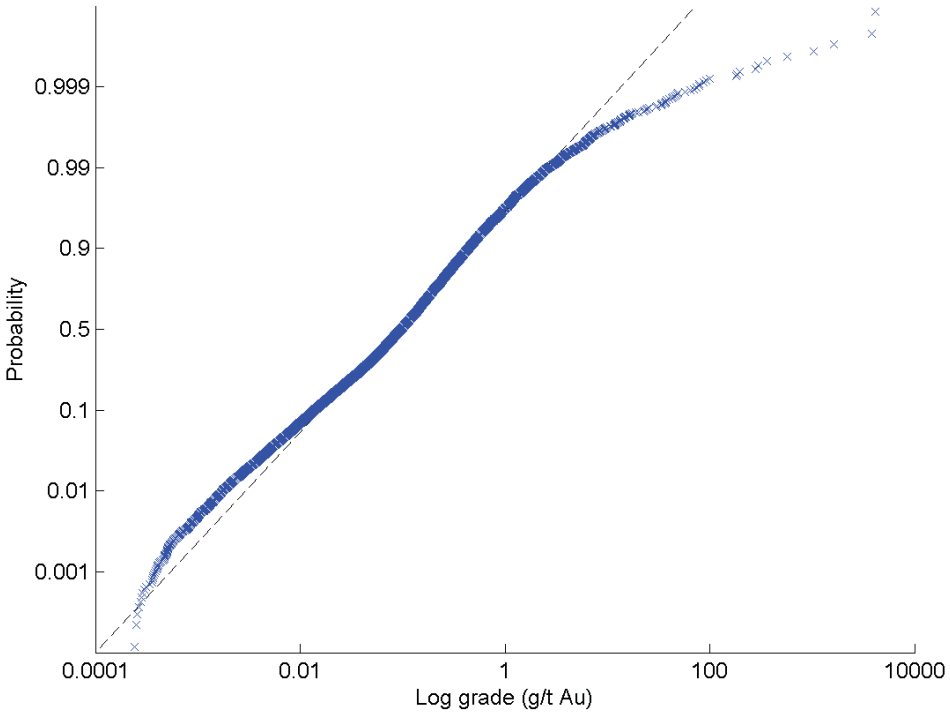

Figure 1.2: Probability plot of gold grade in an epithermal vein deposit. Samples in the upper percentiles depart significantly from log-normality.

Another common method is to define outliers as values that fall outside a specified interval, such as plus or minus two or three standard deviations from the mean or median (Rossi and Deutsch, 2014). Another statistical method proposed by Parker (1991) involves plotting the cumulative coefficient of variation and looking for inflection points. Points above the inflection point could be considered outlier values.

In a mining context, a single high value surrounded by low values will have a more severe consequence on grade estimation than a single high value surrounded by moderately high values. Babakhani and Deutsch (2013) employs a method of detecting spatial outliers by rank transforming the true values and their cross-validated estimation values to the uniform distribution between zero and one and then projecting them on the 135 degree line on a cross plot. Data points that fall on the extreme ends of the 135 degree line are classified as spatial outliers. Finally, the breakdown of variogram structure at

increasing grade thresholds can also indicate an outlier population (Goovaerts, 1997). Figure 1.3 shows a schematic example of the breakdown of variogram structure with increasing grade capping thresholds.

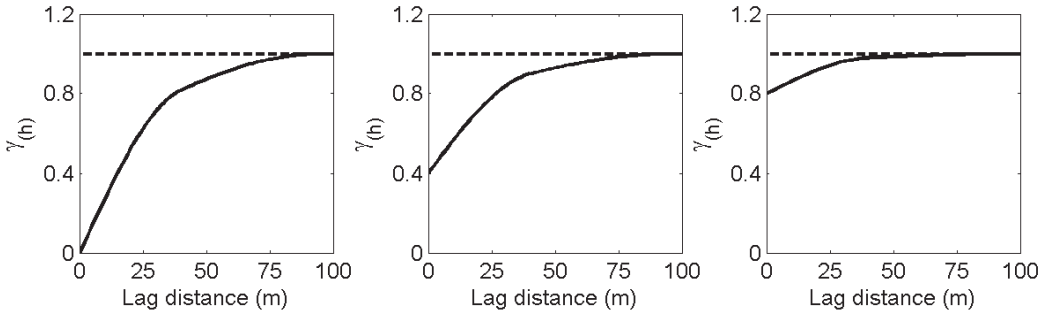

Figure 1.3: The breakdown in variogram structure with increasing capping thresholds.

Outlier values can have a strong effect on commonly used summary statistics. Non-robust statistics such as the mean and standard deviation are strongly effected by even a few outlier values. In a mining context, a single high assay value can significantly inflate the mean and variance of the reference distribution. In addition, the variogram is calculated with a squared statistic and is extremely sensitive to influence from outlier values.

If outlier data are left untreated, estimates may suffer from bias, which can lead to overestimation of the recoverable resources (Rossi and Deutsch, 2014). Figure 1.4 shows the influence that a single outlier value can have. In the left hand side of the diagram, an estimated model is created using a drill string with no outlier values. In the right hand side of the diagram, the same model is created using the same drill string but with a single, high outlier value. In this schematic example, a single outlier value nearly doubles the sample mean (Figure **??**c). If the outlier value represents a chance encounter, such as a drill string hitting a coarse gold nugget, the effect is smeared well beyond the true spatial range of the sample. The single outlier value increases the estimate for all blocks within the variogram range (Figure 1.4e). If the outlier value represents a spatially restricted population (such as a gold nugget) then it

is “smeared” throughout the blocks and can lead to overestimation of grade (Figure 1.4f).

Here, the term outlier will be used to refer to valid, assayed samples which are extreme manifestations of the inherent variability in the distribution, not samples which are a consequence of measurement or labratory error.

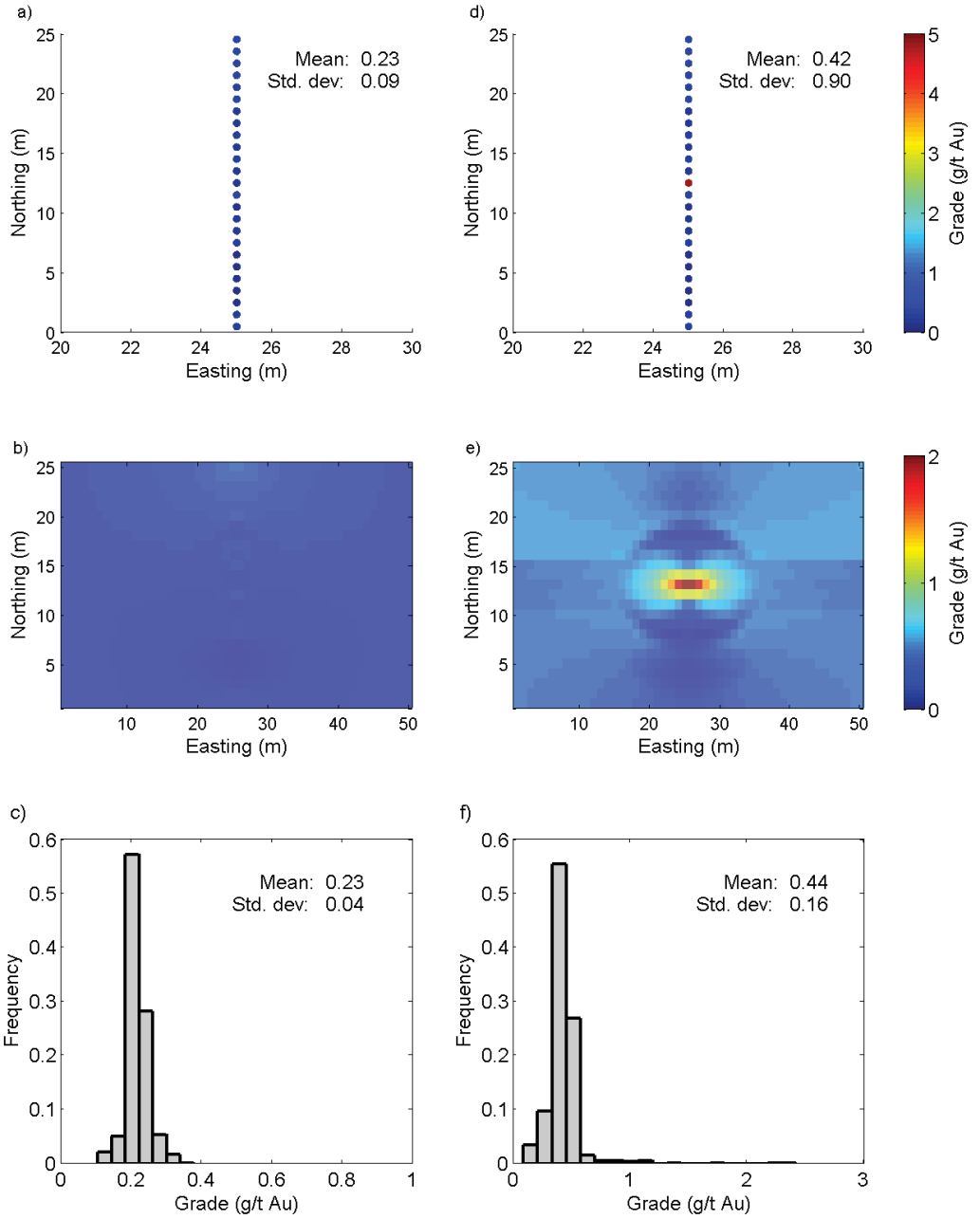

Figure 1.4: Left: a) drill string with no outlier values, b) estimated model from the drill string and c) distribution of block values. Right: d) drill string with a single outlier value, e) estimated model using the outlier value and f) distribution of block values.

1.1.3 Capping Values

Currently, the most common practice in the mining industry for dealing with outlier values during resource and reserve estimation is to cap or topcut outlier values to a predetermined threshold, then proceed with estimation (Rossi and Deutsch, 2014; Sinclair, 2002). To cap assays, all values greater than a threshold are set to equal that threshold. The choice of capping threshold varies among methods and among practitioners. Some simply regard the outlier values as erroneous and do not use them; however, Srivastava (2001) warns that, while these values should be checked, they should not be discarded as they may represent a previously unseen statistical population. Commonly, a fixed top cut value is chosen for the last few percentiles of the distribution and is used in the calculation of resouces (Dagbert, 2005; David, 1988; Krige, 1999). While capping outlier values may be less extreme than removing them all together, using capped data omits some of the information contained in the data and may invoke a bias in the results. In the case of precious metals deposits or other economically challenged deposits, overly aggressive capping may result in a sub-economic resource calculation (Rossi and Deutsch, 2014). Capping assay values is accepted in current international codes for mineral resources (JORC, 2012; SAMREC, 2007) but it is often difficult to select the 'correct' capping threshold.

In this thesis, no top cutting or capping of assay values is done; the data are presented in their original form.

1.1.4 Mixed Statistical Populations

Mineralizing systems responsible for the formation of precious metals deposits are complex and dynamic systems which evolve over time (Sillitoe, 2010). For example, a gold deposit might contain a pervasive, low-grade, background mineralization deposited by circulating meteroic fluids and a separate, vein-hosted, high-grade population caused by the boiling of rising mineralizing fluids. Parker (1991) recognizes that these dynamic geologic processes result in complex grade frequency distributions. His work involves separating the low-

and high-grade populations, modelling them separately then recombining them in a probabilistic framework. The method involves fitting the high-grade population with a log-normal model and produces unbiased results; although, he notes that errors are still large locally and large amounts of data are required to obtain a good model fit.

This work relies on the assumption that coarse gold mineralization occurs as a separate and distinct statistical population compared to the low-grade, background mineralization. For the majority of grade modelling, the low and high-grade populations are treated separately. The novel contribution here is that the high-grade population is modelled using a spatial point process.

1.2 Limitations of Traditional Geostatistics

Heavy-tailed distributions and high outlier values cause a number of problems in geostatistical modelling. Non-robust statistical measures, such as variogram calculation, are difficult because experimental variograms often appear very noisy. Outlier values can lead to bias and overestimation. A single high value, surrounded by low values, if left untreated will cause overestimation of nearby blocks. If the value is simply capped, the total metal content of nearby blocks could be reduced to the point where it is no longer classified as ore (Costa, 2003). Finally, accurately accounting for change of support is impaired when dealing with heavy-tailed distributions.

1.2.1 Variograms

The geologic processes that lead to the formation of a mineral deposit are not random because they follow physical laws. As such, these processes impart patterns of spatial correlation that must be understood. In geostatistics, the most common measure of spatial correlation is the variogram (Equation 1.2); the expected squared difference between two data values separated by a distance vector $\mathbf{h}$.

$$\gamma(\mathbf{h}) = E[Z(\mathbf{u}) - Z(\mathbf{u}+\mathbf{h})^2] \tag{1.2}$$

When calculating experimental variograms, care must be taken to ensure that data comes from the same statistical population. Geologically distinct or intermingled populations must be treated carefully because the variability between the two populations could vary significantly (Armstrong, 1984). Experimental variograms of heavy-tailed distributions are often noisy and display very little spatial structure; in the extreme case, the variogram is pure nugget effect (Figure 1.5a) (Krige and Margi, 1982). Highly variable minerals, such as gold and uranium, can have values which vary over several orders of magnitude, making it very difficult to get a reasonable estimate of the variogram.

Several robust solutions have been proposed as an alternative to the traditional variogram including the use of scale transformation (eg. by taking logarithms or normal scores) or by simply capping the extreme values. One of the most commonly used of these robust measures of spatial continutity is the pairwise relative variogram (Equation 1.3) (Srivastava and Parker, 1989). Similar to the traditional variogram, the pairwise relative variogram is a measure of the semivariance; however, it is normalized by the squared average of the tail and head values. This measure of spatial continuity is remarkably robust in the presence of outlier values (Figure 1.5b).

$$\gamma(\mathbf{h}) = \left\{ \frac{E[Z(\mathbf{u}) - Z(\mathbf{u}+\mathbf{h})^2]}{\left[\frac{E[Z(\mathbf{u}) - Z(\mathbf{u}+\mathbf{h})^2]}{2}\right]} \right\} \tag{1.3}$$

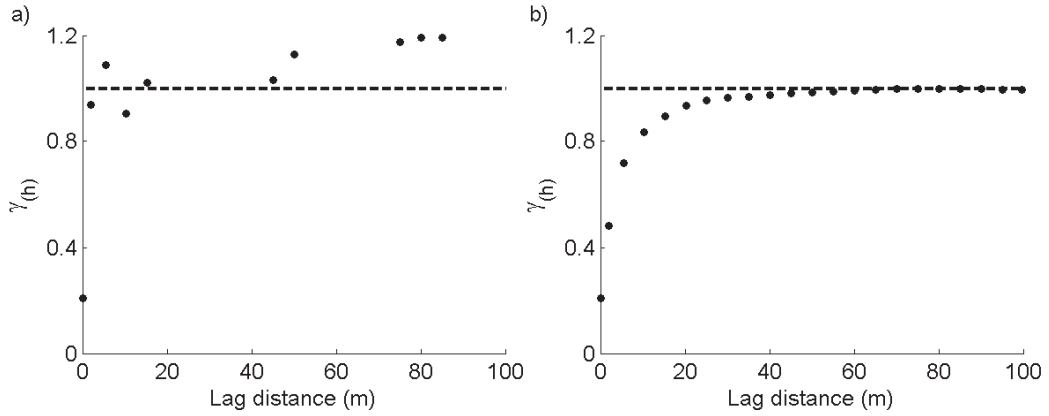

Figure 1.5: Experimental variograms calculated using a) standard method, and b) pairwise relative method

1.2.2 Estimation Methods

Most common modelling techniques such as simple kriging (SK), ordinary kriging (OK) and indicator kriging (IK) produce poor results in the presence of outliers. These techniques linearily average variables to produce a best estimate at a location in space. The smoothing effect of kriging can be seen in Figure 1.6. The standard deviation of the estimated distribution is much smaller than that of the original distribution. In addition, the smearing effect can be seen in the gridded estimates surrounding the outlier values.

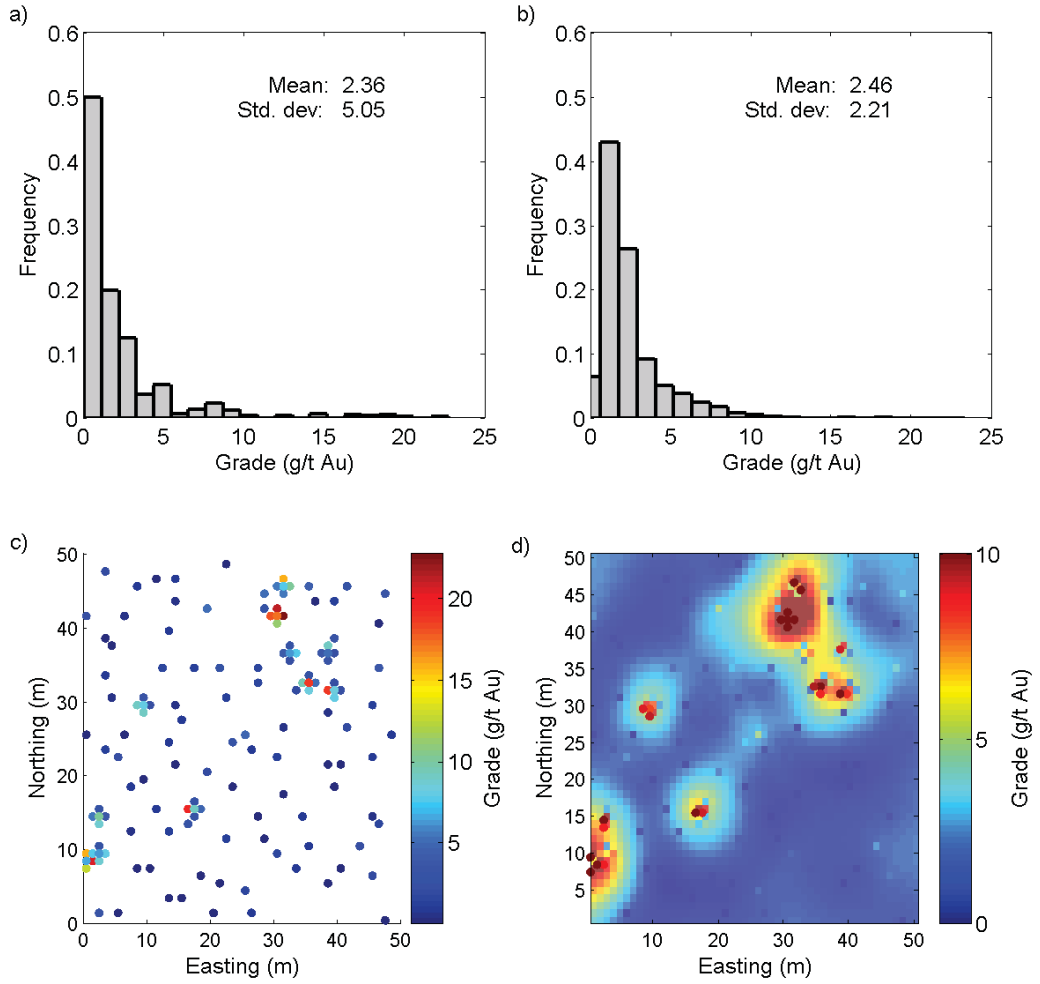

Figure 1.6: The smoothing effect of kriging. a) the original grade distribution, b) the estimated grade distribution, c) location map of original samples and d) gridded map of kriged estimates.

Due to the smoothing effect of all linear estimation techniques, kriging included, estimates offen suffer from conditional bias. Conditional bias occurs when the the expected value of the true grade, conditional on the estimated grade, is not equal to the estimated grade (McLennan and Deutsch, 2004). In high grade areas, the true grade is typically less than the estimated grade. In low grade areas, the estimated grade is typically higher than the true grade. In the case of heavy-tailed, precious metals deposits, this can have serious implications including overestimation of recoverable reserves. The penalty for over-estimating grade is typically more severe than under-estimating an area.

A number of solutions have been proposed to reduce the smoothing and conditional bias caused by heavy-tailed distributions: lognormal kriging (Journel, 1980); three-parameter lognormal kriging (Hawkins, 1979); indicator kriging (Journel, 1982); multi-Gaussian kriging (Verly, 1983); restricted kriging (Pan, 1994). Costa (2003) provides a thorough overview of the advantages and disadvantages of estimation techniques used to account for the effect of outliers when estimating a mineral resource. Lognormal kriging is shown to be sensitive to the sill of the variogram and deviations from the permanence of lognormality. Indicator kriging is commonly used to model heavy-tailed deposits; however, final estimates depend strongly on the choice of grade thresholds used for each indicator class as well as the extrapolation of the upper tail of the cumulative frequency distribution (CDF). Multi-Gaussian kriging assumes that the mean value of normal scores data is perfectly known.

1.3 Thesis Statement and Outline

The primary motivation of this thesis is two fold: i) to understand the limiations of traditional geostatistical methods in the context of heavy-tailed deposits, and ii) examine the use of a spatial point process to model grade as a discrete event. The described contributions should cumulatively achieve the objective of this dissertation, which is summarized in the following thesis statement.

The use of a spatial point process to model a coarse gold population as a discrete event reduces the influence of outlier values without resorting to subjective, ad-hoc manipulation of assays.

This thesis consists of seven chapters and one appendix. Chapter Two is a brief geologic review of gold mineralizing systems. The modelling techniques developed in this thesis are developed with coarse gold deposits in mind and, as such, it is important to understand the geologic background of these systems. The chapter covers gold mineralization, gold deposit types and briefly

summarizes the regional and local geologic setting of the case study area.

Chatper Three discusses spatial point processes and their application to grade modelling. A brief overview and literature review on spatial point processes is presented. Following that, the methodology is discussed and demonstrated on a small, synthetic dataset.

Chapter Four discusses discrete fracture networks and their application to modelling mineralized veins in a deposit. A short review of discrete fracture networks is presented before discussing the required input distributions necessary to generate a fracture model. Following that, the methodology is demonstrated schematically.

Chapter Five is a slight departure from grade modelling to discuss the automatic processing of drill core photos. Point location intersections and the thickness distribution of vein sets can be automatically measured from the core photo database and used directly as inputs to the discrete fracture network. An image processing algorithm is presented along with parameter optimization and a comparison to manually measured vein locations.

Chapter Six is a detailed case study which is divided into two parts. The first models a dense vein stockwork system with an identified coarse gold population using a spatial point process. The high-grade population is separated from the background mineralization and modelled as a discrete event using Poisson and Cox processes. Following that, a vein-hosted system is modelled using a discrete fracture network to sptially limit the extents of the discrete gold population.

Chapter Seven concludes the work and discusses the results and limitations of the proposed methodologies. Future work is set out.

The appendix contains descriptions of the programs used and their associated parameter files.

Chapter 2

Geologic Overview

The following section is a brief overview of the geologic processes that give rise to gold deposits. Gold mineralizing systems are covered first. Following that is an overview of the gold deposit types which are relevant to this work; free-gold deposits and vein-hosted deposits. Finally, regional- and property-scale geologic descriptions are provided for the case study area.

The research presented in this work focuses primarily on coarse gold deposits. In addition, the case studies presented in Chapter Six are done on an epithermal gold deposit in north-western British Columbia. The following chapter is intended to give a geological motivation for the techniques developed.

2.1 Epithermal Gold Mineralization

Mineralizing systems are complex combinations of multiple dynamic processes which may lead to an economic concentration of metal. The geologic processes responsible for epithermal gold deposits are partially responsible for the nature of the grade distribution. Sillitoe (2010) provides a thorough review of porphyry systems and their related mesothermal and epithermal systems. Of particular note is how these systems evolve both spatially and temporally. Initial magmatic fluids are oxidized, aqueous solutions saturated with metal and sulfur-complexes. As the fluids rise through the rock column, they undergo temperature, pressure and phase changes from a high-temperature, two phase hypersaline liquid and vapour to a lower temperature, single phase, moderately

saline fluid. The high-temperature solution is responsible for potassic alteration and early, overlying advanced argillic alteration with associated early-stage mineralization. Thermal pertubations and reinjection of fresh magmas result in an overlapping succession of alteration and mineralization imprints. In addition, this dynamic process leads to the remobilization and concentration of existing mineralization in the form of discrete nuggets of gold throughout the system.

2.2 Gold Deposit Types

Economic concentrations of gold occur across a wide variety of geologic settings. Classification of deposit types is difficult and an area of on-going work. Robert et al. (2007) provides a thorough work on the classification of gold deposit types. Their work identifies thirteen major gold deposit types belonging to three main types which correspond to the underlying genetic model responsible for forming the deposit. The three main types are: i) orogenic, ii) reduced intrusion-related, and iii) oxidized intrusion-related (Figure 2.1). This work is not concerned with the subtleties of classification. Instead, gold deposits will be classified based on the spatial nature gold mineralization. Two cases are considered here: i) free or nugget-y gold deposits, and ii) vein-hosted gold deposits.

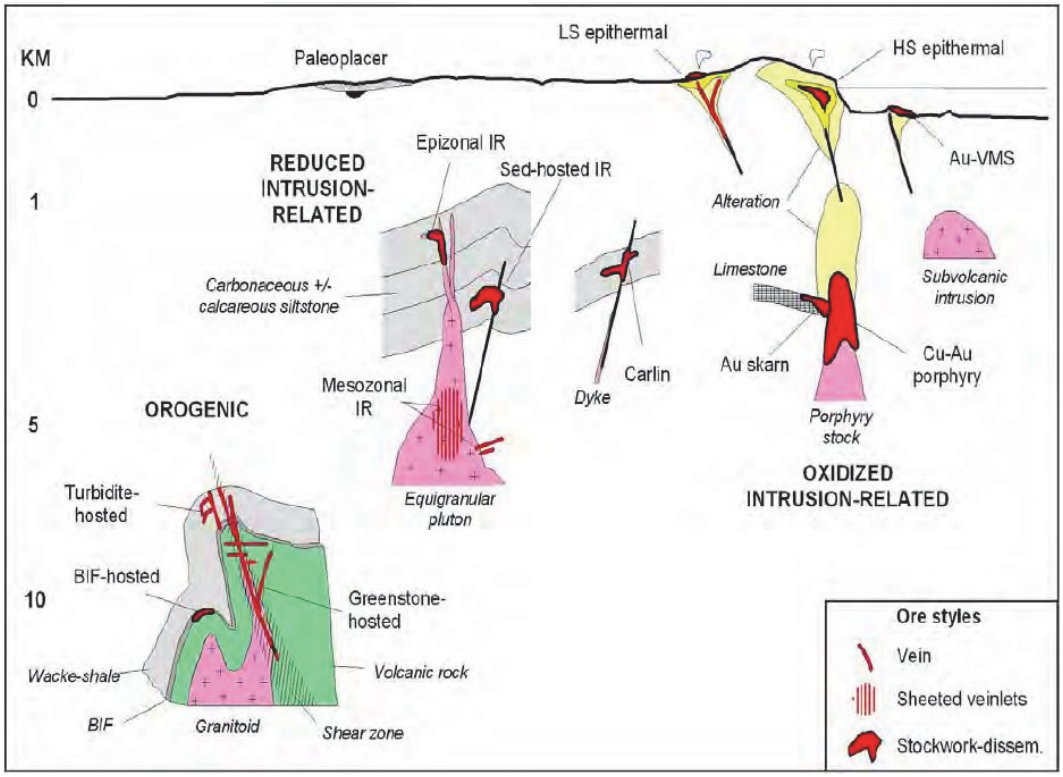

Figure 2.1: Schematic cross-section showing the three clans of gold deposits. Source: Robert et al. (2007)

Free-gold or nugget-y gold deposit types include placer deposits and modified paleo-placer deposits. These deposits are characterized by a coarse gold population with very little to no spatial structure. Also considered here are porphyry-style gold deposits. While porphyry-style deposits are technically vein-hosted, they are considered separately here because the density of the vein stockwork allows the mineralization to be thought of as random points in space with very little spatial structure. In this work, deposits of this type will employ a spatial point process to model the discrete nature of the high-grade gold population.

Vein-hosted gold deposits are the most common type of gold deposit with over one half of worldwide deposits having some form of vein-hosted gold mineralization (Poulsen, Robert and Dube, 2000). They are characterized by gold mineralization which is spatially restricted to narrow vein structures (Taylor, 2007). Often, vein-hosted deposits are characterized by nugget-y gold. Grade is localized and erratic within the veins (Johansen, 1998; Pelham, 1991,

1992). In this work, deposits of this type will use a discrete fracture network to spatially restrict the influence of the high-grade population.

2.3 Fractures, Veins and Veinlets

This work deals with the modelling of fracturs, veins and veinlets. Quartz veins are modelled as a discrete fracture network. Rock fractures are broadly divided into two classes: i) joints and ii) faults. The international Society of Rock Mechanics defines a joint as "a break of geological origin in the continuity of a block of rock occuring either single, or more frequently, in a set or system but not attended by a visible movement parallel to the surface of discontinuity". Faults are defined as "a fracture or fracture zone along which there has been displacement of the two sides relative to one another parallel to the fracture" (Mandl, 2005). While faults are important geological features in understanding mineralization, they are not suited to modelling with a DFN and are outside the scope of this work. In this work, the term fracture will refer to a set of breaks in a block of rock.

Fractures form in response to tectonic or hydrothermal stresses that exceed the strength of the rock. They form in predictable ways which can be modelled. Fractures tend to form in a regularly spaced and predictable manner. Fractures form first in the plane of parallel in the plane parallel to the maximum principal stress and second in the perpendicular plane of minimum stress. This leads to the development of sub-parallel sets of joints and conjugate sets at 90 degrees. Fracture spacing is regular because once a fracture is formed, stress is locally relieved so another fracture will not form immediately next to it (Mandl, 2005).

Geologic veins form in a variety of ways. This paper deals with veins formed by the hydrothermal fluids responsible for deposition of an epithermal gold deposit. These types of veins are recognized to be the consequence of the release of water from sedimentary-volcanic rock sequences as they pass through the orogenic cycle of burial, metamorphism and subsequent uplift and erosion, sometimes with evidence of associated magmatism. During metamorphism, devolatilization occurs on the scale of individual mineral grains, extracting

H_20, CO_2 and S. Gold readily enters this solution by complexing with reduced S and by H_2CO_3 acid buffering near the optimal fluid pH for gold solubility (Phillips and Powell, 2010). Average crustal abundance of gold is approximately 1 - 4 ppb. These systems are capable of enrichment to 10,000 times background concentration (Kerrich and Hodder, 1981).

This gold enriched fluid then migrates upwards from the source area to the sink area via shear zones and/or hydraulic fracture zones. Cox (2005) suggests that without tectonic strain, there is exceptionally low permeability in the rock mass. With relatively minor tectonic strain, permeability may rise sharply and allow fluid movement. As the gold-bearing hydrothermal fluid rises, gold deposition occurs from the breakdown of the complexes that carry it in solution. This occurs by two main processes: i) reaction of the fluid will surrounding wallrock and ii) boiling of the fluid as the pressure drops from decreasing lithostatic pressure. Evidence of deposition by wallrock interaction is given by the presence of alteration minerals such as muscovite and biotite. Evidence of boiling can often times been seen as 'vugs' or open spaces in the vein (Phillips and Powell, 2010).

In summary, fractures typically form in rock masses as a result from tectonic stresses. They form in predictable ways which can be modelled statistically. The hydrothermal fluid responsible for vein formation are the result of geologic processes which are independent of fracture formation; however, the these fluids exploit pre-existing weaknesses, such as fractures, in the rock mass. As a result, veins form from the repeated sealing and cracking of fractures by rising hydrothermal fluids. The term veinlet is often used to describe veins which are smaller than 10 mm in thickness. This distinction has no implications on this work. The term vein is used to describe both veins and veinlets.

2.4 Case Study Area

Two case studies are presented in this work. Data from both case studies comes from the Brucejack deposit in north-western British Columbia. The de-

posit is best described as a transitional to intermediate sulfidation epithermal stockwork vein system. A significant coarse gold population has been identified on the property. The information in this section has been excerpted and summarized from Board and McNaughton (2013).

2.4.1 Regional Geologic Setting

The Brucejack property is located in the western Stikinia terrane in the Intermontane Belt of the Canadian Cordillera. It is interpreted to be an intraoceanic island arc terrane which formed during the mid-Palaeozoic to Middle Jurassic time by accretion to the North American continental margin (Evenchick et al., 2007; Gagnon et al., 2012; Nelson and Colpron, 2007). Western Stikina was subsequently deformed by the accretion of the outboard Insular terranes during the early-Cretaceous period (Kirkham and Margolis, 1995). The volcano-sedimentary rocks and associated Early Jurassic plutons in Stikina host an exceptionally metal-rich assemblage. The area includes deposit types such as volcanogenic massive sulphide (VMS), alkaline porphyry copper-gold deposits and transitional epithermal intursion related precious metal deposits (Nelson, Colpron and Israel, 2013) (Figure 2.2).

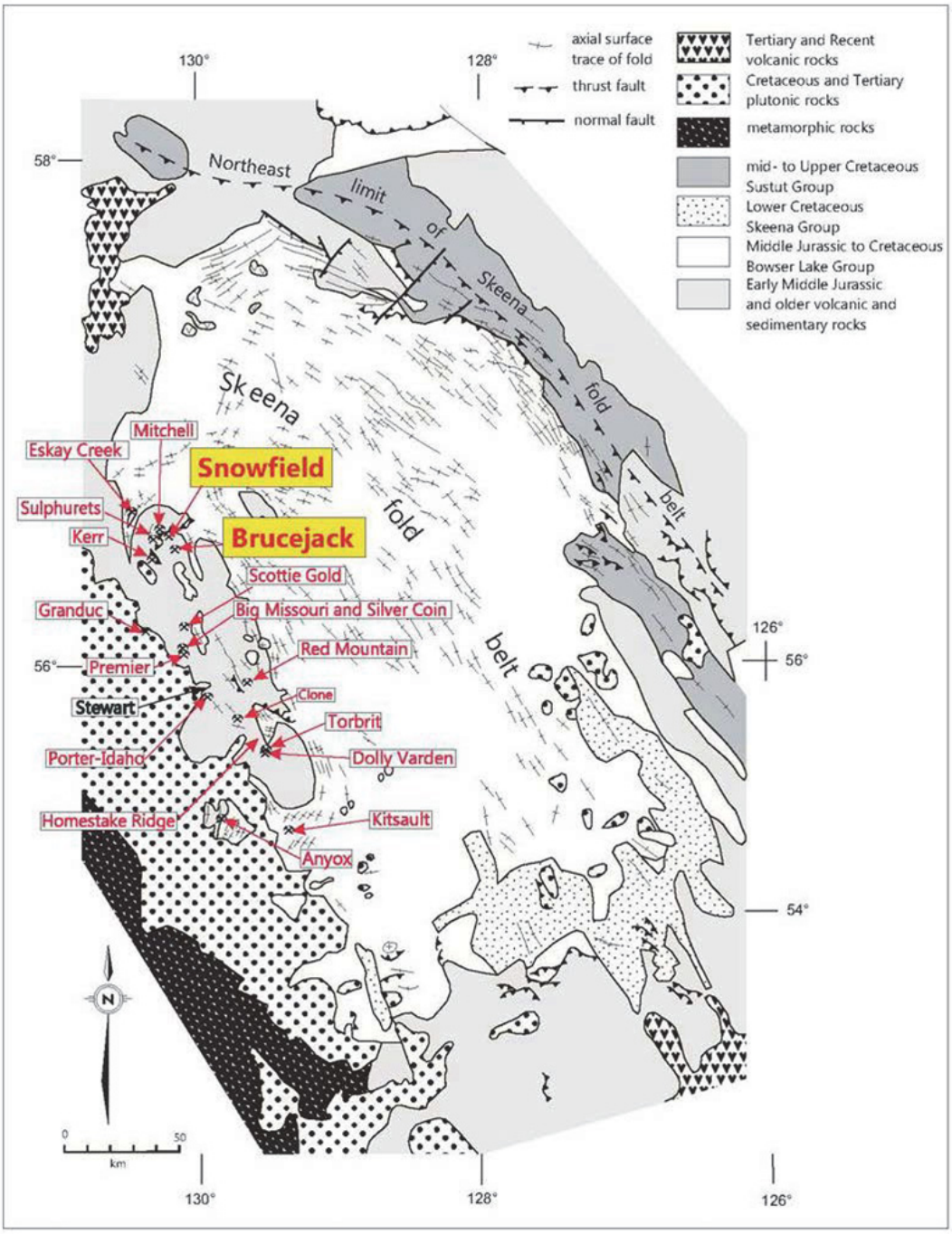

Figure 2.2: Location of the Brucejack deposit relative to the regional geologic setting. Figure includes past producing mines in the area. Source: Ghaffari et al. (2012)

Fold-and-thrust belt deformation in the Cretaceous period resulted in the formation of a major northwest trending structural culmination in western Stikina. This folding helped bring the older, mineralized volcano-sedimentary

rocks close to surface in this region. The Brucejack property is located on the eastern limb of this structural culmination. As a result, rocks on the property are strongly deformed and tilted and display a progressive younging to the east. The core of the deposit is comprised of volcanic, arc-related rocks of the Triassic Stuhini Group which are successively replaced outwards by volcanic rocks of the Lower Jurassic Hazelton Group and clastic, basin-fill sedimentary rocks of the Middle to Upper Jurassic Bowser Lake Group (Gagnon et al., 2012).

Immediately to the northwest of the Brucejack property are the plutonic rocks of the Mitchell Intrusions which host porphyry-style, copper-gold-molybdenum mineralization. The intrusive complexes are surrounded by large hydrothermal alteration halos. The inner core of the deposit is characterized by potassic alteration which is overprinted by propylitic and chlorite-sericite alteration. Associated quartz-sericite-pyrite alteration is widely developed in the region (Kirkham and Margolis, 1995). The multiple stages of overpinted alteration indicate a telescoping porphyry system (Sillitoe, 2010) (Figure 2.3).

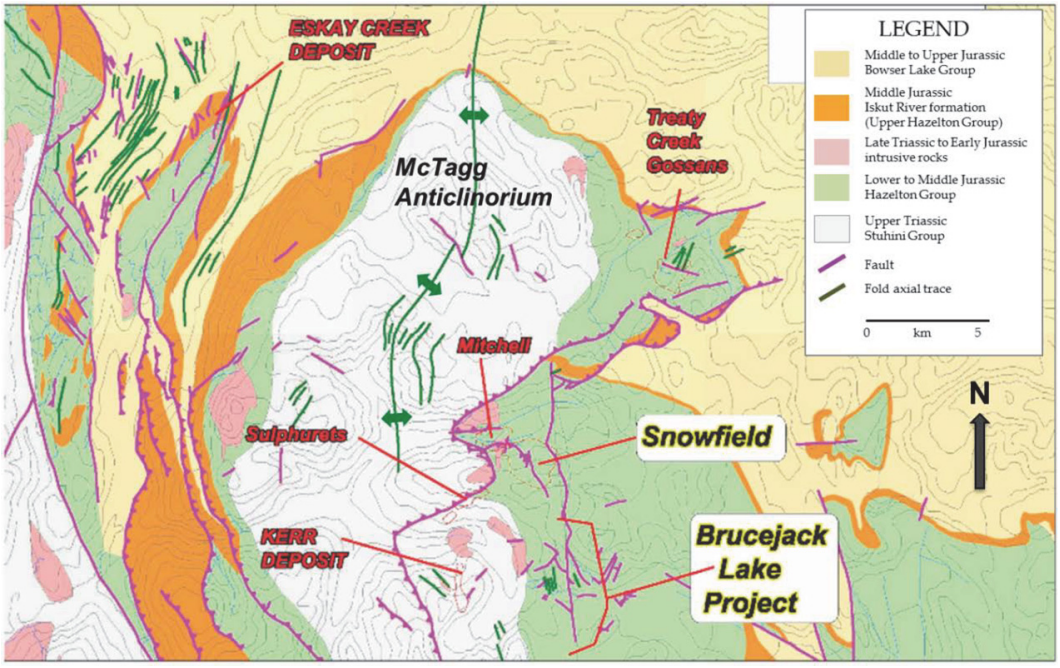

Figure 2.3: Location of the Brucejack deposit relative to the local area geology. Source: Pretium Resources

2.4.2 Deposit Geology

The information in this section has been excerpted and summarized from Jones (2013).

The Brucejack propertry is comprised of volcano-sedimentary rocks of the Lower Jurassic Hazelton Group which unconformably overie volcanic arc sedimentary rocks of the Upper Triassic Stuhini Group. Hazelton Group rocks on the property include volcanic flows, pyroclastic fragmental rocks, heterolithic volcanic pebble conglomerate, volcanic sandstone, siltstone and mudstone. The rocks are interpreted as having been deposited in an extensional setting. Alteration on the property is characterized by generally intense quartz-sericite-pyrite altered rocks that define a continous north-south band that measures approximately 5 km along strike and 0.5 km across strike (Figure 2.4).

Gold (and silver) mineralization on the property is hosted predominatly in sub-vertical veins and vein stockworks throughout the alteration band. The vein systems are relatively continuous along strike and are characterized by the presence of millimeter- to decimeter-scale transitional to epithermal veins of pyrite, quartz, quartz-carbonate and quartz-adularia. Mineralization recognized in different stockwork vein generations includes: pyrite, tetrahedrite, chalcopyrite, galena, sphalerite, arsenopyrite, pyrargyrite, native silver, native gold and electrum. Alteration, mineralization and vein texture variation suggest a spatial and/or temporal down-temperature gradient towards the east. Several mineralized zones have been identified on the property. The case studies in this work focus on the two largest mineralized zones: The VOK Zone and the West Zone (Figure 2.5).

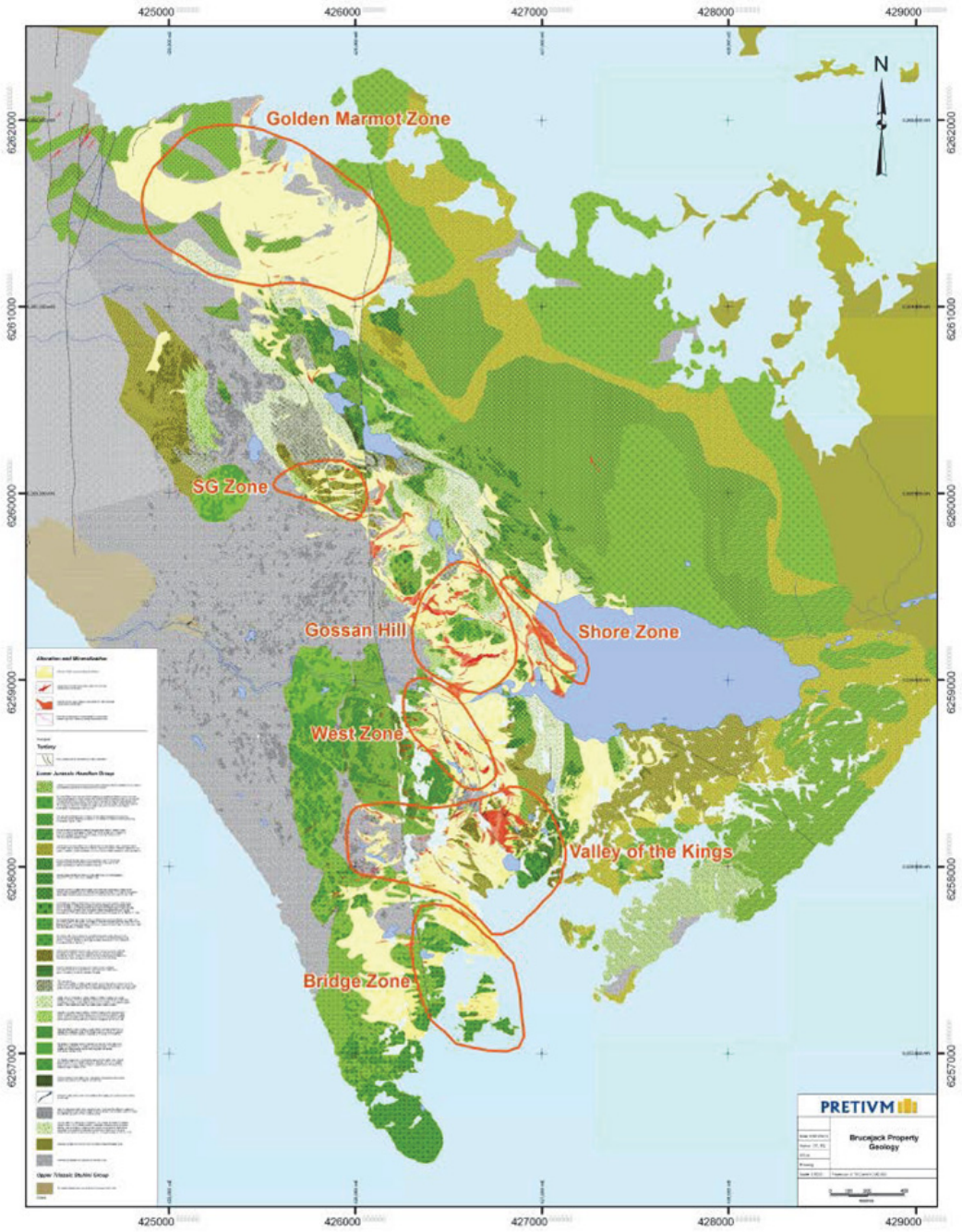

Figure 2.4: Geologic map of the Brucejack property showing the defined mineralized zones. Source: Pretium Resources

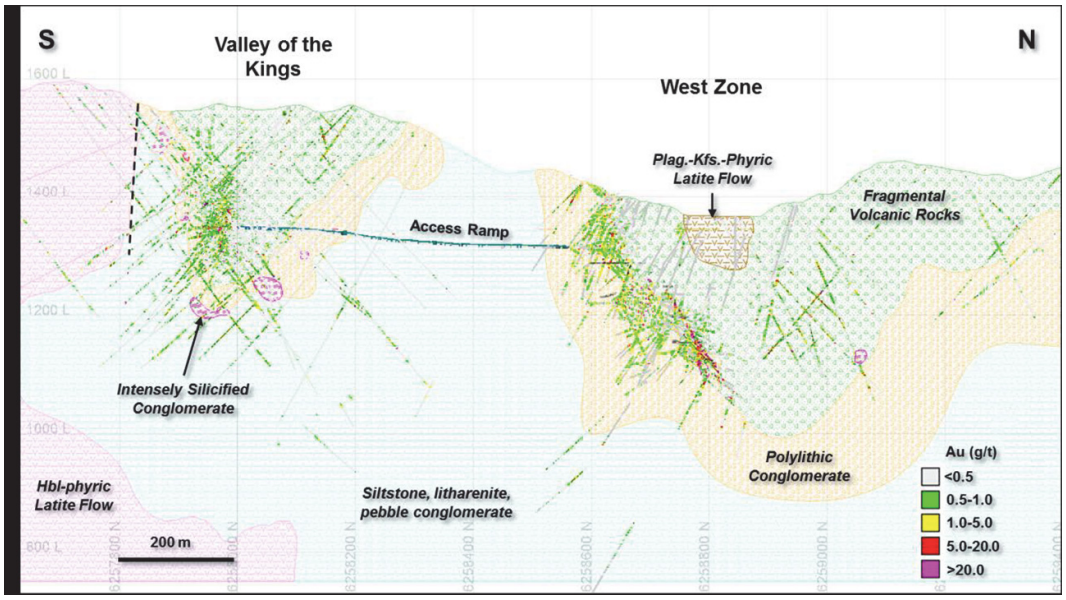

Figure 2.5: General cross section (south-north) showing two mineralized zones. Source: Pretium Resources

Chapter 3

Spatial Point Processes

3.1 Background

In statistics and probability theory, point processes are used to model discrete events or points in time. A spatial point process (SPP) is the multidimensional generalization of a point process and extends the counting process to an interval of space. In a mining context, the discrete events represent gold nuggets within a block or selective mining unit (SMU) and are modelled as a Poisson process. Kroese and Botev (2013) provides an overview of spatial process generation. The relavant aspects are summarized here.

Let E represent a subset of $\mathbb{R}^d$ and let ε be the collection of sets on E. Let X represent a random counting measure $X(A), A \in \varepsilon$, defined by:

$$X(A) = \sum_{i=1}^{n} I_{\{X_i \in A\}}, A \in \varepsilon \tag{3.1}$$

The mean measure, denoted by $\mu(A) = E\left\{X(A)\right\}, A \in \varepsilon$, has a density, λ, referred to as the intensity.

$$\mu(A) = E\left\{X(A)\right\} = \int_A \lambda(\mathbf{u})\, du \tag{3.2}$$

A random counting variable, X, is said to be a Poisson random variable with mean measure, μ, if two conditions are met. First, the sets $A_1, ...A_N \in \varepsilon$ and the random variables $X(A_1, ...X(A_N))$ are independent. Second, any set $A \in \varepsilon$ of the random variable $X(A)$ has a Poisson distribution given by:

$$Prob(X = x) = \frac{\lambda^k e^{-\lambda}}{k!} \tag{3.3}$$

If the intensity function is constant, the Poisson process is said to be homogeneous. If the intensity function varies over A, it is said to be non-homogeneous. An extension of this is the Cox process, where the intensity function itself is also a random function (Cox, 1955). The Cox process is best described as a doubly stochastic Poisson process where the intensity parameter, (λ), is itself a stochastic process. In a mining context, suppose that the propensity for the coarse grade population to exist is a random intensity function, Λ. The random variable X is a Cox process driven by the random intensity function Λ if the conditional point process X is a Poisson process with intensity function λ. The random intensity function is described by:

$$\Lambda(A) = \int_A \lambda(\mathbf{u})\, du, A \in \varepsilon \tag{3.4}$$

Thus in this case, the Cox process is carried out in two steps: First, simulate a realization of $\lambda = \lambda(x), x \in \epsilon$ of the random intensity function Λ; second, given that $\Lambda = \lambda$, simulate X as a non-homogeneous Poisson process with intensity λ.

The Poisson and Cox processes have been used extensively in modelling diamond deposits. Rombouts (1995, 2003) discusses the problems associated with sampling diamonds. Because the exploration samples are small compared to the SMU, a Poisson or chance effect is introduced when hitting (or not hitting) a diamond. This leads to an overrepresentation of barren areas of the deposit. He identifies that the chance effect appears in the variogram as an increased nugget effect. Lantuejoul and Millad (2008) explore modelling a diamond deposit using a Cox process which draws from a size frequency distribution. Kleingeld et al. (1996) explore modelling deposits where mineralization takes place as discrete particles with a conditionally simulated Cox process. The authors discuss placer deposits with a known size frequency distribution and model the random intensity function based on geological traps for the particles. They do not consider in-situ deposits where size and intensity

parameters must be inferred from core data. Monestiez et al. (2006) discuss the difficulty in obtaining accurate maps of relative abundance on the basis of spatially heterogeneous sampling efforts and infrequent encounters with a sparse population. Although this work uses an ecological example, many corollaries can be drawn to the mining industry. Sampling (drill holes) are spatially heterogeneous and there is a random element involved when hitting or missing a coarse gold nugget.

3.2 Methodology

The proposed methodology is demonstrated on a small, synthetic example to describe the steps involved. First, the samples are separated into high- and low-grade populations, and the low-grade population is modelled with standard geostatistical techniques, such as kriging. This methodology also requires a high-grade population that exhibits very little spatial structure (high nugget effect). In this case, the high-grade population approximates random points in space and is modelled independently using a Poisson or Cox process. The high-grade assays are fit with a particle size distribution (PSD) from which the point process will draw.

Specifically, the steps involved are:

Step 1: Determine the high-grade threshold and separate the populations into high and low grades.

Step 2: Estimate or simulate the background mineralization with OK.

Step 3: Model the intensity map for the Poisson (estimation) or Cox (simulation) process.

Step 4: Model the PSD and apply the Poisson or Cox process to locate the gold nuggets.

Step 5: Combine the low- and high-grade models to obtain the final grade model.

The details of each step are described below. The synthetic example demonstrates only the Poisson process. The case study considers both the Poisson and Cox processes.

3.2.1 Step 1: Separate statistical populations

The data for the synthetic example is obtained by simulating the drilling of an exhaustive dataset with properties mimicking an epithermal gold deposit; the synthetic deposit contains a significant coarse gold population. The exhaustive dataset is created on a 1m x 1m x 1m grid by combining a realization of low-grade, background mineralization (generated using Sequential Gaussian Simulation [SGS]) with a realization of discrete particles (generated using a Poisson process with a known intensity map). Simulated drilling is conducted on a regularly spaced grid (Figure 3.1). The grade distribution collected from drilling the synthetic dataset exhibits a heavy-tailed, skewed distribution commonly seen in precious metal deposits (Figure 3.2). Of the 2,800 samples collected, 132 samples (or 4.94%) are classified as high grade, using a cutoff threshold of 5.0 g/t Au. Note that the selection of a threshold is an important practical consideration but here the focus is on the demonstration of the methodology.

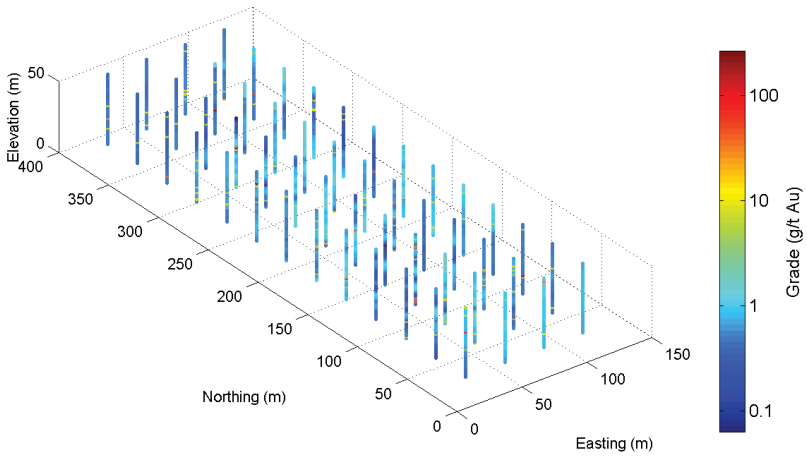

Figure 3.1: Drill assay locations collected by drilling the synthetic truth model.

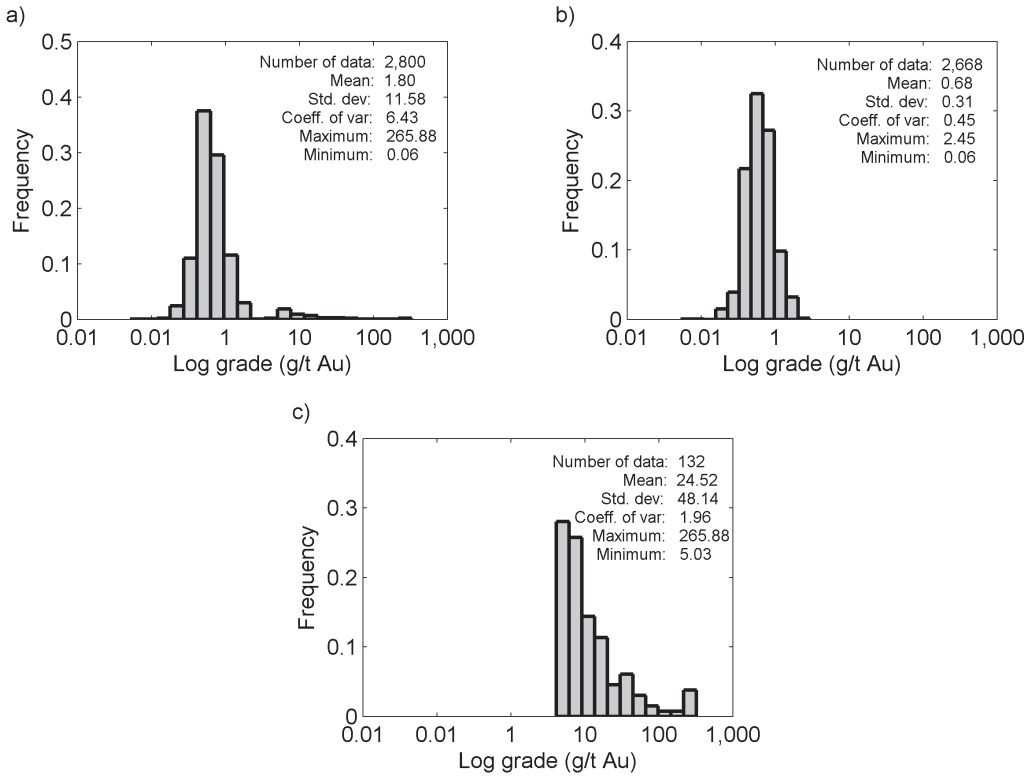

Figure 3.2: Histograms showing the a) entire, b) low-grade only, and c) high-grade only grade distributions of the synthetic model.

3.2.2 Step 2: Model the low grade

The background mineralization is estimated from the low-grade samples of the synthetic dataset using OK with no top cut (Figure 3.3) and the variogram model (Figure 3.4). The assumption inherent in independently modelling the high- and low-grade populations is that the low-grade mineralization is pervasive and each block of the model comprises an (unknown) proportion of high- and low-grade mineralization.

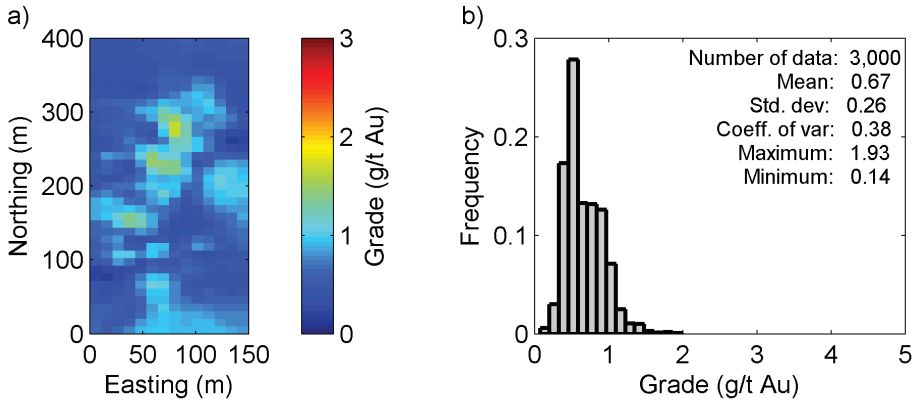

Figure 3.3: OK model of the a) background mineralization, and b) associated histogram.

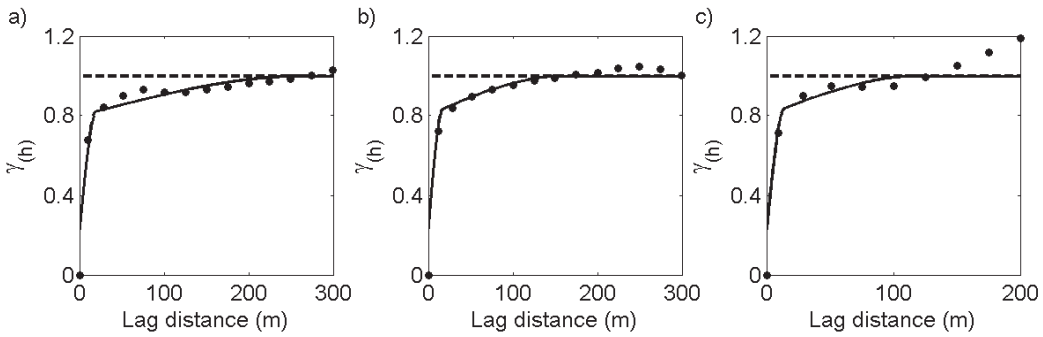

Figure 3.4: a) Major, b) minor, and c) vertical semivariogram models used to estimate the low-grade population. The major direction of continuity is 240 degrees.

3.2.3 Step 3: Model the intensity map

An input map of intensity, $\lambda(\mathbf{u})$, is required to build the conditional Poisson distribution at each location. Given the highly selective nature of sampling coarse gold deposits and the fact that drilling campaigns often over sample high-grade zones, the high-grade assays are unreliable for directly modelling the intensity function. Instead, the local proportion of high-grade assays relative to all samples is used. Each assay location is visited and a local search, using the variogram range of the high-grade population, counts the proportion of coarse gold samples in the local area. This new proportion information is used as conditioning data and the intensity, λ, can be estimated or simulated

in the domain (Figure 3.5). A non-homogeneous Poisson process uses a single value of λ at each location (Figure 3.5) but a Cox process requires multiple realizations of the intensity map. In this case, multiple realizations of the intensity map can be generated using SGS.

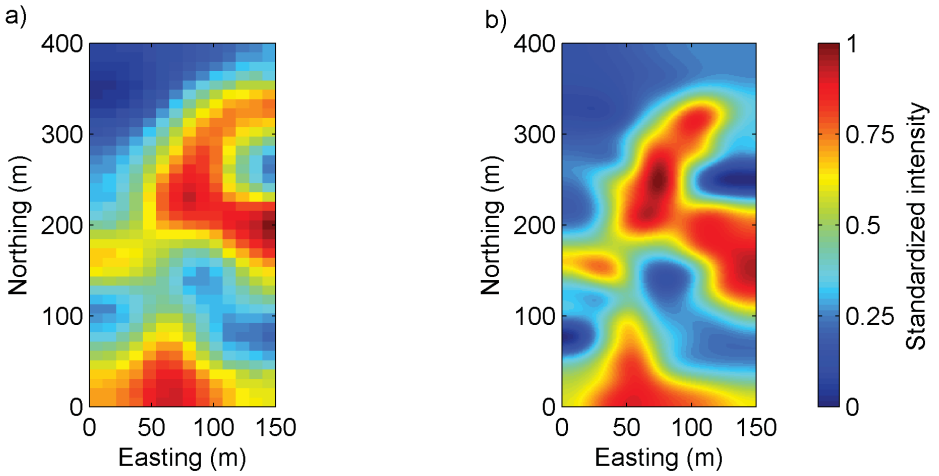

Figure 3.5: a) estimated intensity map for the synthetic example using OK and b) the true intensity map

3.2.4 Step 4: Model the particle size distribution (PSD)

A conditional Poisson distribution is built at each location in space with the intensity map as an input. For each realization, a random number is drawn from the Poisson distribution that determines the number of particles in each block. Once the nuggets are located in the model, the quantity of gold in each nugget is required to obtain the final grade model. The coarse gold population is fit with a PSD, which could come from a number of sources. If available, metallurgical data should be used. These are not available for the synthetic example or the case study: Each nugget is assumed to be a sphere of pure gold and the particle size that would generate a sample of that grade is calculated for each high-grade sample in the drill holes. For a nugget simulated in the Poisson or Cox process, a particle size is drawn randomly from the PSD of the high-grade assays. A single global PSD is assumed, but it would be trivial

to modify the methodology to use locally varying PSDs if that information is available. For this synthetic example, the PSD of the case study is used. The grade of each block can be calculated knowing the location and size of each particle in the model (Figure 3.6).

The Poisson process is continued until there are sufficient particles simulated to match the target mean of the high-grade population (this is equivalent to scaling the intensity map by a constant). The nature of drilling coarse gold nuggets results in extremely inflated assay values when a nugget is encountered and barren results when that nugget is missed. With the background mineralization removed, the global average of the high-grade population can be determined with traditional declustering or debiasing techniques. In this small synthetic example, more than 71 million discrete points were simulated to obtain the desired high-grade global mean (Figure 3.6). The program `SPPSIM` is provided for this step of the methodology. Details of `SPPSIM` are discussed in the appendix of this work.

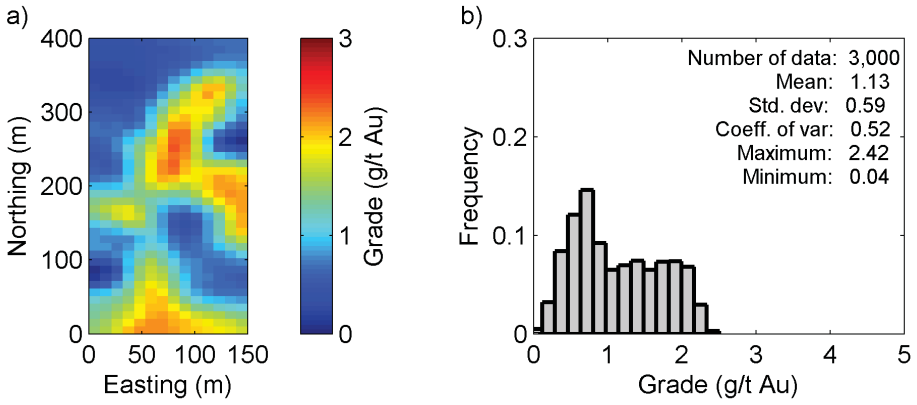

Figure 3.6: a) Grade map from the Poisson process and b) associated block-scale histogram.

3.2.5 Step 5: Combine low and high grade

Once both populations have been estimated, the two models can be combined into a final grade model. The mean of the data is reproduced but the maximum value is significantly lower than that of the input data because this is the distribution of blocks (Figure 3.7), rather than point data (Figure 3.2). The

modelled grade distribution is compared to the true grade distribution (from the exhaustive synthetic dataset) in Figure 3.8.

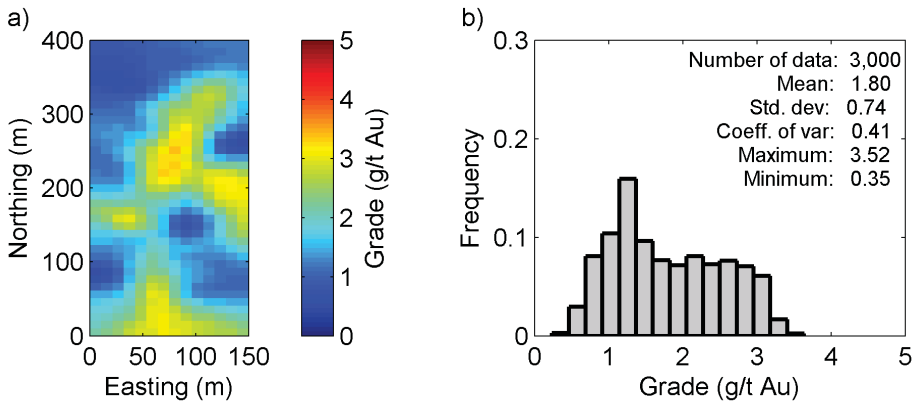

Figure 3.7: a) Grade map from the combined low- and high-grade models, and b) associated block-scale histogram.

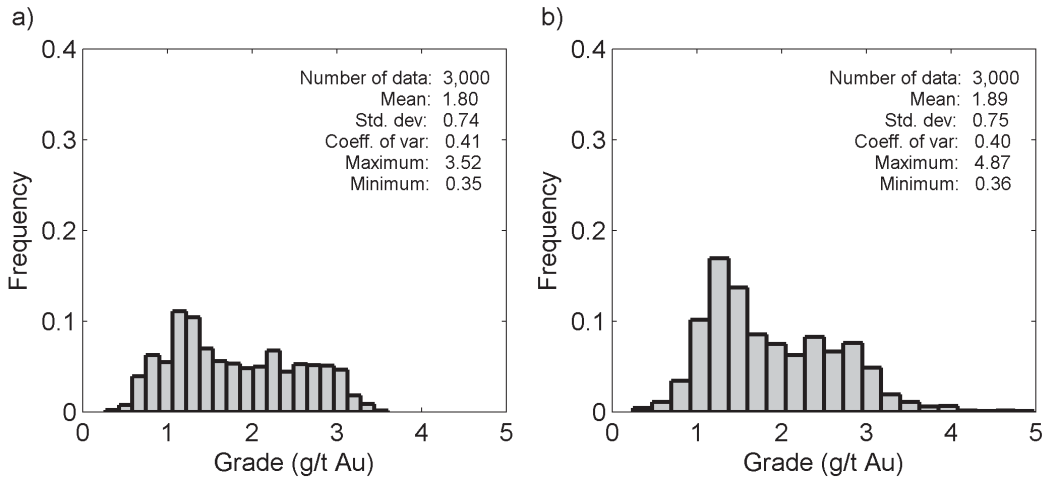

Figure 3.8: Histograms showing the a) modelled grade distribution and b) the true grade distribution

3.3 Discussion

The proposed workflow uses a spatial point process to model the coarse gold population as a series of discrete points with a known volume. This methodology assumes that the true, under-lying coarse gold population exhibits very

little spatial structure and can reasonably modelled as random points in space. The spatial structure that is present in the coarse-gold population is captured in the input intensity map. The goal of this workflow is to limit the influence of high-grade assays by spatially restricting them to a simulated discrete volume of gold.

When applying this methodology to a real dataset, care must be taken to ensure that a coarse gold population exists and there is an accompanying lack of spatial structure. The variogram of the high-grade population should exhibit a very high nugget effect. A spatial point process simulates points randomly within each modelling cell so care must be taken to ensure that this assumption is realistic. The nature of gold mineralization should be visually confirmed in drill core.

Chapter 4

Discrete Fracture Networks

4.1 Background

The assumption that coarse gold mineralization takes place as random points in space is unrealistic. In some geological settings, mineralization is spatially restricted to vein structures. Veins are planar structures which form in fractured rock from hydrothemal fluids which are often associated with mineralizing systems. Fracture formation, and associated vein formation, are the result of large, regional-scale tectonic stresses and they form in predicatable ways which can be modelled.

A common technique for modelling fractures is to simulate them as a Discrete Fracture Network (DFN). In a DFN, fracture centroids are simulated randomly conditional to an input intensity map of vein density using a Poisson process. Other fracture statistics, such as bearing, dip, length, height, thickness etc are randomly drawn from user-defined input distributions. In this chapter, a methodology is presented to model mineralized veins using a DFN.

4.1.1 Natural fractures

Observations of natural fractures indicate that it is possible to describe fracture attributes with a variety of statistical distributions. Fracture pole trend and pole dip tend to follow normal distributions. Fracture length, height and thickness tend to follow a log-normal distribution (Niven, 2010). Other studies have suggested that fracture properties are best described with a power-law

or fractal distribution (Bonnet et al., 2001). Work by Narr, Schechter and Thompson (2006) suggests that fracture spacing is log-normally distributed.

Johnston and McCaffrey (1996) and Roberts et al. (1999) suggest that there is an empirical relationship between vein length and vein thickness using fractal statistics. Their work noted that veins appear to have consistent axial ratios in parallel sections and are approximate ellipsoids in shape. Veins grow concurrently in thickness and length. They examined five vein sets across a variety of tectonic regimes and geologic settings and concluded that vein thickness can be used to approximate vein length. Renard et al. (2005) examined the statistical properties of three different vein sets, including a mineralized vein set from the Val d'Or region in the Abitibi region of Canada. They concluded that all three datasets show similar statistical properties. He concludes that the thickness of fractures is best described by an exponential distribution.

4.2 Discrete Fracture Network Simulation Algorithm

In order to generate a DFN, a number of input distributions are required. A gridded map of vein density controls the number of simulated fractures. Fracture density can be estimated from drill core data. The fracture orientation is described by the trend and plunge of a pole normal to the plane of the fracture. This information comes from surface and underground mapping of veins. Vein thickness can be measured directly from drill core data. Vein length and height can be measured by surface or underground mapping, or infered from a relationship to vein thickness.

DFNs created solely using a Poisson process do not have realistic spatial properties. These codes simulate fracture orientation independent of location resulting in fracture sets which do not honor spatial correlation (Cacas, Daniel and Letouzey, 2001; Gauthier, Garcia and Daniel, 2002; Hitchmough et al., 2007). Fractures generated solely with a Poisson process result in two undesirable features. First, due to the random nature of a Poisson process, it is possible generate fractures which are extremely close or extremely far apart; they do not honor the correct spatial relationship. Natural fractures form as

a response to stress in the rock. Once a fracture is formed, stress is locally relieved and another fracture will not form immediately next to it. Second, if the distribution of fracture orientation is wide enough, it is possible for two fractures in the same set to cross at extremely low angles by random chance. Fractures form first in the plane parallel to the maximum principal stress and second in the perpendicular plane of minimum stress. This leads to the development of sub-parallel sets of joints and conjugate sets at 90 degrees. Fractures intersecting at extremely low angles are unrealistic (Mandl, 2005).

The DFNSIM algorithm of Niven (2010) aims to correct these problems by simulating a pool of fractures three to five times greater than necessary then iteratively removing them until the target statistics are reached. An overview of the steps used in the algorithm is provided. For further details, see Niven (2010).

Step 1: Visit a grid cell and randomly simulate fracture centroids

Step 2: For each simulated centroid, draw fracture statistics randomly from user-defined distributions

Step 3: Repeat until the entire pool of fractures is simulated (target number * multiplication factor)

Step 4: The target number of fractures are actived and the fracture spacing and intersection angle are calculated as an objective function

Step 5: A fracture from the entire pool is selected and its activation state is changed. If the objective function decreases, that change is kept.

Step 6: The process is repeated until the desired number of iterations are complete.

As a result of the optimization process, the DFNSIM algorithm simulates a fracture network which better honors the spatial correlation of natural fracture spacing as well as prevents unrealistic fracture intersection angles.

4.3 Methodology

The proposed methodology is demonstrated on a small, synthetic example to describe the steps involved. The data for the synthetic example were obtained by simulating the drilling of an exhaustive model with properties mimicking a vein-hosted gold deposit. The sampling was conducted on a regular grid (Figure 4.1). The exhaustive dataset is created on a 1 m x 1 m x 1 m grid by combining a realization of low-grade, background mineralization (generated with SGS) with a realization of high-grade mineralization. The high-grade model is created by simulating a DFN using a known intensity function. The grade distribution collected from drilling the synthetic data exhibits a heavy-tailed, skewed distribution commonly seen in precious metals deposits (Figure 4.2).

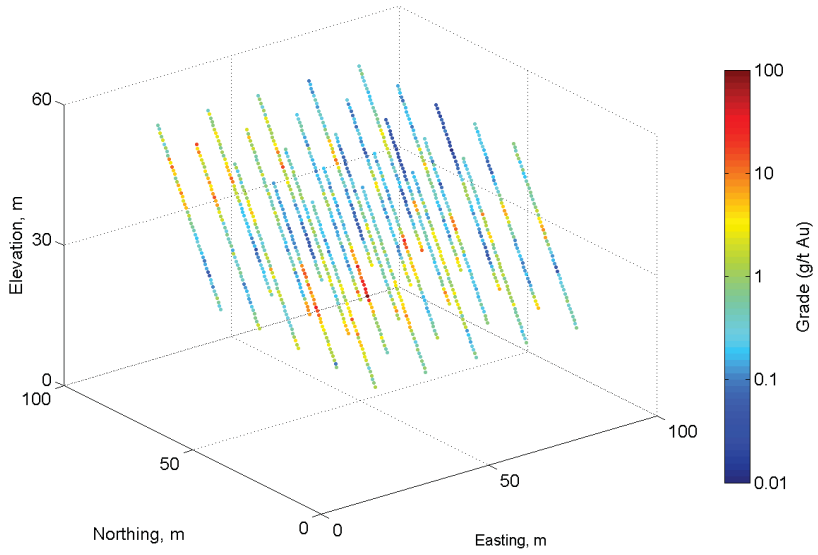

Figure 4.1: Drill assay locations collected by drilling the synthetic truth model

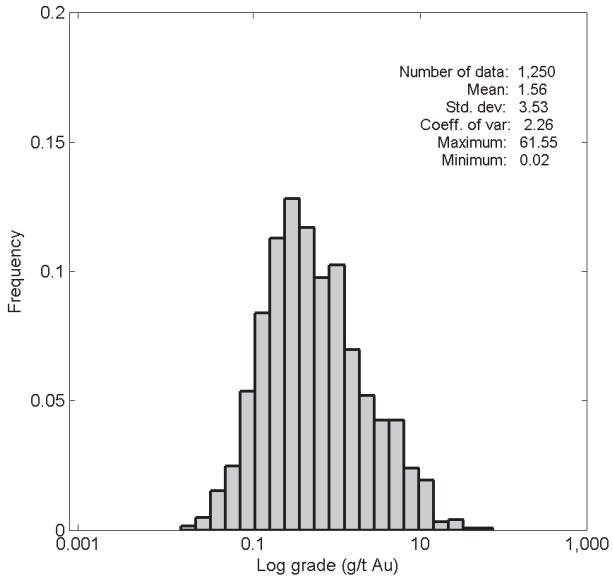

Figure 4.2: Histogram showing the gold grade distribution of samples from simulated drilling

The statistical populations are separated and treated separately. The high-grade population is modelled with a DFN; so the required input distributions must be inferred prior to generating the DFN. Specifically, the steps involved are:

Step 1: Separate statistical populations and model background mineralization separately

Step 2: Infer DFN input distributions and vein intensity from drill core data plus external sources

Step 3: Model the intensity map of vein density

Step 4: Simulate mineralized veins using the DFNSIM program

Step 5: Combine background mineralization and mineralized veins into final grade model

The details of each step are described below.

4.3.1 Step 1: Model low grade

This methodology relies on the assumption that background mineralization and coarse gold mineralization belong to separate statistical populations. The background mineralization is estimated from the low-grade samples of the dataset using standard geostatistical techniques such as OK or SGS. The assumption inherent in independently modelling the high- and low-grade populations is that the low-grade mineralization is pervasive and each block of the model comprises an (unknown) proportion of high- and low-grade mineralization (Figure 4.3).

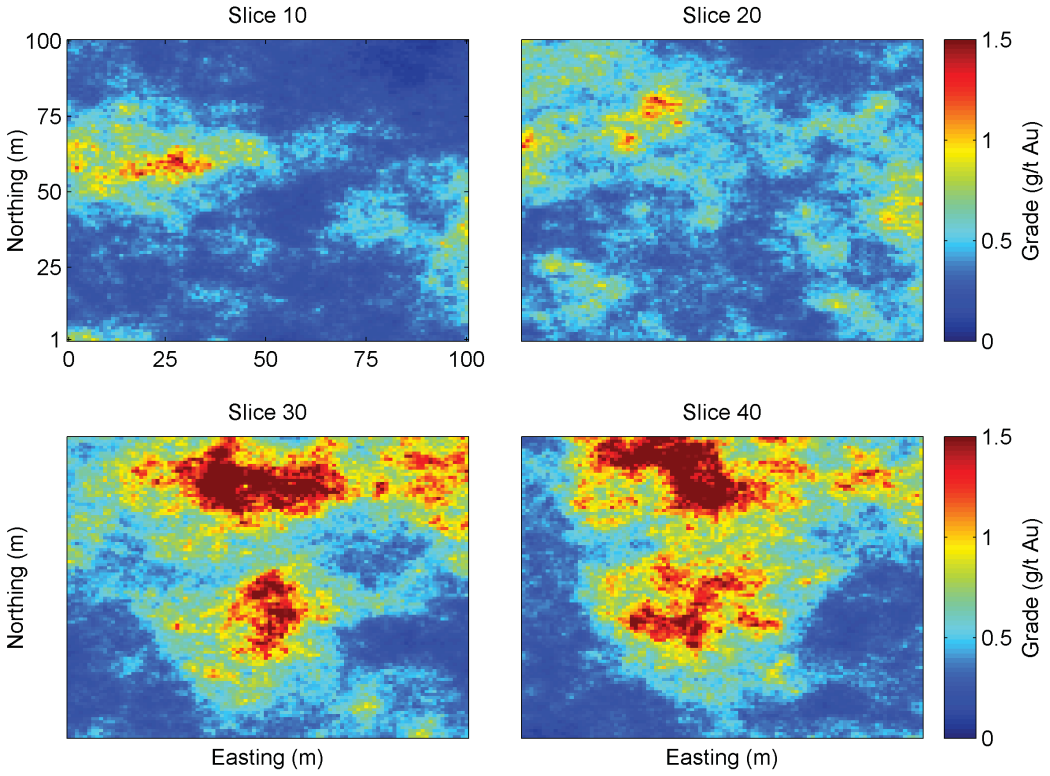

Figure 4.3: Slices through the block model of low-grade, background mineralization

4.3.2 Step 2: Infer DFN distributions

The next step in modelling a DFN is obtaining the representative distributions of input statistics from which DFNSIM (2010) will draw while creating fractures. The program DFNSIM (Niven, 2010) requires input distributions for vein orientation (pole trend and pole plunge), vein size (length, height and

thickness), and vein density. Vein orientation and thickness can be measured reliably from drill core. Vein size cannot be measured from core data and requires information from geological mapping or expert knowledge. Three dimensional vein density cannot be measured from core data; however, it can be infered from the one dimensional fracture spacing which can be measured from core.

In order to condition the fracture model, the point location interesection for each drilled vein is needed. These are obtained from drill core logs and drill core photos. The vein thickness distribution also comes from core logging. The pole trend and pole plunge of the veins are recorded from a mixture of underground and surface mapping and fit with a Normal distribution. Since the length and width of veins cannot be measured directly, the fractal relationship suggested by Johnston and McCaffrey (1996) is used:

$$L = k * T^a \tag{4.1}$$

The length of veins, L, (measured in meters) is related to thickness, T, (measured in mm) by the constant, k, and the exponent, a. The k and a parameters were borrowed from an epithermal gold deposit cited in Johnston and McCaffrey (1996) which is similar to the study area of interest. For the synthetic example, known input distributions of vein statistics are used. They are summarized in table 4.1 below.

Table 4.1: Summary of DFN input distributions

Statistic	Thickness (mm)	Length (m)	Trend (deg)	Plunge (deg)
Distribution	Log-Normal	Fractal	Normal	Normal
Mean	6.17	1.27	000	90
Variance	103.9	1.91	3.0	3.0
Max	368.4	20.6	-	-

4.3.3 Step 3: Model intensity

The DFNSIM program uses a Poisson process to generate the initial fracture network and requires an intensity model, $\lambda(\mathbf{u})$, of fracture count at each location. Fracture intensity is often measured in one dimension along a borehole;

however, to simulate a DFN, a three dimensional count of fractures is needed. There is a multivariate relationship between the number of intersections along a borehole, the length of fractures and the 3D density of fractures (Dershowitz and Herda, 1992; Zhang and Einstein, 2000).

To convert between 1D fracture count and 3D fracture density, a conversion factor is needed. This can be obtained either analytically or through simulation. Analytical methods include Terzaghi-weighting (Terzhagi, 1965) or Wang approximation (Wang, 2005) but they are difficult to implement. This work uses Monte Carlo Simulation (MCS) to solve for the conversion factor. Niven (2010) presents a methodology and a series of programs necessary for computing the conversion. In summary:

Step 1: Define a small DFN with known input distributions

Step 2: Simulate a series of these DFNs with incrementing 3D vein density and fracture size

Step 3: Project a series of scan lines, normal to the mean vein orientation, through each DFN (Figure 4.4a)

Step 4: Measure the average vein spacing along each scan line and compile the results

Figure 4.4b shows a contour plot with the results of the simulation study. The color values indicate average 1D spacing. To create conditioning data, the average fracture spacing is measured along intervals down each drill hole and then compared with the contour map to obtain a value of 3D fracture density. Intensity over the domain can then be estimated with OK or simulated using SGS. Figure 4.5 shows the distribution of intensity values from simulated drilling as well as variogram models showing the range of continuity.

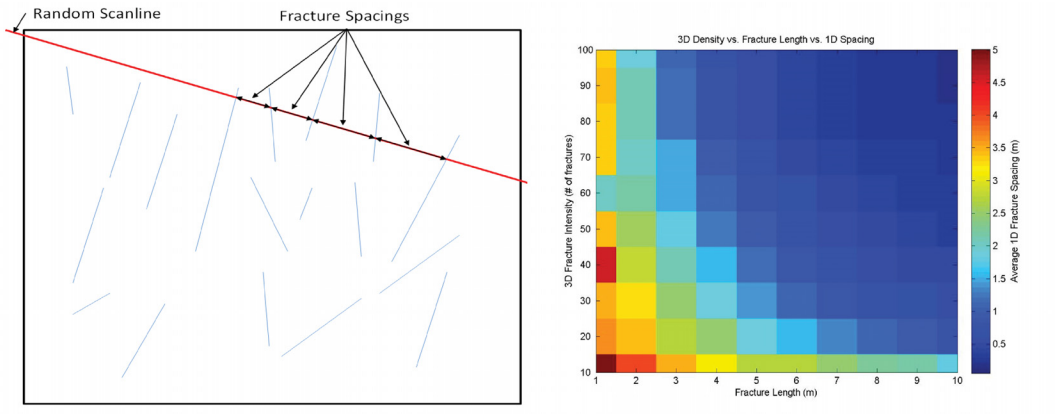

Figure 4.4: a) Random scan line through fracture model and measured spacing; b) contour map showing the relationship between lineal spacing and 3D density

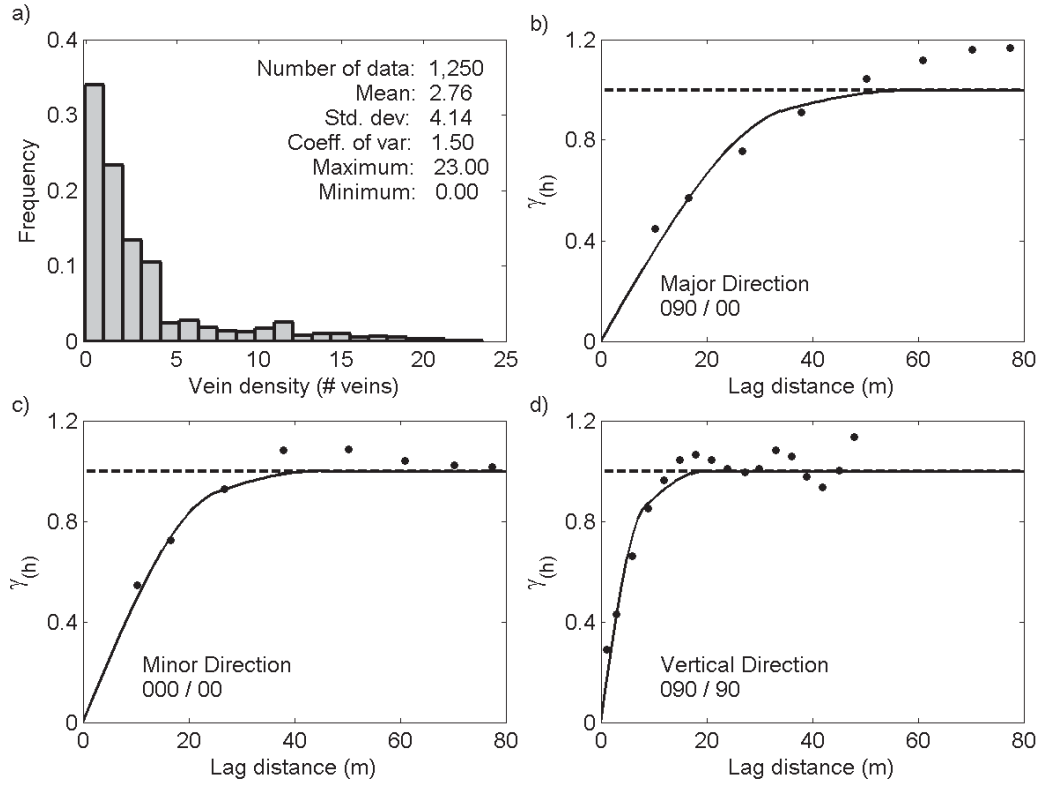

Figure 4.5: a) Distribution of 3D vein density after conversion and variograms showing a) the major direction of continuity, b) the minor direction of continuity, and c) the vertical direction of continuity

4.3.4 Step 4: Simulate mineralized veins

To simulate mineralized veins, the input distributions of vein orientation, vein size and vein thickness are used in DFNSIM. Additionally, an initial DFN

comprised of the intersection point locations from drillhole data are also input. The intensity map of 3D vein density is the final input into the program. DFNSIM generates realizations of DFNs consisting of vein centroids, with corresponding pole trend, pole plunge, thickness, height and length. A realization of a simulated DFN is shown in Figure 4.6. For purposes of plotting, the DFN has been thinned by a factor of 100.

With a conditioned map of mineralized veins in the study area, the high-grade gold population is simulated within the vein structures in two ways:

i) each vein is given a constant gold grade and total gold is proportional to the volume of the vein

ii) gold is simulated as discrete particles (with a spatial point process) which are spatially restricted to the veins (Figure 4.7)

In this example, the first case is used to simulate the high-grade population; mineralization is assumed to be constant across each vein. The input intensity function (which controls the number of simulated veins) is scaled until the desired mean of the population is reached. Figure 4.8 shows slices through the model of high-grade mineralization. The program `DFNSPP` is provided for this section of the methodology. Details of `DFNSPP` are discussed in the appendix of this work.

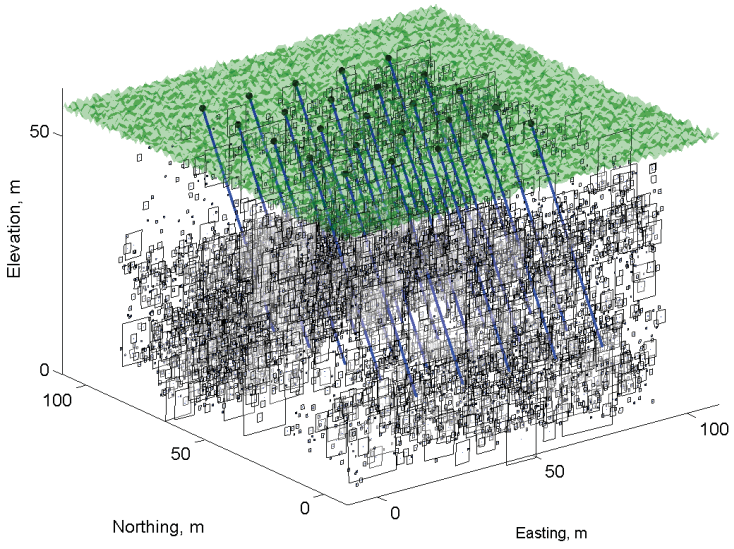

Figure 4.6: A realization of quartz veins simulated as a DFN

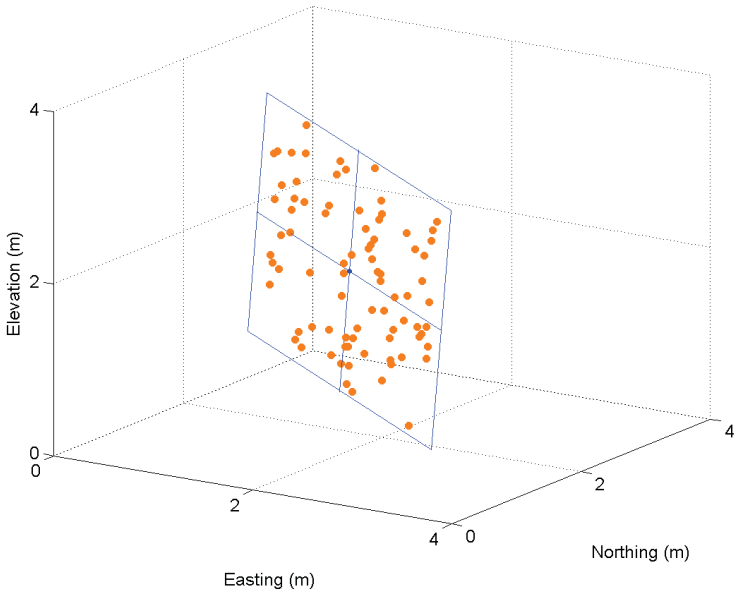

Figure 4.7: Schematic showing discrete particles of gold (generated with a spatial point process) placed along the plane of a simulated vein

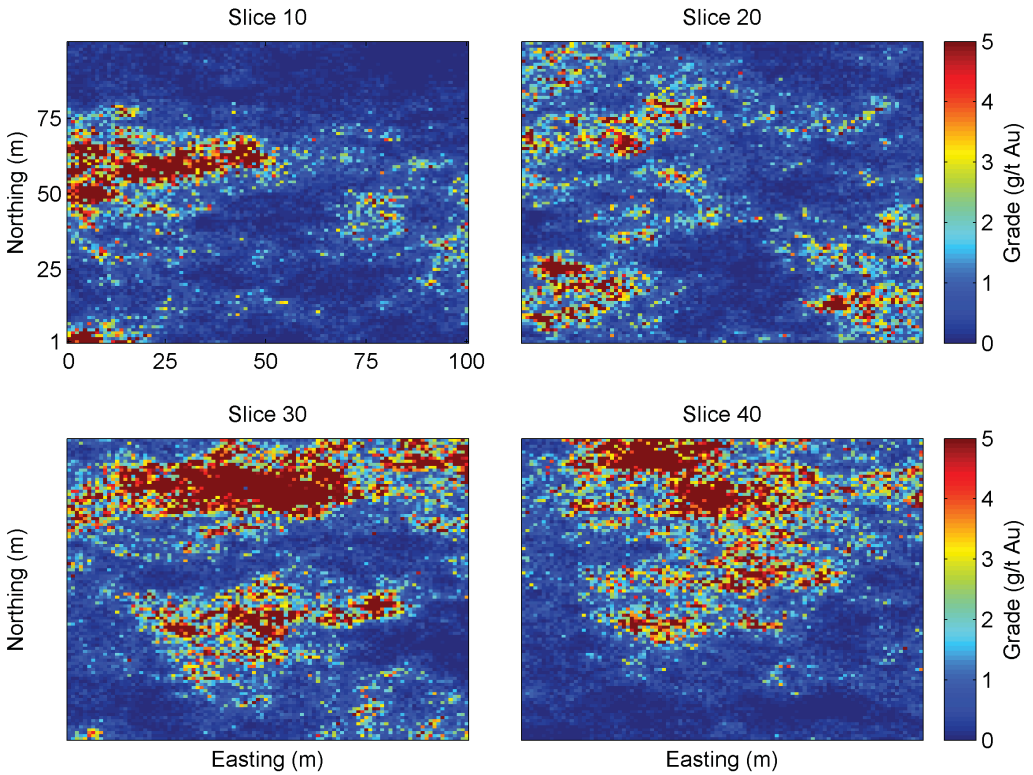

Figure 4.8: Slices through the model of high-grade mineralization

4.3.5 Step 5: Combine low- and high-grade models

Once both populations have been estimated, the two models can be combined into a final grade model. The background mineralization is pervasive whereas the high-grade population is spatially restricted to simulated veins. Slices through the final model of grade are presented in Figure 4.9.

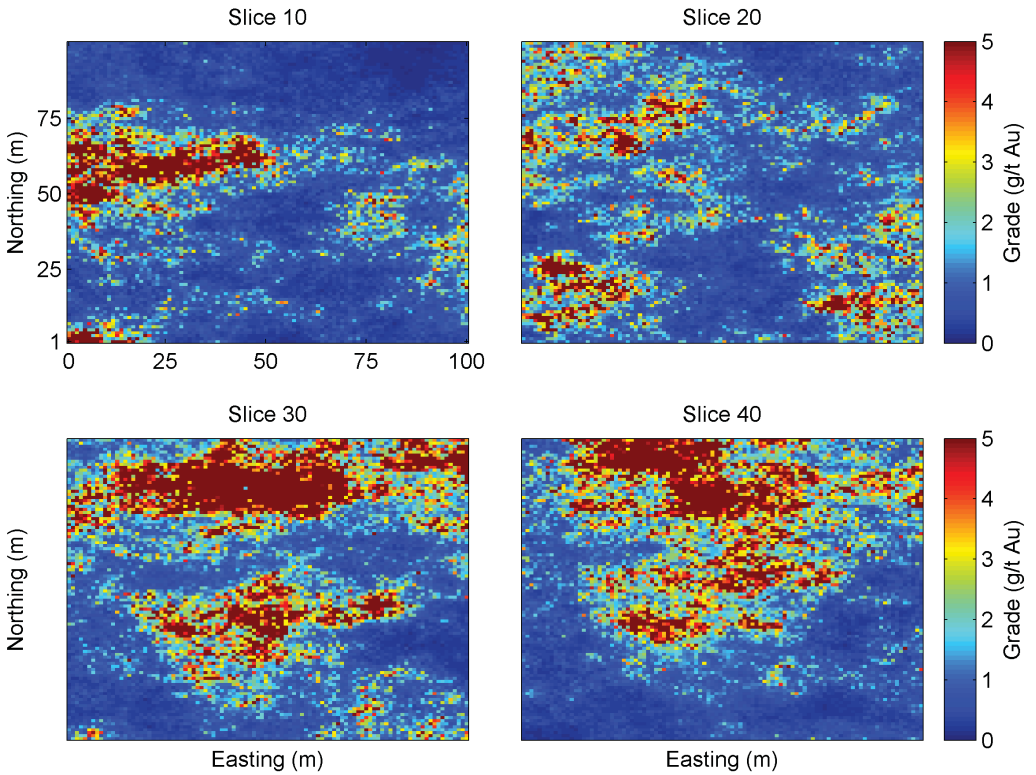

Figure 4.9: Slices through the final grade model after combining low- and high-grade models

4.4 Discussion

The proposed workflow uses a discrete fracture network to model mineralized veins in the study area of interest. Vein-hosted gold deposits are characterized by a coarse gold population which is spatially restricted to veins. The goal of this workflow is to prevent smearing of grade by only allowing coarse gold mineralization to exist where a vein exists. It is assumed that all veins are mineralized in this synthetic example. It is also assumed that gold grade is, on average, constant across each vein. These assumptions lead to the high-grade population being proportional to the volume of simulated veins.

In order to test the methodology, a synthetic dataset was created using completely known properties. One of the assumptions used in creating this synthetic dataset is that, on average, grade is constant across each vein. There is a constant proportion of gold to vein across each vein. This assumption is not realistic in practice; however, for the purposes of demonstrating the

methodology, it is justified. In reality, grade is highly variable throughout each vein because gold mineralization is localized, erratic and nugget-y. It is suggested to model grade within each simulated vein using a spatial point process. This will honor the inherent variability of gold mineralization within quartz veins.

When applying this methodology to a real dataset, care must be taken to ensure that the assumptions are realistic. As best as possible, only mineralized veins should be modelled. In addition, if mineralization takes place as discrete particles within the vein, a spatial point process should be used to model grade within the veins rather than making the assumption that grade is constant across each vein.

Chapter 5

Image Processing

5.1 Background

As discussed in Chapter Four, modelling quartz veins as a DFN requires a number of input distributions and conditioning data. Some of these distributions can be measured from drill core data. Specifically, the point location intersections, apparent dip and vein thickness can be measured from drill core data. During an exploration drill campaign, veins may not be logged in sufficient detail to generate the conditioning data and input distributions needed to model veins with a DFN.

Drill core is typically logged by geologists during the exploration phase of a project. Often, vein density is too great to log each vein individually. In some cases, it is determined at the time of logging that only a rough estimation of vein density is needed. It is typically not possible to go back and re-log all veins from historic drill core because of the time and cost constraints. An automatic method of processing core photos for information is desirable because it saves time and helps remove the inherent subjectiveness from having multiple people collecting the data.

This chapter presents a practical application of existing work in image processing. Plataniotis and Venetsanopoulos (2000) provide an excellent overview of color image processing and image segmentation.

5.1.1 Core Photo Dataset

The dataset for this workflow is a set of core photos from an underground drill program. There are photos of 408 drill holes with a total of over four thousand photos. The photos were taken with a Canon G12 camera on a tripod with flourescent overhead lighting. A typical photo comprises three boxes of HQ core, approximately 10 meters of down hole depth. The core is sprayed with water before being photographed to enhance contrast.

The quality of the photos is highly variable because several people were involved in collection of the photos. Lighting conditions vary across the photos and not all photos are taken exactly square. This has implications for the image processing workflow. A pre-processing step can help eliminate some of these irregularities by making the photos as similar as possible. Examples of core photos can be seen in Figure 5.1.

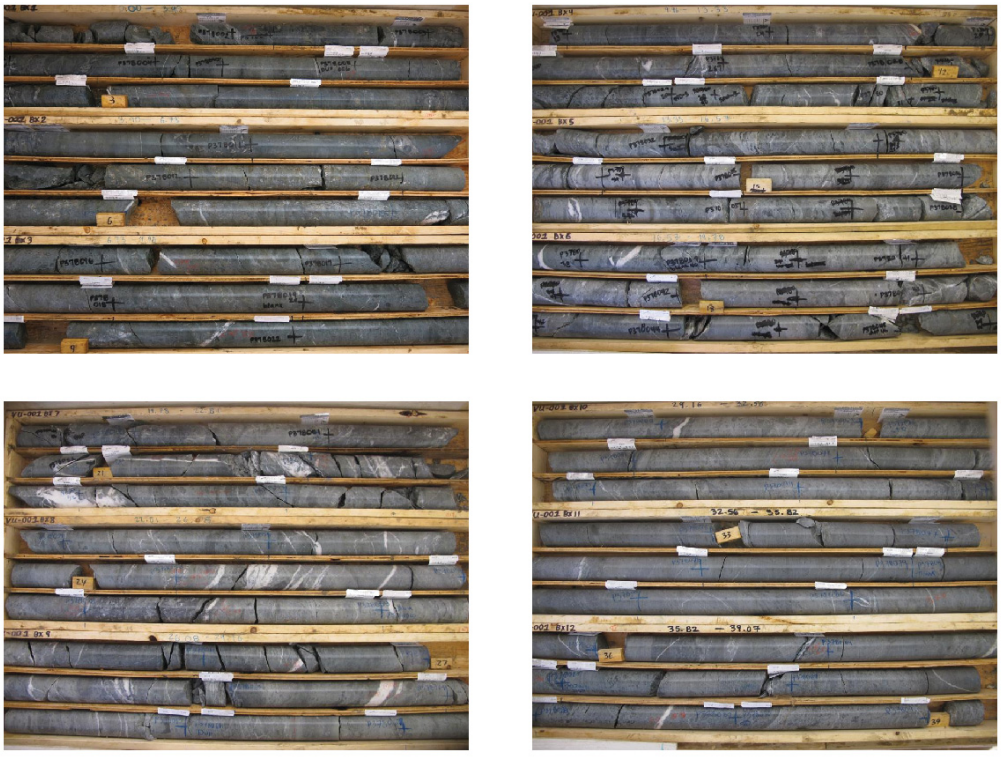

Figure 5.1: Example photos of drill core from the photo library. Photos are in their original form.

5.1.2 Challenges

There are a number of challenges to implementing an automatic image processing workflow. First, the quality of core photos is highly variable. In blurry photos, edges and features are not well defined. If the photos are rotated, it is more difficult to automatically locate features because it is assumed that rows of core occur as straight lines across the photo. Second, there can be very poor separation between color groups in the photos. Figure 5.2a shows an example core photo with each pixel mapped in three different color spaces: b) red-green-blue (RGB), c) lightness-scaled (Lab) and d) hue-saturation-value (HSV). In the core photo, there appears to be fairly well defined color groups (grey stone and brown core box); however, when looking at the distribution of pixels in each color space, there are no clearly defined boundaries between color groups. Instead, grey pixels of stone gradually change into brown pixels of core box. This makes defining the boundary of each color class difficult.

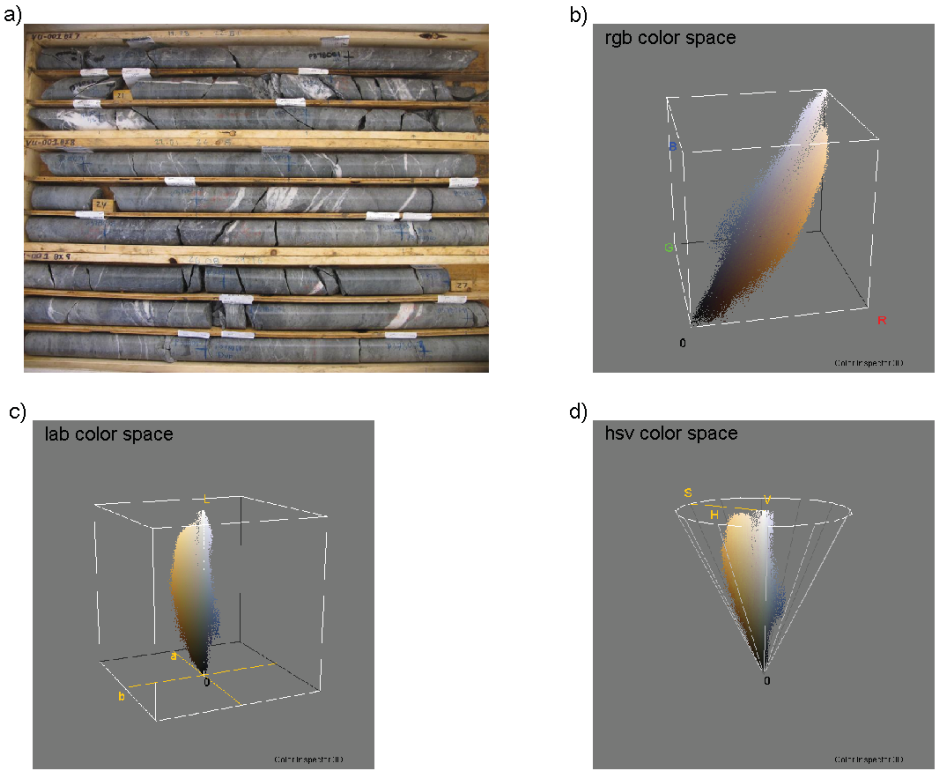

Figure 5.2: a) example core photo and the distribution of pixels in three different colour spaces: b) RGB, c) Lab and d) HSV.

5.2 Methodology

Each image is processed in a number of steps in order to isolate the individual veins from the overall photo. The pixels of rock must be isolated from background pixels such as the core box, floor, sample tags etc. Each set of photos provides a downhole record of the geology with each subsequent row of core being deeper down the drill hole. Individual rows of core must be identified in order to provide down hole depth information. Finally, the individual veins must be isolated from the rows of drill core. Specifically, the steps involved in the image processing workflow are the following:

Step 1: Pre-process core photos

Step 2: Isolate pixels of stone from boxes and other photo features

Step 3: Identify rows and create a row mask

Step 4: Isolate veins from core

Step 5: Locate and count veins

Step 6: Optimize parameters to obtain best fit

The details of each step are described below.

5.2.1 Step 1: Pre-Process core photos

The first step in the image processing workflow is to pre-process each photo to be as similar as possible. Image pre-processing techniques fall into two broad classes: i) image corrections, and ii) image enhancements. Image corrections include correcting for lens distortion, fixing dead sensor pixels and reducing noise. Image enhancements include color histogram equalization, illumination (brightness, contrast and saturation) and sharpening. Additionally, this step should include cropping photos to the area of interest.

In this work, each photo in the library is corrected in the following ways using pre-existing MATLAB functions:

1. Corrected for lens distortion using the default settings

2. Noise reduction by linear filtering

3. Histogram equalization to enhance contrast

4. Consistent illumination across all photos

The above techniques can be applied automatically to each photo in the library. Images are not cropped because this must be done manually and it was determined to be too time consuming for the purposes of this exercise.

5.2.2 Step 2: Isolate pixels of stone

The next step is to isolate the pixels of stone from the background pixels. Plataniotis and Venetsanopoulos (2000) cover nine different classes of image segmentation techniques. Three classes were explored: i) region-based, ii) edge-based, and iii) pixel-based techniques. Region-based techniques work by merging neighbouring pixels into homogeneous regions if their attributes (eg. color) are sufficiently similar. Edge-based techniques work by computing the gradient of color change then looking for rapid slope changes in the gradient's first derivate. Pixel-based techniques work by grouping like pixels into groups based on their position in color space. Discontinuities and breaks in the core cause the region-based and edge-based techniques to over segment the image into far too many classes so these methods were abandonded in favour of a pixel-based segmentation technique.

One of the most commonly used pixel-based segmentation techniques is clustering, the process of partitioning an image in subsets of similar colors. As shown in Figure 5.2, there are no clearly defined clusters of pixel color; there is a smooth transition among the different colors groups in the photo. Despite the lack of well-defined color groups, this segmentation method out-performed the other tested methods.

One of the most popular and fastest clustering method is k-means, which is also the technique recommended by Plataniotis and Venetsanopoulos. The original k-means algorithm was developed by MacQueen (1967) as an unsupervised method of classifying multivariate data. It is commonly used in image

processing to automatically partition an image into k initial color groups then iteratively refining the groups as follows:

1. Each pixel p_i is assigned to the nearest colour group center, C_j
2. Each color group is updated to the mean of its constituent pixels

The algorithm converges when there is no further change of pixels to color groups. The initial algorithm has undergone many refinements and the current MATLAB implementation is used in this work.

Figure 5.3 shows the result from clustering with three classes. Despite a lack of clear separation between pixel colors, the clustering algorithm is able to separate the predominantly grey pixels of the core from everything else. The clustering algorithm is applied to the pre-processed, original core photo (Figure 5.3a) to create the clipping mask (Figure 5.3b) which is then applied to obtain the isolated core (Figure 5.3c). There are three clusters in the mask: i) white pixels isolate the core, ii) grey pixels isolate the core box, and iii) black pixels isolate shadows and darker spots on the core.

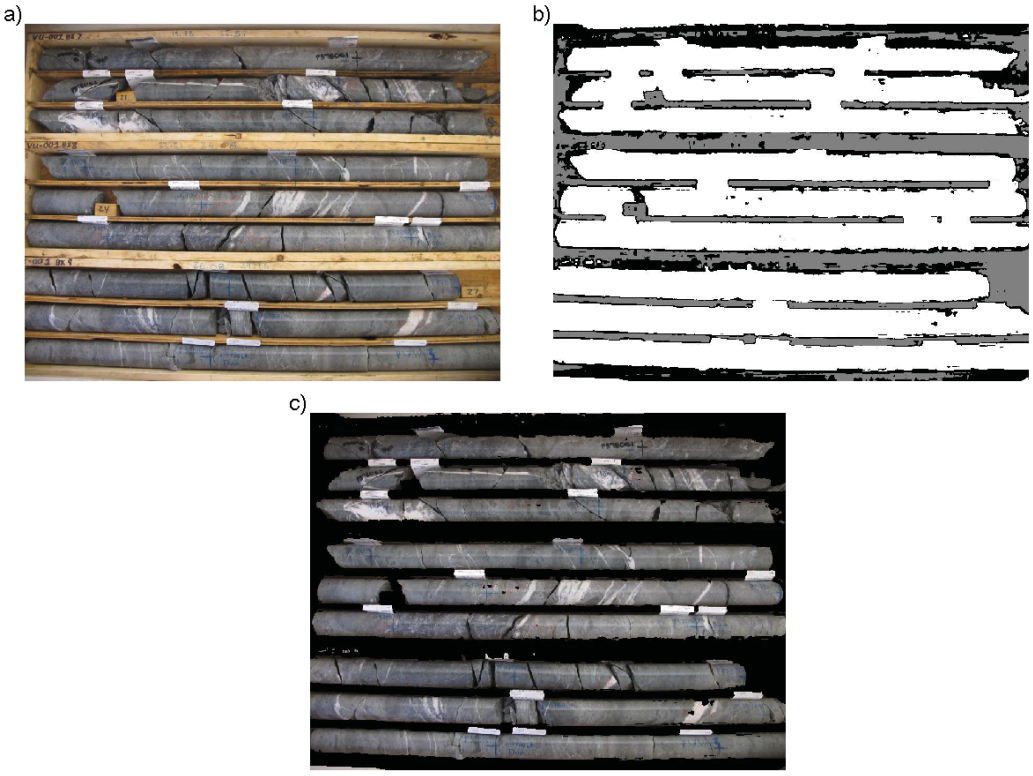

Figure 5.3: a) original image, b) Image mask created from k-means clustering, and c) the core photo after the mask has been applied

5.2.3 Step 3: Identify individual rows of core

The clustering algorithm is effective in isolating pixels of rock from everything else; however, the rows must be further defined before veins can be located in space. Drill core is laid out sequentially from the top of the drill hole to the bottom before photographing. Additionally, each box is marked with a start and end depth. In order to use this information, each individual row of core needs to be further isolated with a mask. Figure 5.4a shows a core photo after being processed with k-means. To isolate the rows, the following steps are applied to each photo:

1. Count non-black pixels for each row of pixels in the photo and normalize to 1

2. Plot the normalized count for each row of pixels (Figure 5.4b)

3. Select a threshold which is just low enough to capture each row of drill

core

4. Keep each row of pixels with a count greater than the selected threshold to create the mask (Figure 5.4c)

5. Apply the mask to further isolate each row of drill core (Figure 5.4d)

With each row of core isolated in this manner, the start and end depth of each row can be approximated from the start and end depth of the box and the number of rows of core. This assumes that each row of core is the same length which is not true; however, each box begins at the correct depth so the slight shift in true vein location is considered negligible. On a block-scale, these minor differences will not effect vein count.

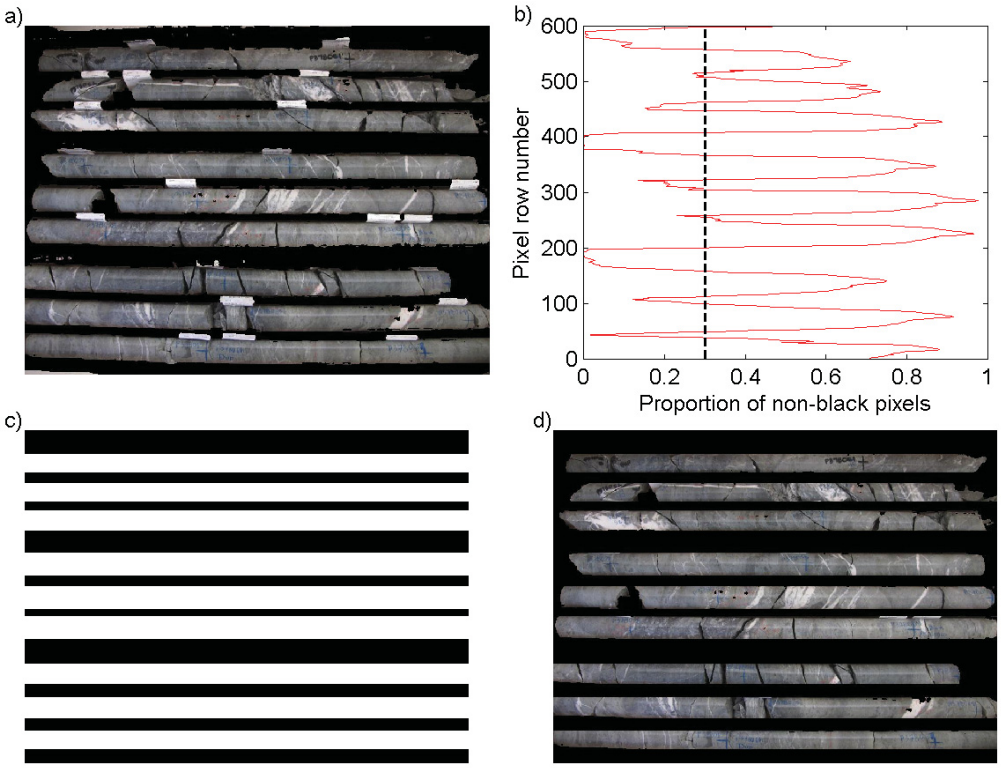

Figure 5.4: a) isolated core from clustering, b) row-by-row threshold of non-black pixels, c) row mask, and d) isolated rows of core

5.2.4 Step 4: Isolate Veins

The next step is to isolate each vein from the drill core. The International Commission on Illumination (CIE) defines a standard for detecting colour

difference. The latest iteration of the formula is called CIEDE2000. For details of the colour difference formula, see Luo, Cui and Rigg (2001). The MATLAB implementation by Sharma, Wu and Dalal (2004) is used in this thesis.

$$\Delta E_0 0 = \sqrt{\left(\frac{\Delta L}{k_L S_L}\right)^2 + \left(\frac{\Delta C}{k_C S_C}\right) + \left(\frac{\Delta H}{k_h S_H}\right) + R_T \frac{\Delta C \Delta H}{k_C S_C k_H S_H}} \tag{5.1}$$

The steps are summarized as follows:

1. Each photo is converted to Lab color space
2. Colorfulness (Luminosity) of each pixel is calculated
3. The colorfulness of each pixel in the image is compared to the mean colorfulness of veins in the image
4. The perceptual difference (ΔE) for each pixel is calculated using equation 5.1
5. A range of perceptual differences around the mean value of the veins is selected

Figure 5.5 shows the results of isolating veins with the above method. Most veins in the image are isolated; however, there is some noise. In particular, glare from the overhead lights causes reflections on the core that are similar in colour value to the veins. This can be seen in the horizontal lines across some rows.

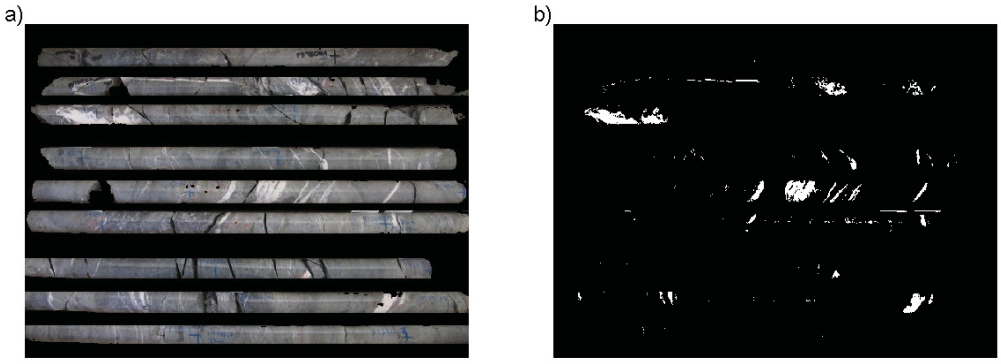

Figure 5.5: a) isolated core from clustering, and b) isolated pixels after colour segmentation

5.2.5 Step 5: Locate and Count Veins

To count and locate each vein, each row of core (as defined by the mask in 5.4c) is treated separately. For each row of pixels, a vein is recorded as a transition from black to white to black pixels. In addition, the pixel thickness of each vein is recorded and converted into milimeters.

One common problem in many of the photos is reflective glare from overhead lighting. It causes high-frequency, horizontal noise to be isolated by the color difference algorithm. The highlighted section of drill core in Figure 5.6a shows an example of this. In the drill core, there is just a single vein. In the vein mask, there is a single vein identified plus horizontal noise from the overhead glare. The count of transitions from black to white to black is counted for each row of pixels and a CDF of count is constructed (Figure 5.6b). Since the vein crosses the piece of core, the noise only occurs in the upper part of the distribution. By selecting a modest quantile, the noise is essentially ignored.

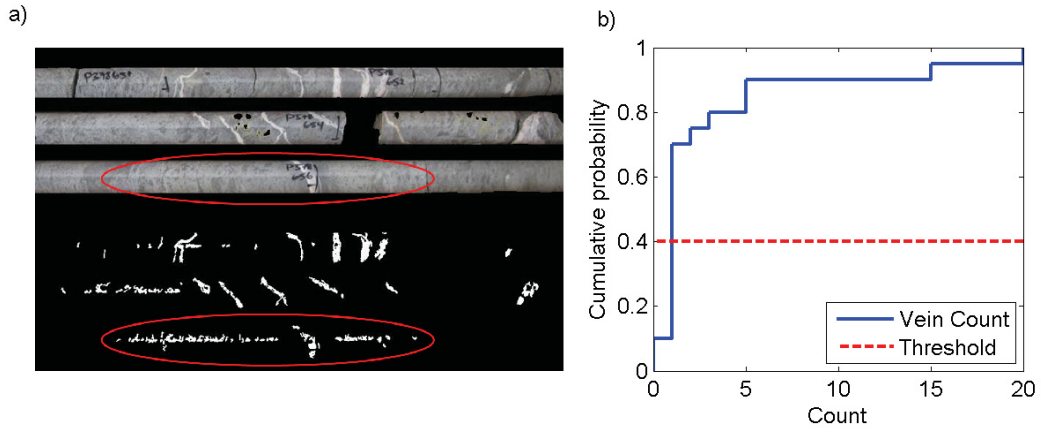

Figure 5.6: a) Highlighted noise from vein segmentation and b) cumulative distribution of vein counts

5.2.6 Step 6: Optimization

The above workflow has many of user-selectable parameters. In order to obtain the best results, the parameters of the automatic workflow are optimized and compared to a set of manually logged core photos. 200 photos were manually logged using a GUI to click on the locations of each vein (Figure 5.7).

A bounded minimization algorithm was implemented using MATLAB. For more information on the minimization algorithm, see Lagarias et al. (1998). The parameters to be optimized are as follows:

1. Size and strength of sharpening filter
2. Row intensity threshold
3. Color difference range
4. CDF quantile to keep

After 10,000 iterations using a derivative-free, bounded minimization search, a correlation of 0.710 is acheived between the manually logged and automatically logged photos (Figure 5.8).

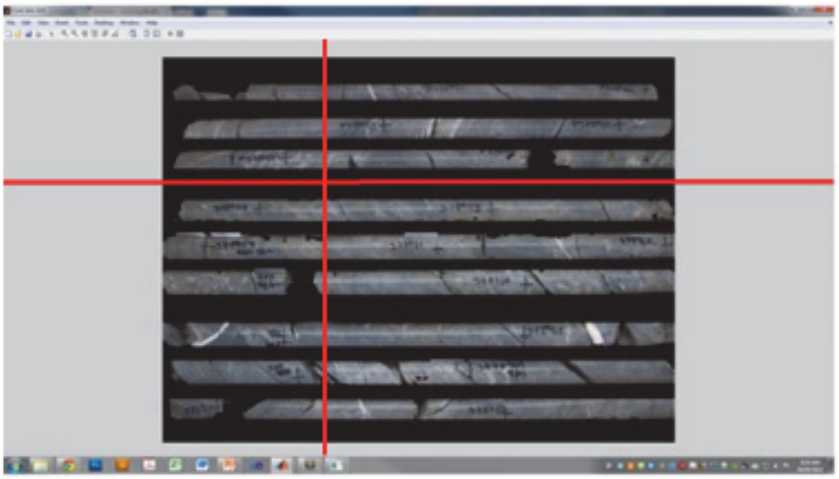

Figure 5.7: GUI used to manually record point location intersections.

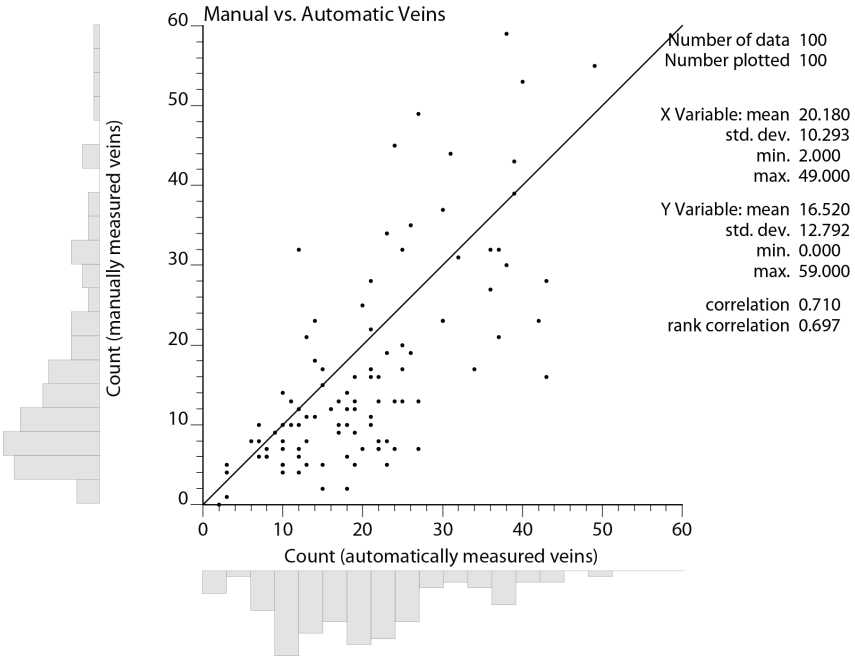

Figure 5.8: Correlation of vein count between automatically measured photos and manually measured photos.

5.3 Results

After optimizing on a random subset of 100 photos, the optimized parameters are used for each photo in the global core photo dataset. A total of 4,107 photos are processed and over 68,000 vein intersections are recorded in the study area. The distribution of measured vein thickness is shown in Figure 5.9.

The mean vein thickness is 6.32 mm with a variance of 147 mm and a maximum thickness of 981 mm. This is consistent with veins which have been measured during underground mapping. Work by Roberts et al. (1999) suggests that vein thickness is best described with a log-normal distribution. The resulting empirical distribution is fit with a log-normal distribution (Figure 5.9).

Figure 5.10 shows the results of locating the veins. The original core photo is compared to the isolated veins with their recorded location plotted in red. Some of the small, fine veins have been missed. This is likely not a problem because these veins are typically not mineralized. Additionally, some of the broken veins have been identified as two separate veins. This could be more of an issue because it will create two conditioning points which are very close together.

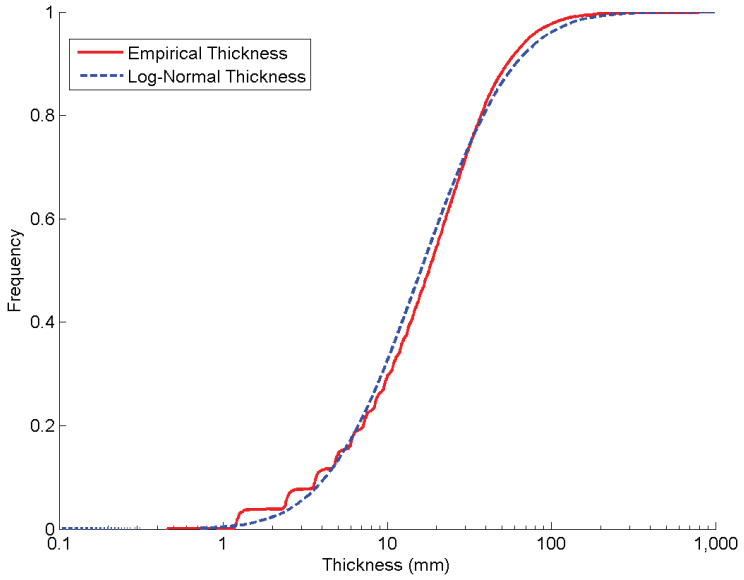

Figure 5.9: Thickness distribution of automatically measured veins fit with a log-normal distribution.

Figure 5.10: a) Original core photo and b) isolated and located veins

5.4 Discussion

Overall, the image processing workflow described above worked sufficiently well for the intended purpose in this work, to create conditioning data for use in a DFN. K-means is sufficiently effective at isolating pixels of stone from everything else in the image. The row identification method also works sufficiently well for its purpose. Identifying invididual veins from the rows of core is an area that could use improvement. The veins are not uniform in color and many are very close to the color of their host rock. Many small veins were missed by the locating step and some broken veins were measured twice. To get around this, photos were quickly checked at each processing step and where the processing step failed, the photos were discarded. The mean vein count of the drill hole was used in place.

Chapter 6

Case Study

This chapter presents a thorough case study implementing the previously described techniques in the case of an epithermal gold deposit. Models of block grade are constructed using a spatial point process and a discrete fracture network. In addition, models of block grade are constructed using the standard geostatistical techniques OK and MIK for comparison. The dataset includes a minor but still significant amount of silver. For simplicity, only gold has been modelled. The silver population is also characterized by a heavy-tailed distribution; although, not as pronounced as that of the gold population. The modelling techniques presented here could be extended to the silver population. For further information on the deposit, see Ireland et al. (2014).

6.1 Case Study A: Spatial Point Process

The spatial point process methodology is demonstrated on an epithermal gold project from north-western British Columbia. The project consists of multiple mineralized domains but this portion of the case study focuses on a single domain. The domain measures approximately 590 m along its northwest strike, 560 m across strike and down to 650 m in depth. The domain is best described as a transitional to intermediate sulphidation epithermal stockwork vein system. While this is technically a vein-hosted deposit, mineralization takes place within a dense vein stockwork with quartz veins representing up to 50% of the rock volume. A significant coarse gold population with a distinct lack of spatial structure has been identified. For the purposes of modelling, the coarse

gold population can be considered as randomly distributed in space.

6.1.1 Data

The area of interest comprises more than 30,000 samples collected via surface and underground drilling and represents one mineralized domain. The gold distribution is characterized by highly skewed grade values with assay values over one percent gold (Figure 6.1). Using a high-grade threshold of 5.0 g/t Au, 1,702 of 36,626 samples (4.6%) are classified as coarse gold. The locations of the drill assays with their associated variograms can be seen in Figure 6.2.

The lack of spatial structure in the upper tail can be clearly seen in Figure 6.2c which shows only the high-grade assays. The discrete nature of coarse gold mineralization can also been seen in the associated variograms in Figure 6.2d. The nugget effect of the population is approximately 0.75, indicating a high chance effect and degree of inherent randomness in the population. This justifies the use of a spatial point process for modelling the high-grade population.

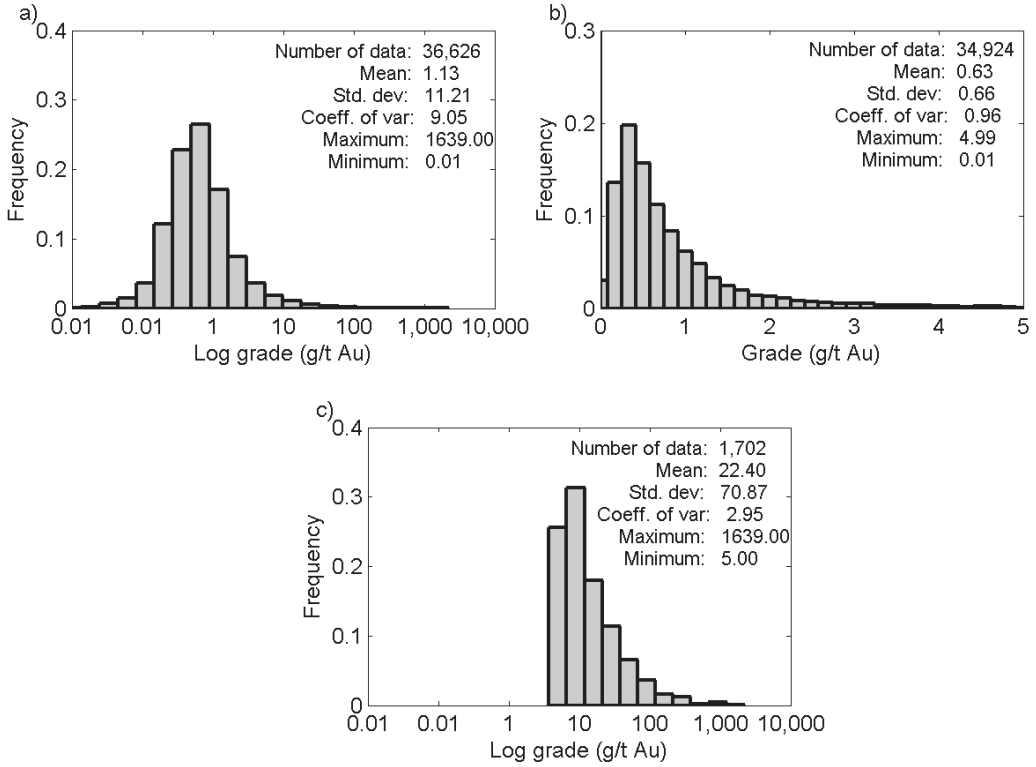

Figure 6.1: Histograms showing the a) entire grade distribution, b) low-grade distribution, and c) high-grade distribution

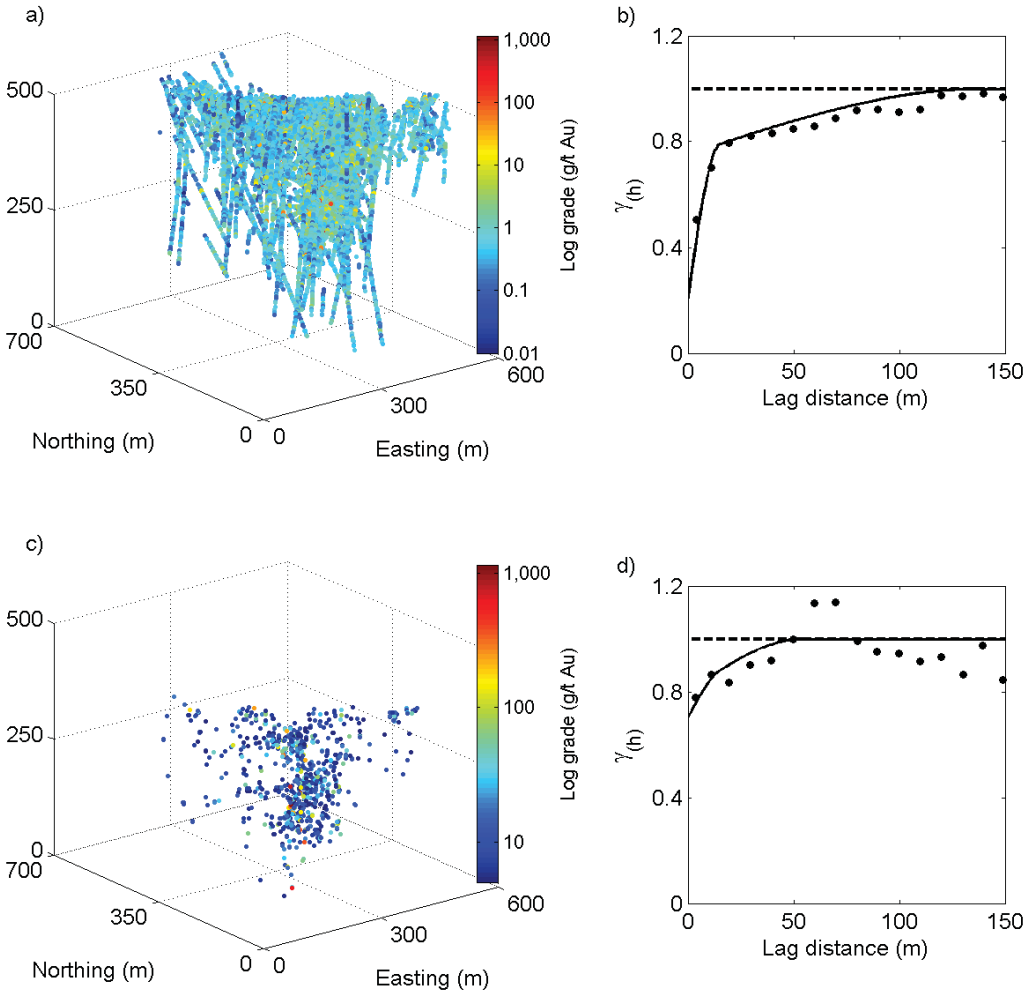

Figure 6.2: a) Drill assays in the mineralized domain and, b) variogram of all samples; c) high-grade assays only and, d) variogram of high-grade samples

6.1.2 Steps

First, low-grade background mineralization is estimated independently from the high-grade population with OK using only the low-grade subset of the data. Next, the local proportion of high-grade assays is modelled to obtain the required intensity fields for the Poisson and Cox processes. The variogram range of the high-grade population is used as the search ellipsoid parameterization when calculating local proportion data. The proportion data are used as conditioning data to generate a single estimated map of the intensity field (OK) and realizations of the intensity field (SGS) (Figure 6.3).

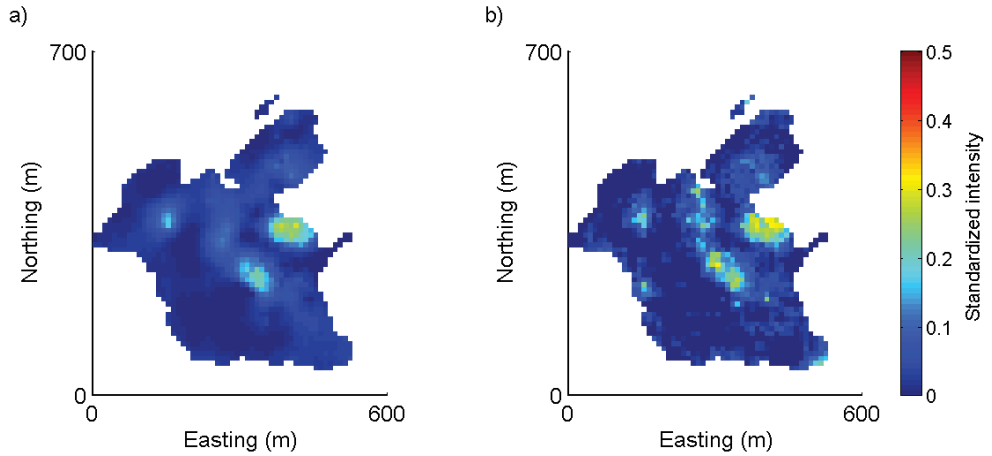

Figure 6.3: a) Ordinary kriged map of intensity for the Poisson process input and b) realization of intensity (SGS)for the Cox process input

The high-grade population is modelled in two ways. First, an estimated model is created using a non-homogeneous Poisson process with a single estimated intensity map. Second, 100 realizations of the high-grade population are created using a Cox process with realizations of the intensity map generated by SGS and the proprtions previously generated. Figure 6.4 shows models for the low- and high-grade populations using the Poisson and Cox processes.

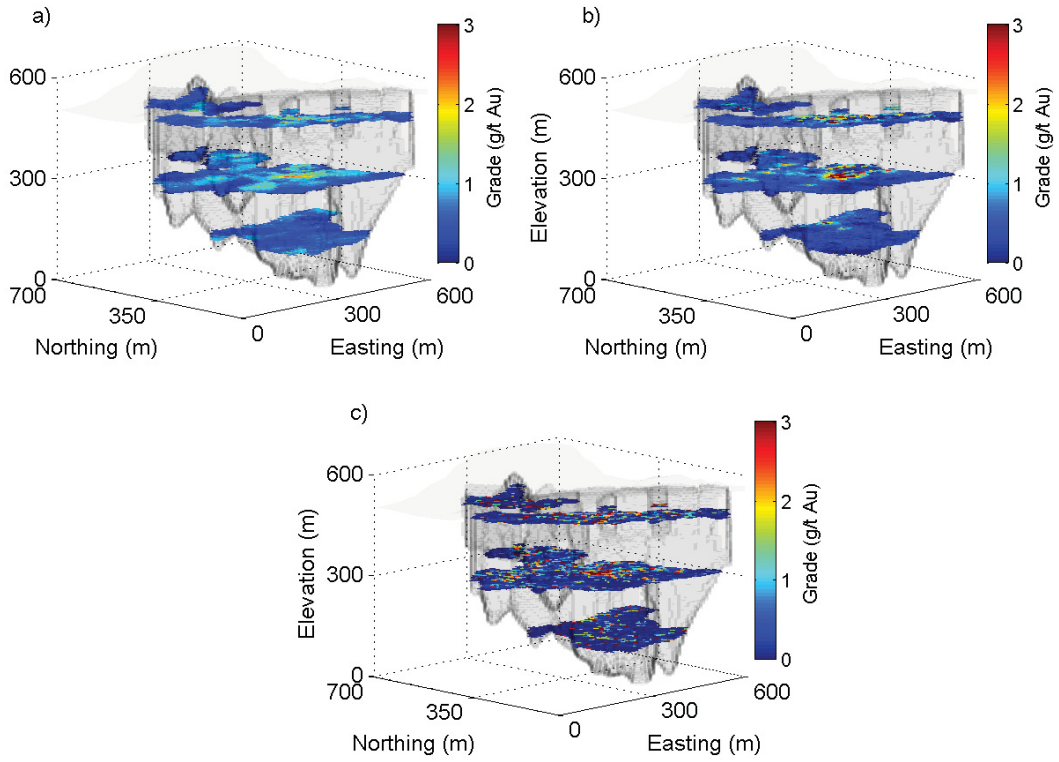

Figure 6.4: Slices through the grade model: a) background mineralization, b) high-grade mineralization from the Poisson process, and c) high-grade mineralization from a single realization of the Cox process

It is important to account for the uncertainy in the input parameters of the modelling methodology, particularly when considering simulation. The most critical input parameter is the global distribution of gold grade. The spatial bootstrap (Leuangthong, Khan and Deutsch, 2008) is used to access the uncertainty in the global mean (Figure 6.5). The global distribution of mean values is slightly skewed due to the presence of high-valued outliers. Each realization of the high-grade population from the Cox process is scaled to a realization of the global mean determined from the spatial bootstrap by scaling the intensity map. The full methodology is described in Chapter Three.

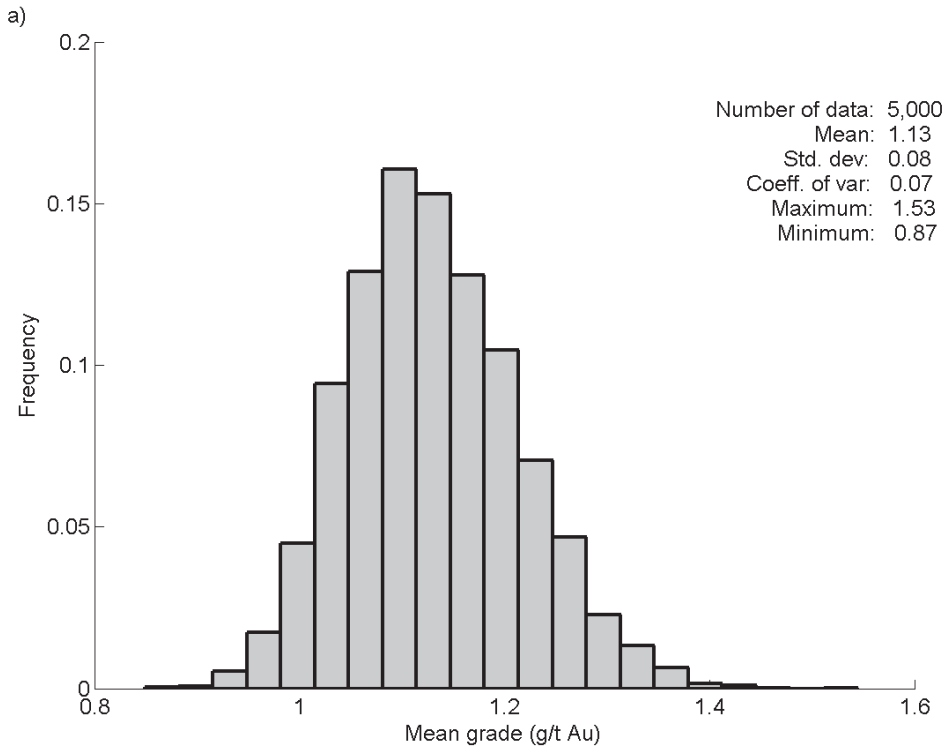

Figure 6.5: Global uncertainty in the mean generated from the spatial bootstrap

6.1.3 Results and Discussion

Final maps from the Poisson and Cox processes show that the resulting final grade model (which includes the low-grade population) is smooth (Figure 6.6) and analogous to an estimated grade model created using OK. The realizations resulting from the Cox process have the correct spatial variability and the correct mean and variance.

Although the Poisson process is a stochastic process in itself, the results approximate an estimation map because of the very large number of points simulated per block. The process could be repeated n-times resulting in very similar maps; thus, it is reasonable to consider the results of the Poisson process to be an estimated map that could be used for mine planning, in the same way an OK map would be used. The global distribution of the model can be tuned much like traditional estimation techniques. Rather than controlling the variance with search and data parameters, as is commonly done with OK (Rossi and Deutsch, 2014), the variance of the global distribution is tuned

by controlling the smoothness of the intensity field. Increasing the variability of the intensity field increases the variability in the final grade distribution. A change of support study can be undertaken to determine the appropriate level of smoothing when upscaling from point- to SMU-scale data. Here, the histogram is rescaled using the discrete Gaussian model (DGM) to a 10 meter block support (Figure 6.7). Change of support is not the focus of this work; the interested reader is referred to Machuca, Babak and Deutsch (2007) for specific DGM considerations.

This workflow does not lead to the reproduction of the assay data because block grades in the final model do not reproduce the input assay data. One of the difficulties of working in a coarse gold environment is obtaining a representative histogram of grade values. Hitting or missing a coarse gold nugget involves a high chance factor due to the extremely high nugget effect of the population. This is not viewed as a drawback of the methodology. Rather, it is argued that when nuggets are hit by a drillhole in a given block, using that assay value to represent the block grade is inappropriate (likely the block grade should be lower, in fact, this is the short-scale effect of smearing). When the drillhole does not strike a nugget, the block grade is also inappropriate (likely the block grade should be higher, nuggets probably exist that drilling did not hit). Realizations of the block grade are compared to the DGM support-corrected input distribution (Figure 6.8) and show good reproduction.

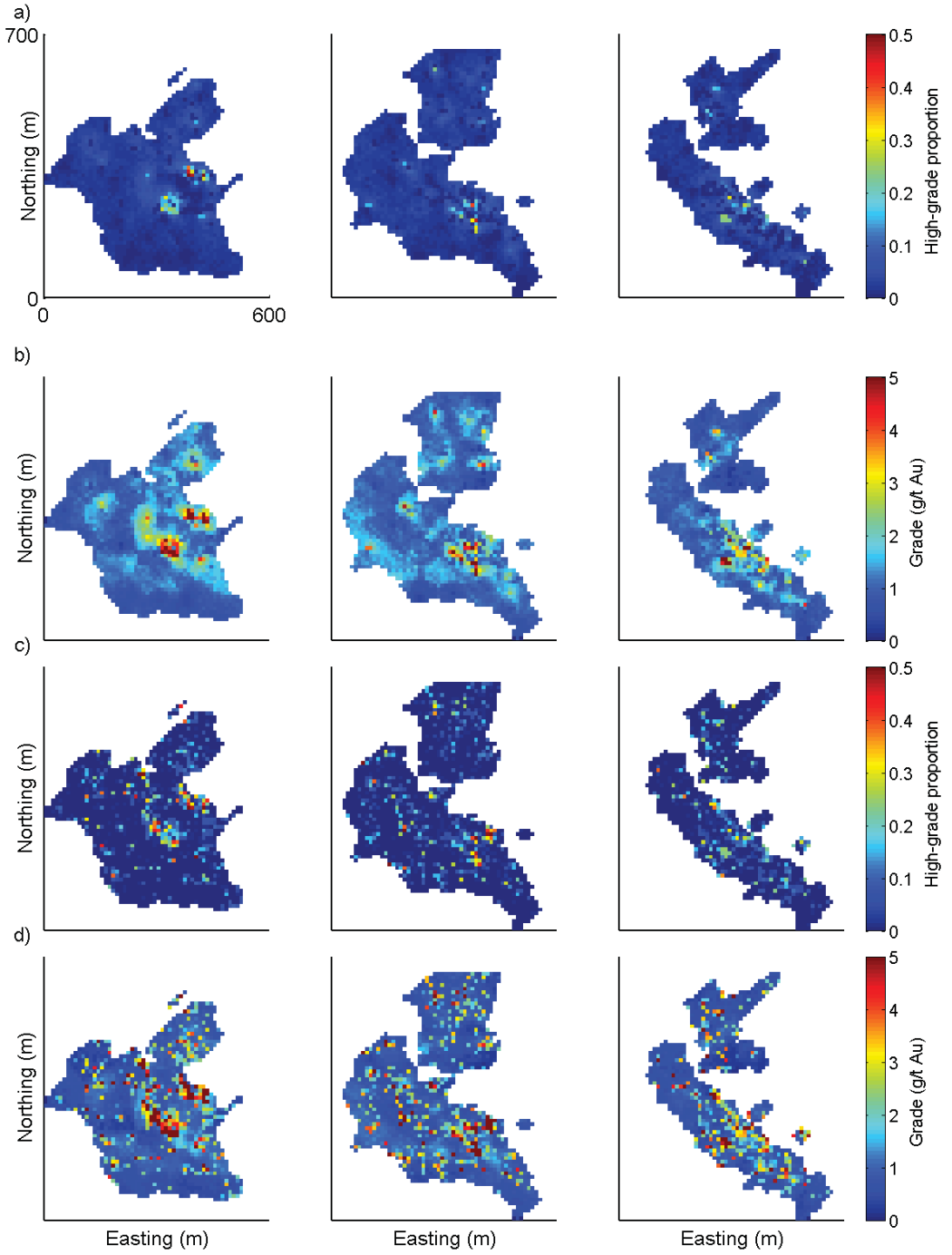

Figure 6.6: Slices through: a) an estimated intensity field, b) the corresponding grade model generated with a Poisson process, c) a single realization of a simulated intensity field, and d) a realization of grade generated from a Cox process

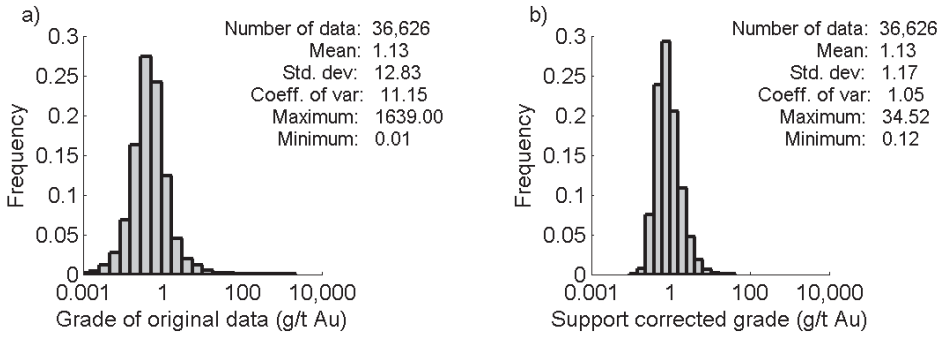

Figure 6.7: a) Point-scale grade distribution and b) selective mining unit (SMU)-corrected grade distribution

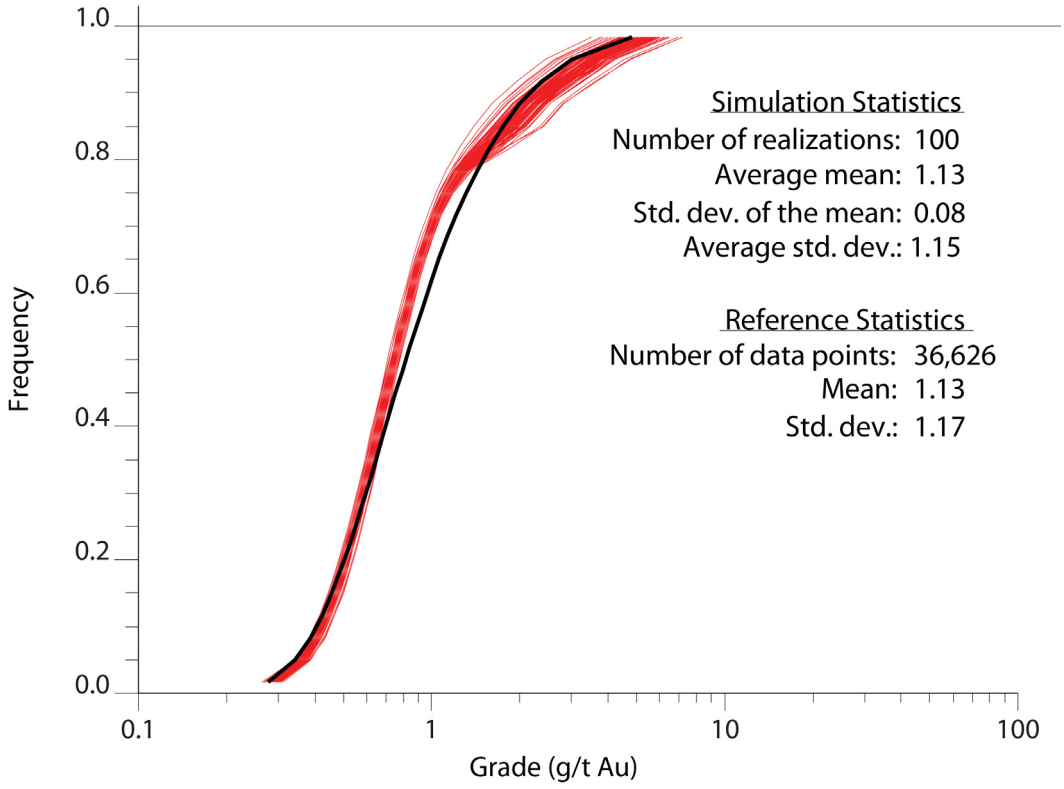

Figure 6.8: Block-grade distribution from 100 realizations (red) and the support-corrected input distribution (black)

6.1.4 Comparison to other techniques

The proposed methodology is compared to more traditional workflows, including capped models at different thresholds and an MIK workflow. Three models are created using OK, uncapped, capped to the P99.5 and capped to the P99.9 grade thresholds. Recall, the support-correct mean of the grade distribution is 1.13 g/t Au.

Table 6.1 summarizes the results of the models. The uncapped results overstate the mean and do not control the smearing of outliers. Capped OK is effective in reducing the variance but results in severe underestimation of the mean (the global declustered mean is 1.13 g/t Au). MIK is an improvement over uncapped OK because the mean is better reproduced and smearing is better controlled. The Poisson approach also reproduces the mean (by construction) but results in lower variance when compared to upcapped OK or MIK.

Table 6.1: Comparison of estimation results (all numbers reported in g/t Au)

Statistic	OK-1 (no cut)	OK-2 (P99.5)	OK-3 (P99.9)	MIK	Poisson
Mean	1.18	0.84	0.95	1.16	1.13
Std. Dev.	3.06	0.93	0.93	1.47	1.17
Min	0.01	0.01	0.01	0.01	0.12
Max	193.94	9.18	25.31	92.29	14.99

Slices through the block models of methodologies can be seen in Figure 6.9. Results from OK with no top cut assays are plotted on the left. Results from the MIK model are plotted on the right. The MIK model is smoother compared to the OK model and the spatial influence from outlier values is reduced.

A further comparison of the modelling techniques is given in Figure 6.10. The average grade above a 3.0 g/t Au cut-off is shown in Figure 6.10a; the proportion of material above cutoff grade is shown in Figure 6.10b and summarized in Table 6.2. Each estimated model provides a single value, whereas the simulated models provide a distribution of values. The smearing effect of the outlier assay values in the MIK workflow is clearly seen in Figure 6.10a. The MIK model reports a significantly higher average grade above cutoff when

compared to top-cut OK and the proposed Poisson and Cox methodologies. In Figure 6.10b, the proportion of blocks above the cut-off grade is higher with the Poisson and Cox methodologies compared to those of OK and MIK because the distribution is less influenced by high outlier values in the tail.

Table 6.2: Proportion of blocks above cut off with different modelling techniques

Technique	Proportion Above Cutoff
Cox	0.070
Poisson	0.068
MIK	0.053
Topcut OK	0.031

Estimated grade models use linear combinations of available data and have an unavoidable smoothing effect due to the averaging of values. Although an estimated model is appropriate for visualizing trends, it is not appropriate for heavy-tailed deposits. The high-valued assays end up having a disproportionately strong effect on the block being estimated and are "smeared" throughout the model (Figure 6.11). Geostatistical conditional simulations provide the same information as an estimated model. In addition, simulations also provide histogram reproduction and a model of uncertainty. For more information on estimation versus simulation, see Rossi and Deutsch (2014).

Figure 6.11 shows a side-by-side comparison of block models generated from the Poisson process, a single realization of the Cox process, and MIK. The cross-sectional slices are plotted alongside the locations of high-grade composites. Visual inspection shows that the same overall features are reproduced in the Poisson and Cox models, whereas the spatial variability is the distinguishing feature between the estimation and simulation models. The effect of the outliers has a more dramatic effect in the MIK model and the visual effect of smearing is clear.

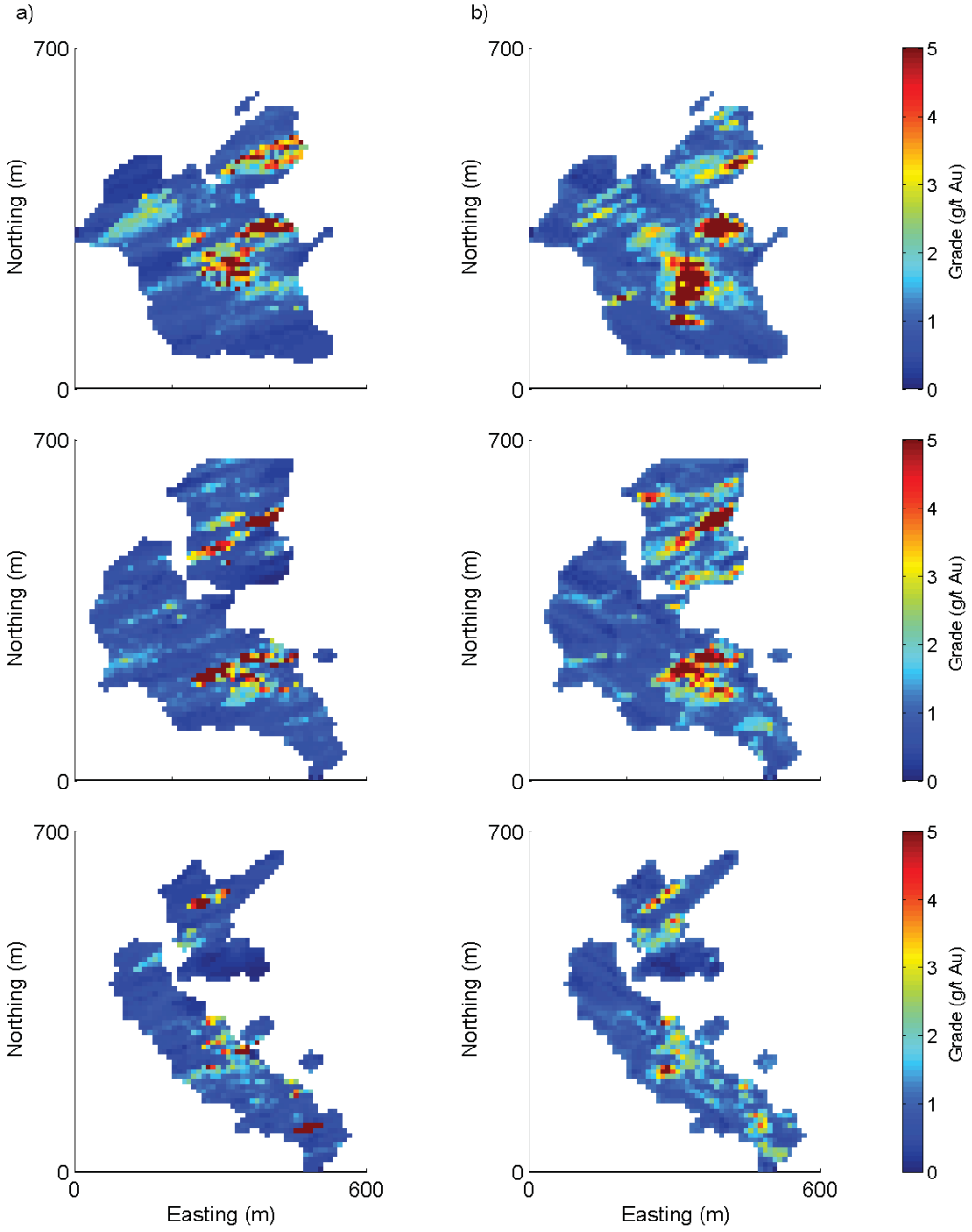

Figure 6.9: Slices through the block model of grade, estimated using a) OK and b) MIK

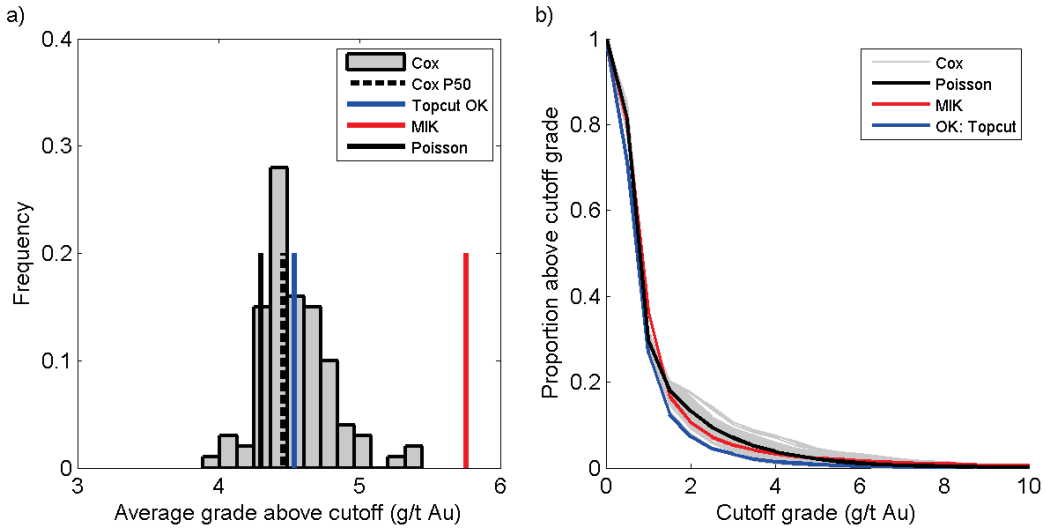

Figure 6.10: a) average grade above a 3.0 g/t Au cut off for each workflow, and b) proportion above cut off for each workflow

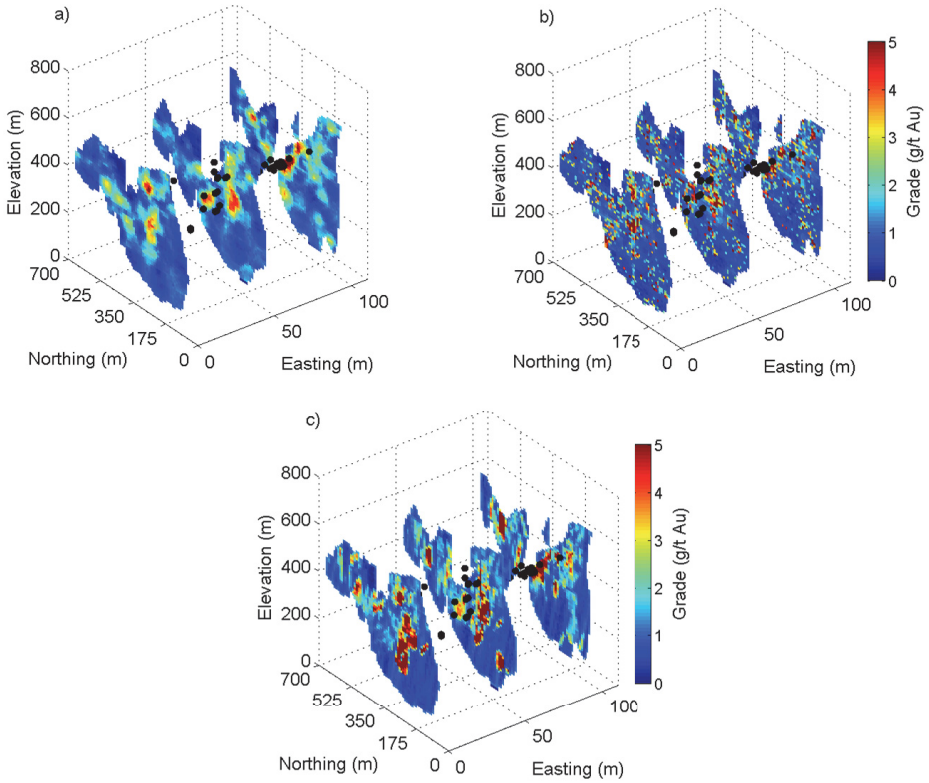

Figure 6.11: Cross sections through the block model highlighting the smearing effect in a) Poisson model, b) Cox model, and c) MIK model

6.2 Case Study B: DFN Grade Modelling

The DFN grade modelling methodology is demonstrated on another mineralized domain from the same epithermal gold project in north-western British Columbia. The entire zone consists of over twenty mineralized domains spanning an area 1,200 m along an east-west strike, 600 m across strike and down to 650 m in depth. The DFN methodology is presented on a single domain which measures 200 m along an east-west strike, 100 m across strike and 50 m in the vertical direction. Gold mineralization occurs as both pervasive background mineralization and discrete, coarse gold mineralization. Coarse gold is visible and restricted to quartz veins. Overall vein density in this domain is much lower compared to case study A, ranging from 5 to 20% volume.

6.2.1 Data

The proposed DFN grade modelling methodology is demonstrated on a subset of data from a vein-hosted, epithermal gold deposit. The grades are altered from their original values and the locations shifted for confidentiality reasons; however, the statistical properties remain representative of the deposit type. The cumulative distribution of of grades (Figure 6.12) show a highly skewed distribution; the locations of the samples are shown in Figure 6.13. The mean grade of the dataset is 1.55 grams per tonne gold and the maximum assay grade is over 9,000 grams per tonne Au. Several assumptions are made regarding the nature of mineralization to demonstrate this methodology:

- All veins in the deposit are mineralized
- Coarse gold occurs as random discrete particles (nuggets) within the veins
- Background mineralization is pervasive across the domain

The information required to generate the DFN is generated by processing core photos using the methodology presented in Chapter Five of this thesis. In summary, over 4,000 drill core photos are processed and the point location intersection and thickness are recorded for each vein. Approximately 68,000

vein intersections were recorded from the image processing workflow. These intersections are used as conditioning data in the DFN. In addition, the thickness of each vein was recorded and fit with a log-Normal distribution (Figure 6.14).

DFN input distributions which cannot be collected from drill core come from different sources. In this case study, the distributions of length and height are inferred from the thickness using the relationship given in Chapter 4 (Johnston and McCaffrey, 1996). The distributions of fracture trend and plunge come from both underground and surface mapping and are fit with a Normal distribution. The input statistics used to generate the fracture network are summarized in Table 6.3.

Table 6.3: Summary of DFN input distributions

Statistic	Thickness (mm)	Length (m)	Trend (deg)	Plunge (deg)
Distribution	Log-Normal	Fractal	Normal	Normal
Mean	6.32	1.26	030	88
Variance	147.1	18,340	3.0	3.0
Max	981.6	22.1	999	999

The grade distribution and the required DFN input distributions are collected from drill core. The next step in the workflow is to model the vein density which is required to control the number of simulated veins in each modelling cell.

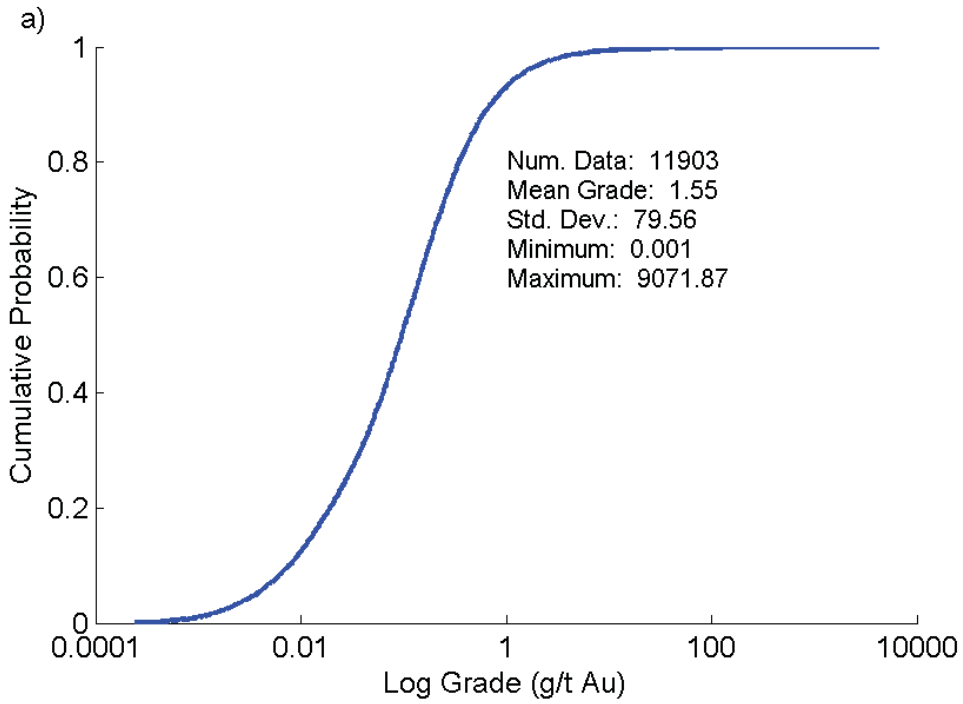

Figure 6.12: Cumulative distribution of assay grades used for modelling

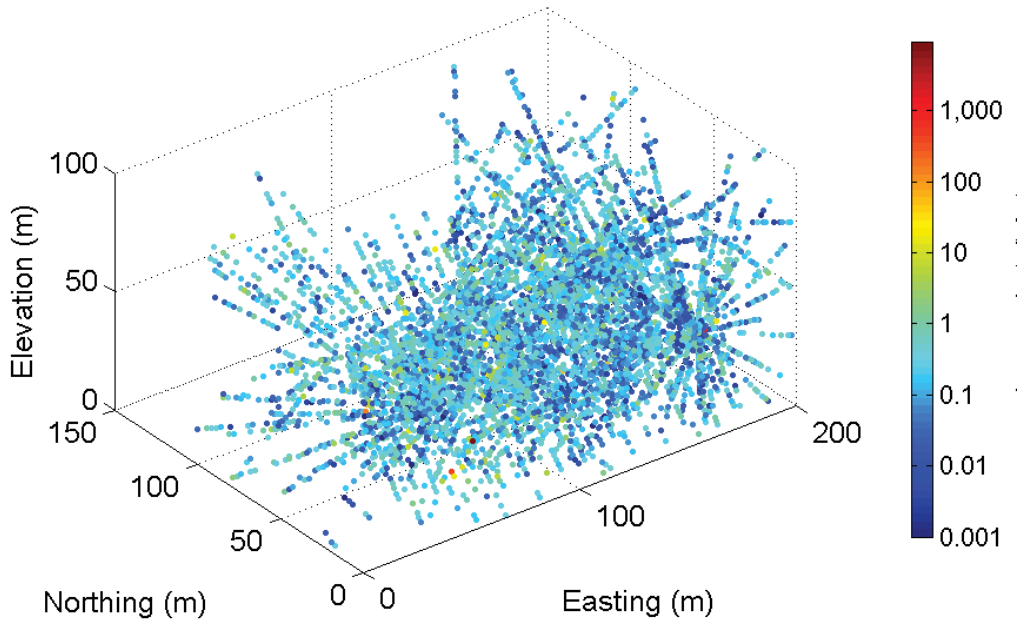

Figure 6.13: Locations of drilled assays

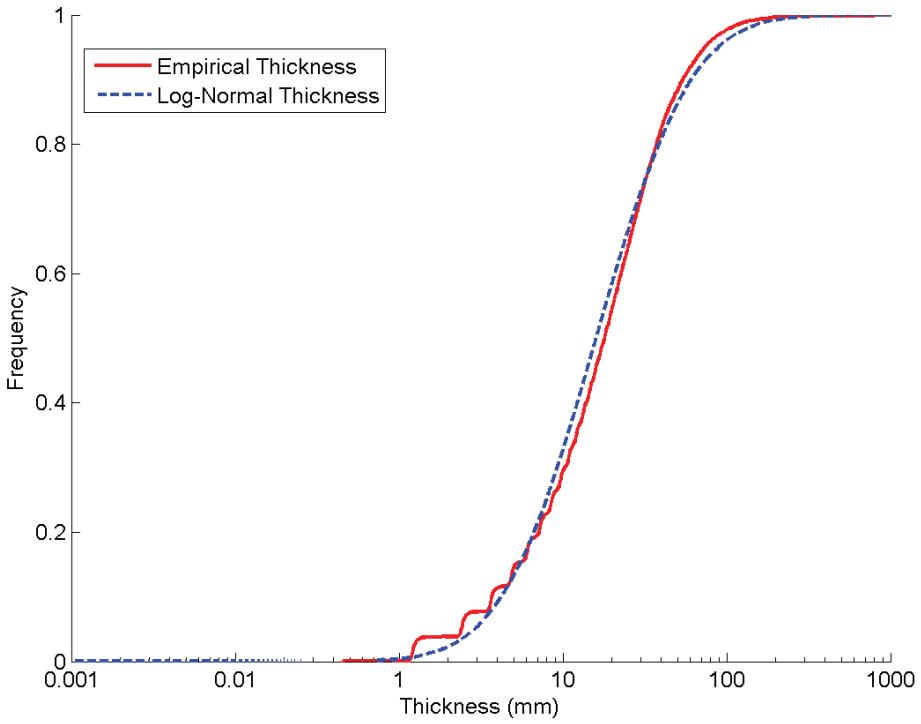

Figure 6.14: Distribution of vein thickness

6.2.2 Quartz vein modelling

Once the distributions of representative vein statistics are gathered, the veins in the domain are modelled using DFNSIM. The program uses a Poisson process to generate the initial fracture network and requires an intensity model of fracture count at each location. Lineal fracture intensity is measured along each drill hole then converted to 3D fracture density using the methods outlined in Chapter Four. Figure 6.15 shows the distribution of intensity values and the variograms. Using these results as conditioning data, the vein density over the entire domain is estimated using SGS (Figure 6.16). Uncertainty in the distribution of intensity can be seen in Figure 6.17.

With the input distributions and intensity map, realizations of a conditional fracture model are simulated. In total, approximately 1.5 million veins were simulated over the study area. An example of a simulated DFN is presented in Figure 6.18.

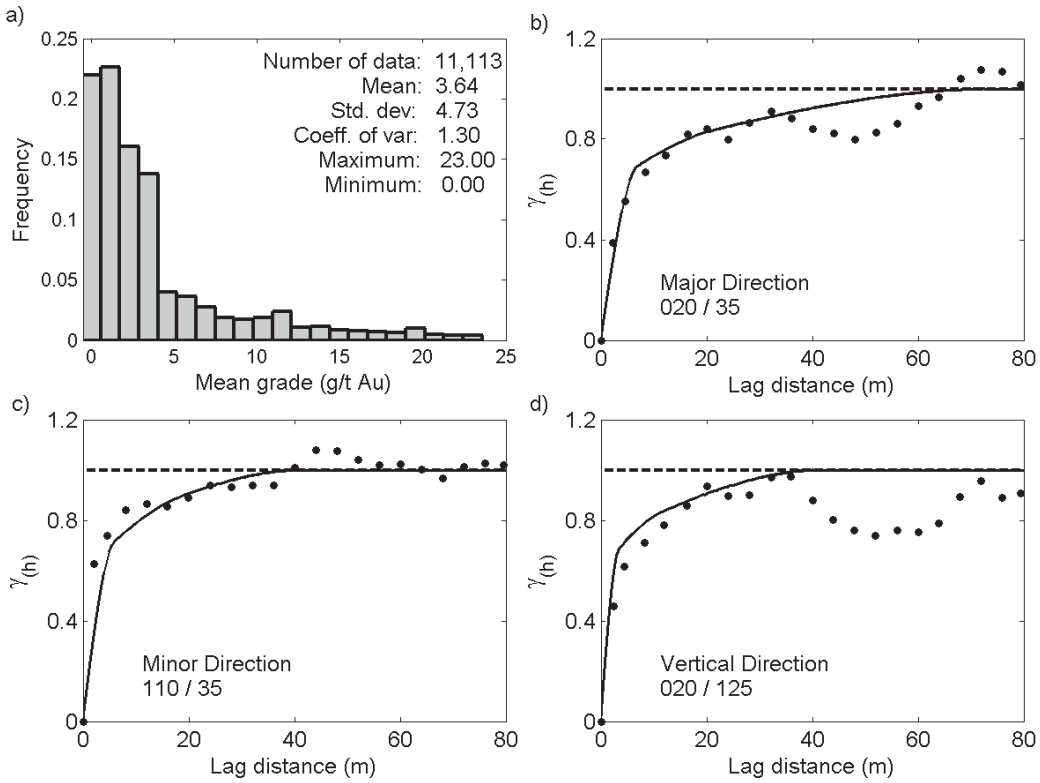

Figure 6.15: a) Distribution of vein intensity values with variograms of the b) major direction of continuity, c) the minor direction of continuity and d) the vertical direction of continuity

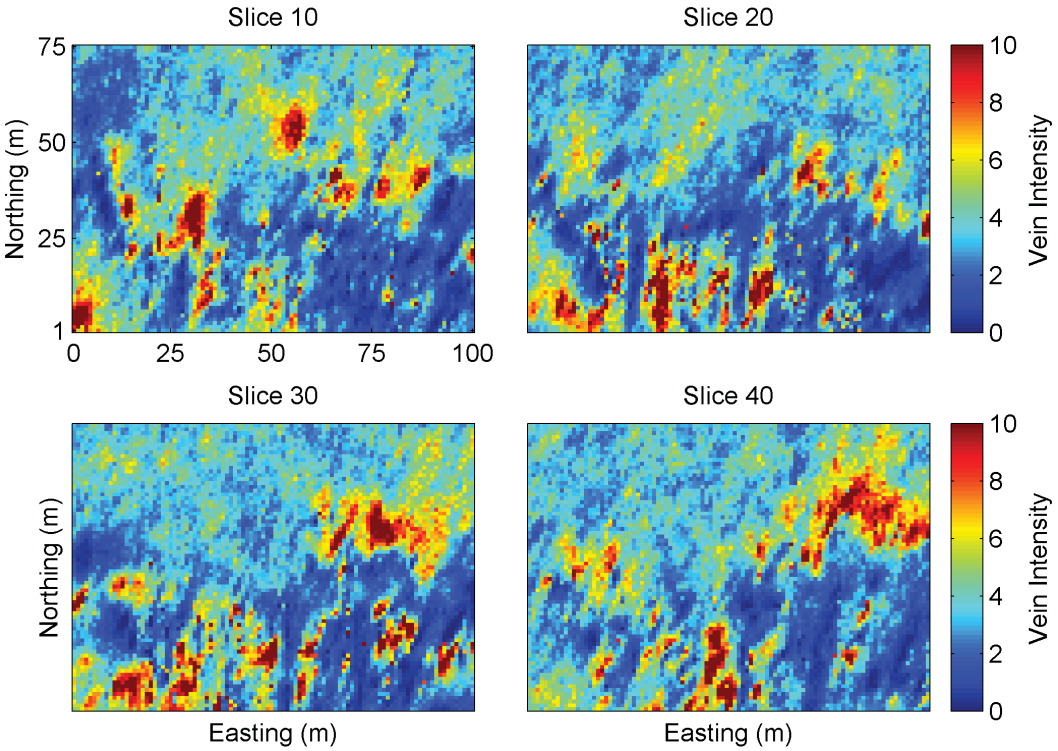

Figure 6.16: Slices through the model of vein intensity

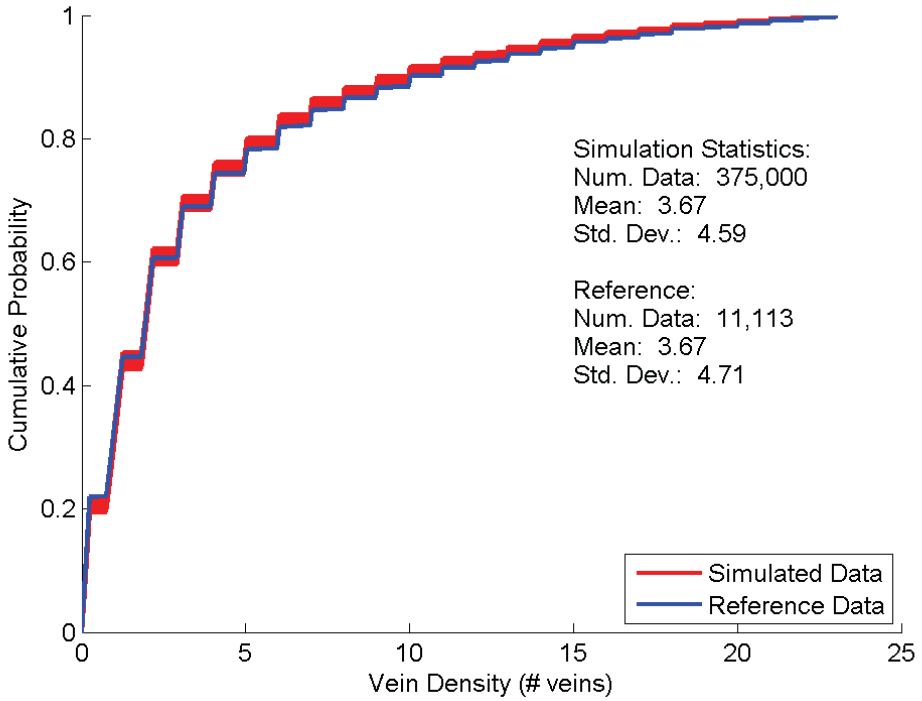

Figure 6.17: Distribution reproduction from simulated models of intensity

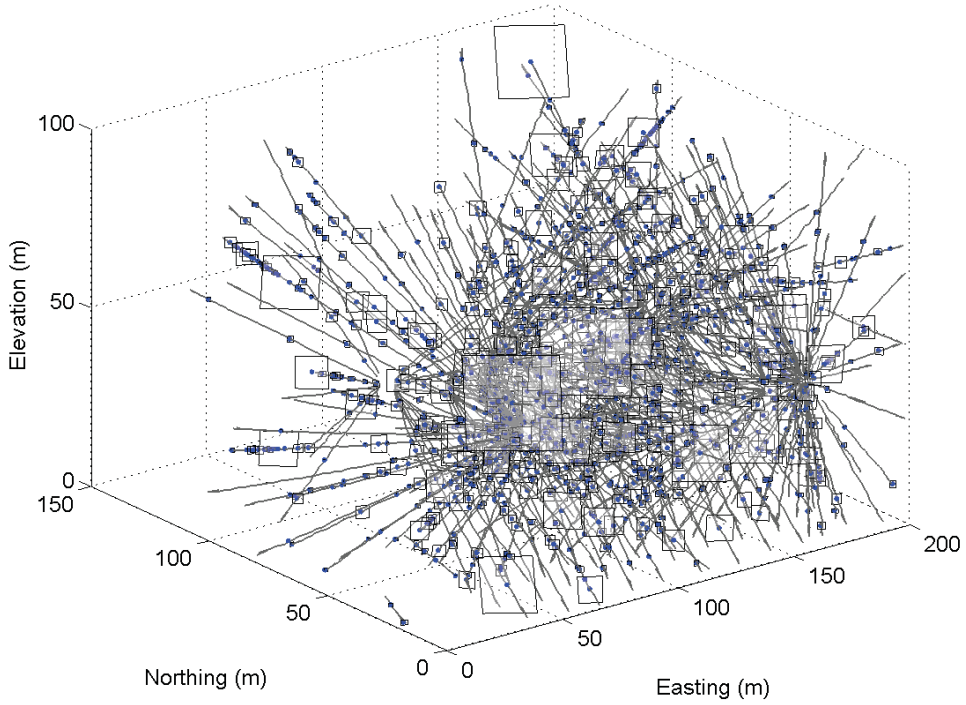

Figure 6.18: A realization of a simulated DFN; plotted only at the drill hole locations

6.2.3 Gold grade modelling

First, low-grade background mineralization is estimated independently from the high-grade population with SGS using only the low-grade subset of the data. Background mineralization is pervasive and smooth across the domain (Figure 6.20). Uncertainty in the low-grade realizations can be seen in Figure 6.19.

Next, high-grade gold is modelled using the DFN workflow outlined in Chapter Four. Gold is simulated as a spatial point process which is spatially restricted to the simulated veins. This work makes the assumption that grade is related to vein intensity. The intensity distribution is transformed on a quantile-by-quantile basis to match the support-corrected grade distribution (Figure 6.21). In this case, areas with more quartz veins will have higher gold grade. The transform approach is implemented using 'trans_trend' Deutsch (2005).

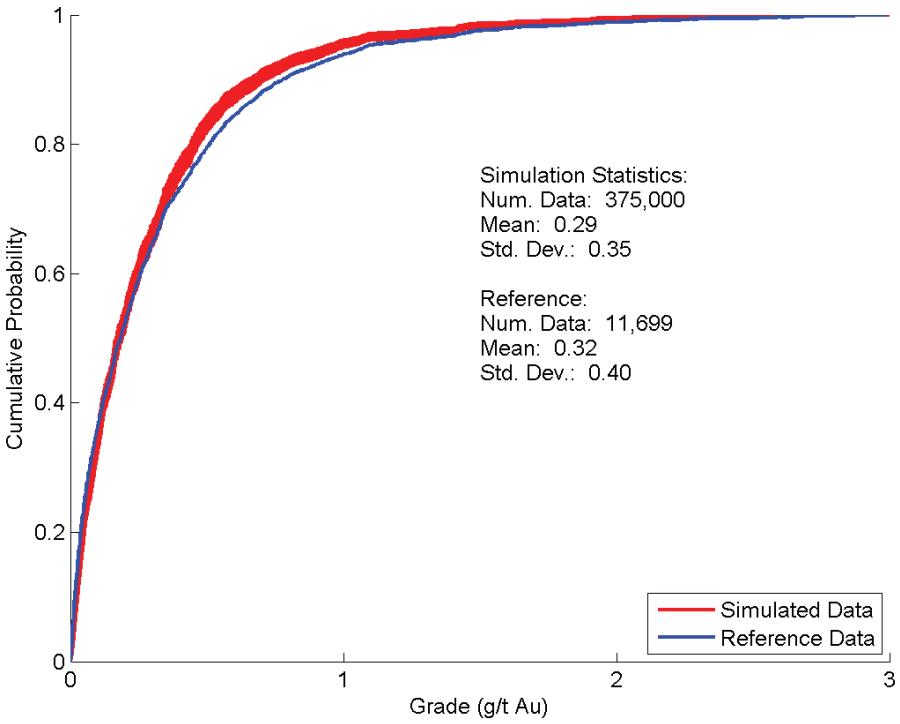

Figure 6.19: Background mineralization distribution reproduction

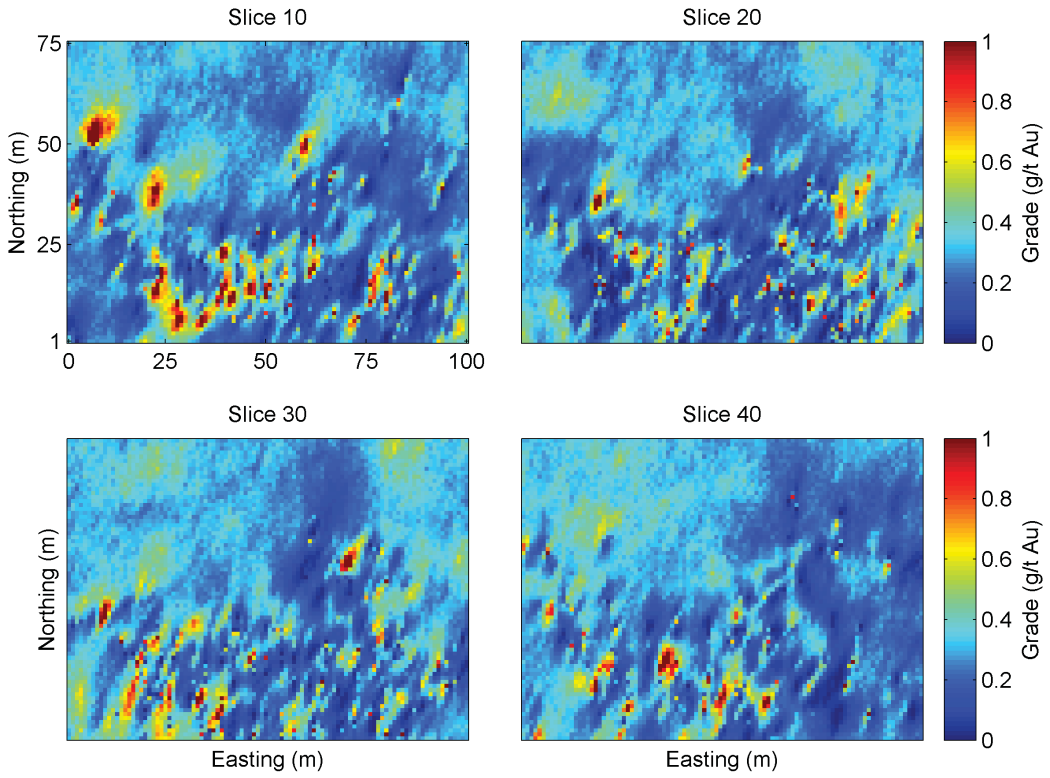

Figure 6.20: Slices through the model of background mineralization

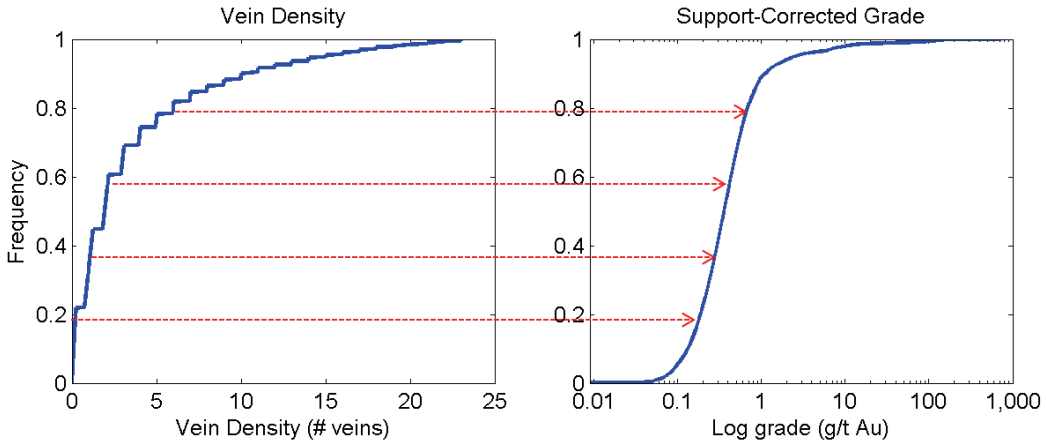

Figure 6.21: Schematic showing the quantile transform of intensity to grade

6.2.4 Results and Discussion

The coarse gold population is assumed to be spatially restricted to only the simulated veins in the discrete fracture network. Coarse gold mineralization

is proportional to the intensity of the simulated veins in the DFN. The spatial location of the discrete gold particles is controlled by the location of the simulated quartz veins; however, the density of gold nuggets in each vein can be changed. In general, this should be scaled until simulated realizations of grade match the support-corrected grade distribution.

Like the spatial point process workflow outlined above, the global distribution of the model can be tuned by controlling the smoothness of the intensity field. Increasing the variability of the intensity field increases the variability of the final grade distribution. A change of support study can be undertaken to determine the appropriate level of smoothing when upscaling from point- to SMU-scale data. Here, the histogram is scaled to a 2 m block support using the discrete Gaussian model (Figure 6.22).

Like the results in Case Study A, this workflow does not lead to the reproduction of the assay data because block grades in the final model do not reproduce input assay data. In a coarse gold setting, it is argued that using the assay grade to represent the block grade is inappropriate. Outlier values represent a chance encounter with a spatially restricted population and their influence should not be spread across the entire block. On the other hand, there are cases where a drill hole does not encounter an outlier value in an area where there is a higher proportion of the coarse gold population ie. where there is greater vein density. In this case, the block grade is likely higher than the input assays. Realizations of the block grade are compared to the support-corrected input distribution (Figure 6.23). The mean and standard deviation of the distribution are reproduced; although, the shape of the distribution is not matched completely. Slices through the final grade model are presented in Figure 6.24. The high-grade population is related to vein density. Areas with more simulated veins have a higher proportion of the high-grade population and a higher final grade value.

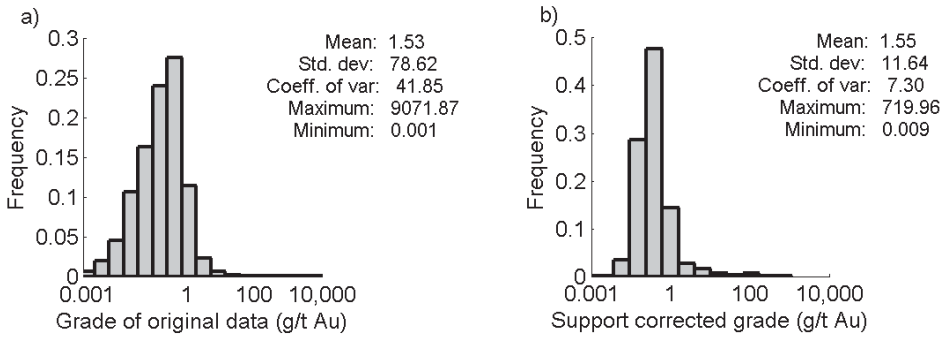

Figure 6.22: Histograms showing the a) point-scale grade distribution and b) support-corrected histogram

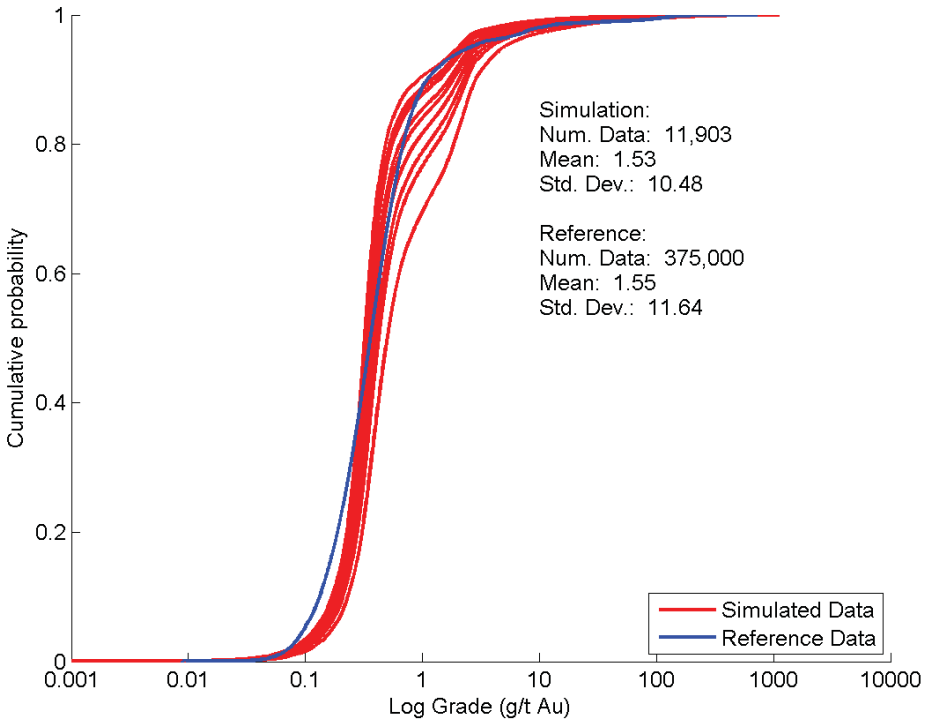

Figure 6.23: Distribution reproduction in the high-grade population

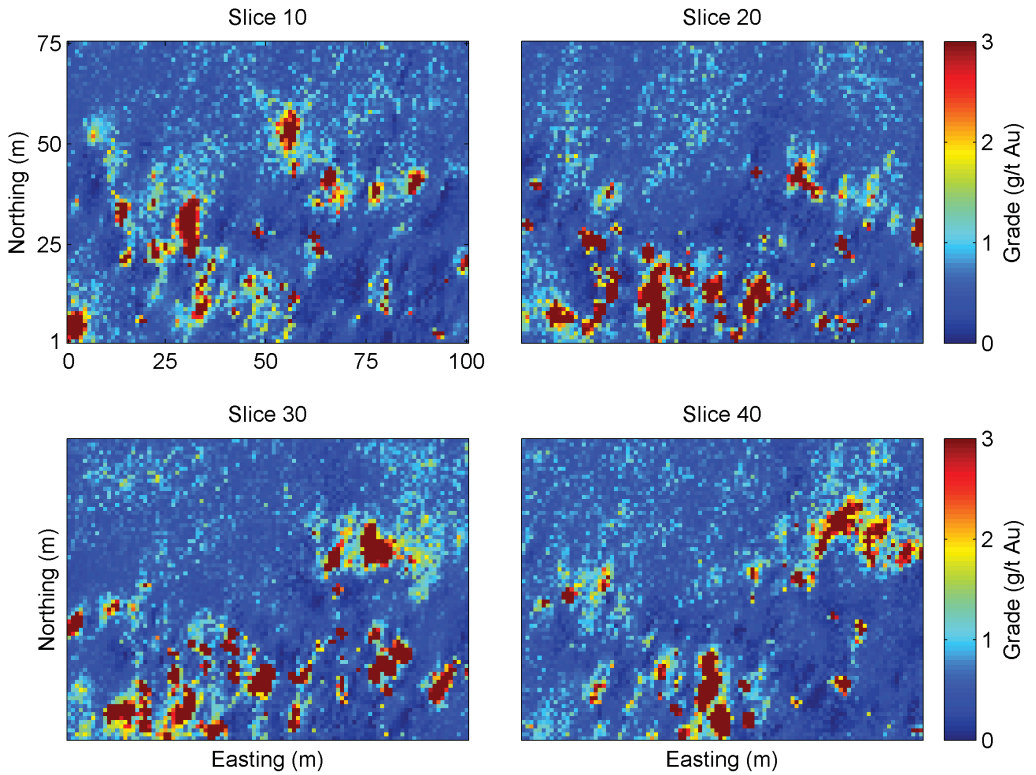

Figure 6.24: Slices through the model of coarse gold mineralization

Chapter 7

Conclusions

Assessment of the value of an ore body is an essential step in any mining project. Exploration samples represent less than one trillionth of the volume of the deposit. Distributions characterized by heavy-tails have an element of inherent randomness that cannot be ignored. This small amount of data, combined with the chance effect of hitting outlier values, means that the scale of variability of the values in the tail of the distribution cannot be ignored.

Outlier values should have their influence reduced in order to prevent potential bias and overestimation of grades. Traditional geostatistical methods often employ subjective, ad-hoc manipulations of the data such as capping assays. This work presents two techniques to reduce the influence of outlier values by spatially restricting their volume of influence. Both techniques attempt to honor the geologic reality of the processes that make up the underlying grade distribution.

7.1 Topics Covered and Contributions

Precious metal deposits are often characterized by heavy-tailed grade distributions. Inherent in these distributions are outlier values. Care must be taken when dealing with these values because they are often the result of an extreme manifestation of the random variability inherent in the data. The economic viability of many precious metals deposits relies on the presence of a few outlier values in the upper tail of the grade distribution. The upper few percentiles of samples may represent ten or more percent of the contained metal in the

deposit. The most common method of dealing with outlier values is to cap them to a pre-determined threshold. This is a subjective practice and overly aggressive capping risks making a deposit subeconomic. Undercapping assays risks overstating the grade. This work provides methods for the inclusion of outlier values and make use of the full grade distribution in the modelling workflow.

The implications of geostatistical modelling in the presence of outlier values is discussed in Chapter One. Outlier values should be examined to determine their validity as assayed samples which represent extreme variability in the grade distribution. It also must be determined if outlier values belong to a separte statistical population. If outlier data are left untreated, estimates may suffer from bias and overestimation when assed by typical geostatistical techniques. Estimation techniques linearly average values and a single outlier value can cause large modelling volumes to have an unrealistically high value. The influence of outlier values is typically restricted by capping assays. The methods presented in this work do not resort to capping or any other subjective, ad-hoc manipulation of the grade distribution. Here, the influence of outlier values is reduced by restricting their volume of influence. Each sample in the high-grade population of the dataset is modelled as an idealized sphere, or nugget, of gold to make up the particle size distribution.

The high-grade population is characterized by a high nugget effect which implies a lack of spatial structure and an element of inherent randomness. There is a chance effect involved when hitting or missing a high-grade sample. This is dealt with in this work by modelling the local proportion of high to low grade samples. The limited range of spatial correlation of the high-grade population is captured here by using a search window which is restricted to the variogram range of the high-grade population. The local proportion data is the intensity parameter in the spatial point process. The high-grade population is modelled (separately from the low-grade population) by simulating discrete volumes of gold using a spatial point process. Each simulated point draws randomly from the particle size distribution. This way, the entirety of the grade distribution is used. The influence of the values is restricted

by limiting their volume of influence. The intensity parameter is scaled until the mean of the modelled high-grade population matches that of the global reference distribution. Uncertainty in the global mean was accounted for by generating realizations of the global mean using the spatial bootstrap. This was incorporated into the point process by scaling each realization of intensity to a realization of the global mean.

The variability of the grade distribution is captured by controlling the variability of the intensity map. In this work, the intensity map was tuned until the variability of the final grade distribution matched that of the support-corrected histogram. By modelling the high-grade population with a spatial point process, the final grade models can be tuned to have the correct mean, variance and spatial variability. In the comparison to ordinary kriging and multiple indicator kriging, the results from using a spatial point process better match the support-correct global grade distribution.

Gold mineralization often takes place as discrete events; however, they are not typically distributed as random points in space but instead are spatially restricted to vein structures. In this work, veins were simulated using a discrete fracture network. The distribution of vein thickness and a set of intersection locations are necessary inputs to model a discrete fracture network. In this work, an image processing workflow was presented to automatically measure this information from a core photo database. The methodology was effective at isolating isolating rows of core. In this step of the processing workflow, over 95 percent of photos were correctly classified. The CIEDE2000 perceptual difference formula was effective at isolating veins from the rows of core; however, it also produced noisy results under some lighting conditions. The methodology presented here for isolating veins from noise was effective and, after optimization, achieved a correlation of 0.710 against a manually logged subset of photos. The locations and thickness of over 68,000 veins were measured from over 4,000 core photos. The measured thickness distribution was approximately log-normal.

The results from the image processing workflow were used to calculate vein density and estimate it over the case study domain. Over 1.5 million quartz

veins in the study area were simulated as a discrete fracture network. The high-grade population was modelled using a spatial point process; however, the the nuggets were only simulated within simulated veins. The high-grade population was assumed to be proportional to the vein density and was scaled, proportional to the vein density, until the mean of the high-grade population matched that of the global distribution. The final models of grade have the correct mean and variance and their spatial continuity is the same as the input DFN.

7.2 Future Work

The techniques outlined in this work show are effective in reducing the influence of outlier values; however, further refinement is needed and future work in this direction remains.

In the spatial point process modelling workflow, two areas that could use refinement are the generation of the intensity field and the selection of the particle size distribution. The intensity field controls the amount of simulated points and is a very important parameter. This work uses the local proportion of high and low grade assays to generate proportion conditioning data. Perhaps other indicator approaches such as sequential indicator simulation (SIS) or truncated pluri-Gaussian (TPG) techniques could be employed. The particle size distribution is generated using the high-grade subset of the original data. The use of metallurgical data could be employed here to find a more realistic size distribution of gold particles.

Using a discrete fracture network is effective in spatially reducing the influence of outlier values; however, one area that needs refinement is the assumption that grade is proportional to vein density. The workflow assumes that grade is greater in areas with more vein density. This may not be a realistic assumption for all deposits.

The image processing workflow worked sufficiently well for the intended purpose in this work; however, refinements are needed before it could be implemented on a larger scale. Specifically, improvements in pre-processing and

reducing noise are needed. The methodology failed to locate veins most commonly on photos with excess noise which was often the result of poor initial photo quality. In addition, further testing on a variety of drill core photo datasets is needed.

For the case study, more care should be taken to model only mineralized veins. This will improve the accuracy of the final models of grade.

Bibliography

Armstrong, M. (1984). Common problems seen in variograms. *Journal of the International Association of Mathematical Geology*, 16(3):305-313.

Asmussen, S.R. (2003). "Steady-State Properties of GI/G1/1". *Applied Probability and Queues*. Stochastic Modelling and Applied Probability, 51, pp. 266-301. New York, NY: Springer.

Babakhani, M., and Deutsch, C.V. (2013). Outlier detection and management in geostatistics. *CCG Report 13*, University of Alberta, Edmonton.

Board, W. and McNaughton, K.M. (2013). The Brucejack high-grade gold project, northwest British Columbia, Canada. *Paper presented at the New Gen Gold Conference 2013*, Perth, Western Australia

Bonnet, E., Bour, O., Odling, N.E., Davy, P., Main, I., Cowie, P., and Berkowitz, B. (2001). Scaling of fracture systems in geological media. *Reviews of Geophysics*, 39:347-383.

Cacas, M.C., Daniel, J.M. and Letouzey, J. (2001). Nested geological modelling of naturally fractured reservoirs. *Petroleum Geoscience*, 7(S):S43-S52.

Costa, J.F. (2003). Reducing the impact of outliers in ore reserves estimation. *Journal of the International Association of Mathematical Geology*, 35(3):323-345.

Cox, D. (1955). Some statistical methods connected with series of events. *Journal of the Royal Statistical Society*, B17(2):129-164.

Cox, S.F. (2005). Coupling between deformation, fluid pressures, and fluid flow in ore-producing hydrothermal systems at depth in the crust. *Economic Geology 100th Anniversary Volume*, pp. 39-75.

Dagbert, M. (2005). Geostatistics in resource/reserve estimation: A survey of the Canadian mining industry practice. In Leuangthong, O. and Deutsch, C.V., editors, Geostatistics Banff 2008, pages 345-350. Springer, Netherlands.

David, M. (1988). Handbook of applied advanced geostatistical ore reserve estimation. Amsterdam, Netherlands: Elsevier.

Dershowitz, W.S. and Herda, H.H. (1992). Interpretation of fracture spacing and intensity. *In 33rd US Symposium on Rock Mechanics, Santa Fe, NM*, pp. 757-766.

Deutsch, C. V. and Journel, A. G. (1998). *GSLIB: A Geostatistical Software Library and User's Guide, 2nd edn.* Oxford University Press, New York.

Deutsch, C.V. (2005). A new trans program for histogram and trend reproduction. In *CCG Annual Report 7*, University of Alberta, Edmonton.

Dominy, S.C., Annels, A.E., Johansen, G.F. and Cuffley, B.W. (2000). General considerations of sampling and assaying in a coarse gold environment. *Applied Earth Science*, 109(3):145-167.

Evenchick, C.A., McMechan, M.E., McNicoll, V.J., and Carr, S.D. (2007). A synthesis of the Jurassic-Cretaceous tectonic evolution of the central and southeastern Canadian Cordillera: Exploring links in the orogen, In: J.A. Sears, T.A. Harms, and C.A. Evenchick (editors), Whence the Mountains?: Inquiries into the Evolution of Orogenic Systems: A Volume in Horor of Raymond A. Price, Special paper 433, *The Geological Society of America*, Boulder, CO, pg. 419

Francois-Bongarcon, D. and Gy, P. (2001). The most common error in applying 'Gy's Formula' in the theory of mineral sampling, and the history of the liberation factor. In: Edwards, A.C. (editor) Mineral resource and ore reserve estimation - the AusIMM guide to good practice, *The Australasian Institute of Mining and Metallurgy,* Melbourne: pg. 67-72.

Gagnon, J.F., Barresi, T., Waldron, J.W.F., Nelson, J.L., Poulton, T.P., and Cordey, F. (2012). Stratigraphy of the upper Hazelton Group and the Jurassic evolution of the Stikine terrane, British Columbia *Canadian Journal of Earth Sciences*, 49(9): 1027-1052.

Gauthier, B.D.M., Garcia, M. and Daniel, J.M. (2002). Integrated fractured reservoir characterization: A case study in a North Africa field. *SPE Reservoir Evaluation and Engineering*, SPE 79105: 284-294.

Ghaffari, H., Huang, J., Hafez, S.A., Pelletier, P., Br, T., Brown, F.H., Vallat, C.J., Newcomen, H.W., Weatherly, H., Wilchek, L. and Mokos, P. (2012). Technical Report and Updated Preliminary Economic Assessment of the Brucejack Property. NI-43-101 Report. *Tetra Tech, Wardrop, Rescan, PE Mining, Geospark and AMC Mining*, 309 pg.

Goovaerts, P. (1997). Geostatistics for natural resources evaluation. New York, NY: Oxford University Presss.

Grubbs, F.E. (1969). Procedures for detecting outlying observations in samples. *Technometrics*, 11(1):1-21.

Hawkins, D.M. (1979). Lognormal - de Wijsian geostatistics for ore evaluation. In Krige, D.G., editor, South African Institute of Mining and Metallurgy monograph series: Geostatistics I. *Computers and Geosciences*, 5(2):279.

Hitchmough, A.M., Riley, M.S., Herbert, A.W. and Tellam, J.H. (2007). Estimating the hydraulic properties of the fracture network in a sandstone aquifer. *Journal of Containment Hydrology*, 93(1-4):38-57.

Ireland, D., Olssen, L., Huang, J., Pelletier, P., Weatherly, H., Stoyko, H.W., Hafez, S.A., Keogh, C., Schmid, C., McAfee, B., Chin, M., Gould, B., Wise, M., Greisman, P., Scott, W.E., Farah, A., Zazzi, G., Crozier, T. and Blackmore, S. (2014). Feasibility study and technical report update on the Brucejack Project. *Pretivm Resources*

Johnston, J.D. and McCaffrey, K.J.W. (1996). Fractal geometries of vein systems and the variation of scaling relationships with mechanism. *Journal of Structural Geology*, 18(2-3): 349-358.

Johansen, G.F. (1998). The New Bendigo Goldfield. *In VICMIN98: The 2nd GPIC Conference on Developments in Victorian Geology and Mineralization*. Australian Institute of Geoscientists, 24:47-51.

Jones, I.W.O. (2013). Mineral Resources Update Technical Report. *Pretium Resources*.

JORC. (2012). *Australian code for reporting of exploration results, mineral resources and ore reserves.* Joint Ore Reserves Committee of the Australasian Institute of Mining and Metallurgy, Australian Institue of Geoscientists and Minerals Council of Australia.

Journel, A.G. (1980). The lognormal approach to predicting local distributions of selective mining unit grades. *Journal of the International Association for Mathematical Geology*, 12(4):285-303.

Journel, A.G. (1982). The indicator approach to estimation of spatial distributions. In T.D. Johnson and R.J. Barnes, editors, *Proceedings of the 17th APCOM International Symposium*, Golden, CO, 793-806.

Kerrich, R. and Hodder, R.W. (1981). Archean lode gold and base metal deposits: evidence for metal separation into independent hydrothermal systems. *Canadian Mining and Metallurgy Bulletin*, 74:144-160.

Kirkham, R.V. and Margolis, J. (1995). Overview of the Sulphurets area, northwestern British Columbia, In: T.G. Schroeter (editor), Porphyry Deposits of the Northwestern Cordillera of North America. *CIMM Special Volume*, 46:473-482.

Kleingeld, W.J., Thurston, M.L. Prins, C.F. and Lantuejoul, C. (1996). The conditional simulation of a Cox process with applications to deposits with discrete particles. In E.Y. Baafi and N.A. Schofield, editors, *Geostatistics Wollongon 1996*, Amsterdam, Netherlands: Kluwer Academic Publishers.

Krige, D.G. (1999). Essential basic concepts in mining geostatistics and their links with geology and classical statistics. *South African Journal of Geology*, 102(2):147-151.

Krige, D.G. and Margi, E.J. (1982). Studies of the effects of outliers and data transformation on variogram estimates for a base metal and a gold ore body. *Journal of the International Association for Mathematical Geology*, 14(6):557-564.

Kroese, D.P. and Botev, Z.I. (2013). Spatial process generation. In V. Schmidt, editor, *Lectures on stochastic geometr, spatial statistics and random fields, volume II: Analysis, modeling and simulation of complex structures.*, Berlin, Germany: Springer

Lagarias, J.C., Reeds, J.A., Wright, M.H. and Wright, P.E. (1998). Convergence properties of the Nelder-Mead simplex method in low dimensions *Society for Industrial and Applied Mathematics*, 9(1):112-147.

Lantuejoul, C. and Millad, M. (2008). Modelling the stone size distribution of a diamond deposit. In J.M. Ortiz and X. Emery, editors, *Proceedings of the 8th International Geostatistics Congress*, Santiago, Chile, pages 779-788

Leuangthong, O., Khan, D.K., and Deutsch, C.V. (2008). Solved problems in geostatistics. Hoboken, NJ: John Wiley and Sons

Luo, M.R., Cui, G. and Rigg, B. (2001). The development of the CIE 2000 colour-difference formula: CIEDE2000. *Colour Research and Application*, 26:340-350.

Machuca, D.F., Babak, O. and Deutsch, C.V. (2007). Flexible change of support model suitable for a wide range of mineralization styles. In *CCG Annual Report 9*, University of Alberta, Edmonton.

Maleki, M., Madani, N., and Emery, X. (2014). Capping and kriging grades with long-tailed distributions. *The Journal of the Southern African Institute of Mining and Metallurgy*, 114:255-263.

Mandelbrot, B.B. (1997). States of randomness from mild to wild, and concentration in the short, medium and long run, In: B.B. Mandelbrot (editor), *Fractals and Scaling in Finance*. New York, NY: Springer

Mandl, G. (2005). *Rock joints: The mechanical genesis.* Berlin: Springer

McLennan, J.A. and Deutsch, C.V. (2004). Conditional non-bias of geostatistical simulation for estimation of recoverable reserves. *CIM bulletin*, 97.

MacQueen, J.B. (1967). Some methods for classification and analysis of multivariate observations. *Proceedings of the Fifth Symposium on Math, Statistics and Probability*, pp. 281-297. Berkeley, CA: Univeristy of California Press.

Monestiez, P., Dubroca, L., Bonnin, E. Durbec, J.P. and Guinet, C. (2006). Geostatistical modelling of spatial distribution of Balaenoptera physalus in the Northwestern Mediterranean Sea from sparse count data and heterogeneous observation efforts. *Ecological Modelling*, 193(3-4), 615-628.

Narr, W., Schechter, D.S., and Thompson, L.B. (2006). Naturally fractured reservoir characterization. *Society of Petroleum Engineers*: Richardson, Texas

Nelson, J. and Colpron, M. (2007). Tectonics and metallogeny of the British Columbia, Yukon and Alaska Cordillera, 1.8 Ga to the present. In: Goodfellow, W.D., (editor) Mineral Deposits of Canada: A Synthesis of Major Deposit-Types, District Metallogeny, the Evolution of Geological Provinces, and Exploration Methods. *Geological Association of Canada, Mineral Deposits Division*: Special Publication Number 5, pg. 755-791

Nelson, J., Colpron, M. and Israel, S. (2013). The Cordillera of British Columbia, Yukon, and Alaska: Tectonics and Metallogeny. In: M. Colpron, B.G. Rusk, J.F.H. Thompson (editors), Tectonics, Metallogeny and Discovery: The North American Cordillera and Similar Accretionary Settings, *Society of Economic Geologists*, Special Publication Number 17, pgs. 53-109.

Niven, E.B. (2010). *Geostatistics for naturally fractured reservoirs.* Unpublished doctoral dissertation. University of Alberta, Edmonton, Alberta, Canada

Pan, G. (1994). Restricted kriging: A link between sample value and sample configuration. *Journal of the International Association for Mathematical Geology*, 26(1):135-155.

Parker, H.M. (1991). Statistical treatment of outlier data in epithermal gold deposit reserve estimation. *Journal of the International Association for Mathematical Geology*, 23(2):175-179.

Pelham, D.A. (1991). The evaluation of vein gold deposits: Part I. *Mining and Quarrying Technology International*, pp. 57-61.

Pelham, D.A. (1992). The evaluation of vein gold deposits: Part II. *Mining and Quarrying Technology International*, pp. 31-34.

Phillips, G.N. and Powell, R. (2010). Formation of gold deposits: a metamorphic devolatilization model. *Journal of Metamorphic Petrology*, 28:689-718.

Plataniotis, K.N. and Venetsanopoulos, A.N. (2000). *Color Image Processing and Applications*. New York, NY: Springer

Poulsen, K.H., Robert, F. and Dube, B. (2000). Geological Classification of Canadian Gold Deposits. *Geological Survey of Canada*, bulletin 540, Vancouver, BC.

Renard, F., Andreani, M., Boullier, A.M. and Labaume, P. (2005). Crack-seal patterns: records of uncorrelated stress release variations in crustal rocks. *Geological Society of London Special Publications 2005*, 243:67-79.

Robert, F., Brommecker, R., Bourne, B.T., Dobak, P.J., McEwan, C.J., Rowe, R.R. and Zhou, X. (2007). Models and exploration methods for major gold deposit types. In: B. Milkereit (editor), Proceedings of Exploration 07: Fifth Decennial International Conference on Mineral Exploration. pg. 691-711. *Decennial Mineral Exploration Conferences*, Toronto, ON, Canada.

Roberts, S., Sanderson, D.J., Lonergan, L. and Gumiel, P. (1999). Fractal analysis and percolation properties of veins. In: K.W.L. McCaffrey, L. Lonergan and J.J. Wilkinson, editors, *Fractures, Fluid Flow and Mineralization*. Geological Society, London, Special Publications, 155:7-16.

Rombouts, L. (1995). Sampling and statistical evaluation of diamond deposits. *Journal of Geochemical Exploration*, 53(1-3), 351-367.

Rombouts, L. (2003). Assessing the diamond potential of kimberlites from discovery to evaluation bulk sampling. *Mineralium Deposita*, 38(4), 496-504.

Rossi, M.E. and Deutsch, C.V. (2014). *Mineral Resource Estimation*. New York, NY: Springer

Royle, A.G. (1995). *The sampling and evaluation of gold deposits*. Unpublished doctoral dissertation. University of Leeds, United Kingdom.

SAMREC. (2007). *South African code for reporting of exploration results, mineral resources and mineral reserves.* South African Mineral Resource Committee, Working group under the joint auspices of the South African Institute of Mining and Metallurgy and the Geological Society of South Africa.

Sharma, G., Wu, W. and Dalal E.N. (2004). The CIEDE2000 colour-difference formula: implementation notes, supplementary test data, and mathematical observations. *Colour Research and Application*, 30(1):21-30.

Sillitoe, R.H. (2010). Porphyry copper systems. *Economic Geology*, 105(1):3-41.

Sinclair, A.J. (2002). *Applied mineral inventory estimation*. Cambridge, UK: Cambridge University Press

Srivastava, M. and Parker, H.M. (1989). Robust measures of spatial continuity. In: M. Armstrong (editor), *Geostatistics* (pp. 295-308). Amsterdam: Springer.

Srivastava, M. (2001). *Outliers - A guide for data analysts and interpreters on how to evaluate unexpected high values: Contaminated sites statistical applications guidance document* (No. 12-8). Victoria, BC: British Columbia Ministry of Environment

Taylor, B.E. (2007). Epithermal gold deposits. In: W.D. Goodfellow, editor, *Mineral Deposits of Canada: A Synthesis of Major Deposit-Types, District Metallogeny, the Evolution of Geological Provinces, and Exploration Methods*. Geological Association of Canada, Mineral Deposits Division, Special Publication, 5:287-304.

Terzhagi, R.D. (1965). Sources of error in joint surveys. *Geotechnique*, 15:287-304.

Verly, G. (1983). The multigaussian approach and its applications to the estimation of local reserves. *Mathematical Geology*, 15:249-286.

Wang, X. (2005). *Stereological interpretation of rock fracture traces on drillhole walls and other cylindrical surfaces*. Unpublished doctoral dissertation. Virginia Polytechnic Institute and State Univeristy, Blacksburg, Virginia, United States

Zhang, L. and Einstein, H.H. (2000). Estimating the intensity of rock discontinuities. *International Journal of Rock Mechanics and Mining Sciences*, 37(5):819-837.

Chapter 8

Appendix - Software

A number of GSLIB style software programs have been developed to support the research presented in this thesis. The conventions used and software developed build upon those set out by Deutsch and Journel (1998). This appendix provides a description of the purpose and parameters for each of the programs developed.

8.1 Spatial Point Process Simulation

The program `SPPSIM` generates a model of discrete gold nuggets using a spatial point process. The two main requirements for the program are a gridded file of intensity and a particle size distribution. The gridded intensity file can be generated using OK or SGS (recommended GSLIB software: `sgsim` or `kt3d` (Deutsch and Journel, 1998)). The size distribution can either come from prior sources or is calculated from assay data. Size must be input in milimeters. The program requires either a single value for the high-grade mean or a file of means if wanting to consider mean uncertainty. The output file contains a conditional count of nuggets per block and the associated block grade. The parameter file is listed below:

```
                  Parameters for SPPSIM
                  *********************

START OF PARAMETERS:
intensity.dat          -file with gridded intensity
  1                    -   column
-1e21   1e21           -trimming limits
0                      -size distribution (see note 1)
size_dist.out          -if 0, provide file, 1 provide grade
  1                    -   column
clipping.dat           -file with clipping data (see note 2)
  1                    -   column
1  0.83                -high-grade mean (see note 3)
bootstrap.out          -file with means (see note 4)
  1                    -   column
0.0  0.0  0.0          -search for LVSD (see note 5)
  0.0 0.0 0.0          -angles for search ellipsoid
100                    -number of realizations
50   0.5    1.0        -   nx,xmn,xsiz
50   0.5    1.0        -   ny,ymn,ysiz
50   0.5    1.0        -   nz,zmn,zsiz
nuggets.out            -output file name

******
NOTES:
******
1.  For the size distribution, provide either a file with
nugget radius in mm or provide a file with high-grade assays
to be converted to size
2.  If no clipping file is used, change to nofile
3.  For single mean, set to 0 and input mean.  For multiple
means set to 1 and enter the file of means from spatial
bootstrap
4.  If not considering different means, change to nofile
5.  Set to 0 0 0 if using a global size distribution
```

Figure 8.1: Input paramters for SPPSIM

.

8.2 DFN Grade Modelling Programs

The program DFNSPP is similar to SPPSIM except it requires an input DFN. To generate a DFN, this work used the GSLIB-style program DFNSIM (Niven, 2010). If using another program to generate a DFN, care must be taken to ensure that the input DFN file follows the same format. This program simulates discrete events along the simulated fracture planes. The locations of the nuggets can be output; however, the output file can be extremely large.

```
                  Parameters for DFNSPP
                  *********************

START OF PARAMETERS:
dfn.dat                 file with DFN (see note 1)
  1                     -   column
-1e21   1e21            -trimming limits
0                       -size distribution (see note 2)
size_dist.out           -if 0, provide file, if 1 provide grade
  1                     -   column
count.dat               -gridded file with nugget counts
  1                     -   column
clipping.dat            -file with clipping data (see note 3)
  1                     -   column
1  1.13                 -high-grade mean (see note 4)
bootstrap.out           -file with means (see note 5)
  1                     -   column
50   0.5    1.0         -   nx,xmn,xsiz
50   0.5    1.0         -   ny,ymn,ysiz
50   0.5    1.0         -   nz,zmn,zsiz
highgrade.out           -file for output grade
1                       -1, print nugget locations
nuggets.out             -file with nugget location (note 6)

******
NOTES:
******
1.  This program is designed to work with standard output
files from DFNSIM.  If using another program, please
convert to the same format
2.  For the size distribution, provide either a file with
nugget radius in mm or provide a file with high-grade assays
to be converted to size
3.  If no clipping file is used, change to nofile
4.  For single mean, set to 0 and input mean.  For multiple
means set to 1 and enter the file of means from
spatial bootstrap
5.  If not considering different means, change to nofile
6.  This file can be extremely large
```

Figure 8.2: Input paramters for DFNSPP

.